ASYMPTOTICS OF THE TURAEV-VIRO INVARIANTS AND THEIR CONNECTIONS IN LOW-DIMENSIONAL TOPOLOGY

By

Sanjay Lakshman Kumar

A DISSERTATION

Submitted to
Michigan State University
in partial fulfillment of the requirements
for the degree of

Mathematics - Doctor of Philosophy

2021

ABSTRACT

ASYMPTOTICS OF THE TURAEV-VIRO INVARIANTS AND THEIR CONNECTIONS IN LOW-DIMENSIONAL TOPOLOGY

By

Sanjay Lakshman Kumar

We study the Turaev-Viro invariants of 3-manifolds as well as their relationship to invariants arising from hyperbolic geometry. We first construct a closed formula for the Turaev-Viro invariants for hyperbolic once-punctured torus bundles. We then examine a conjecture by Chen and Yang [13] which states that the asymptotics of the Turaev-Viro invariants recover the hyperbolic volume of the manifold. Using topological tools, we are able to construct infinite families of new examples of hyperbolic links in the 3-sphere which satisfy the conjecture. Additionally, we show a general method for augmenting a link such that the resulting link has hyperbolic complement which satisfies the conjecture.

As an application of the constructed links in the 3-sphere, we extend the class of known examples which satisfy a conjecture by Andersen, Masbaum, and Ueno [3] relating the quantum representations of surface mapping class groups to its Nielsen-Thurston classification. Most notably, we provide explicit elements in the mapping class group for a genus zero surface with n boundary components, for $n > 3$, as well as elements in the mapping class group for any genus g surface with four boundary components such that the obtained elements satisfy the conjecture. This is accomplished by utilizing the intrinsic relationship between the Turaev-Viro invariants and the quantum representations shown by Detcherry and Kalfagianni in [18].

Dedicated to Chung Ae Kim and Karla Gomez.

ACKNOWLEDGEMENTS

I would first like to thank my advisor, Effie Kalfagianni, for her guidance throughout my time in the mathematics PhD program at Michigan State University. I sincerely appreciate the effort she has dedicated towards my growth as a mathematician.

I would also like to express my gratitude towards Charles Frohman and Rosemary Guzman who were at the beginning of my journey as an undergraduate. Because of them, I have always felt supported in the community.

Additionally, I would like to extend my gratitude towards Robert Bell, Matthew Hedden, Kristen Hendricks, and Ben Schmidt for their involvement and help during the graduate program as well as Renaud Detcherry who provided insightful comments and suggestions on some of the results appearing in this work.

Moreover, I would like to thank my family and friends whose positivity and support has always been a valuable asset in my life.

As a further acknowledgement, the material appearing in this work is based on research partially supported by NSF grants DMS-1404754, DMS-1708249, DMS-2004155 and by a Dr. Paul and Wilma Dressel Endowed Scholarship from the Department of Mathematics at Michigan State University.

TABLE OF CONTENTS

LIST OF TABLES

LIST OF FIGURES

Chapter 1

Introduction

In the 1980's, Witten [60] provided a new interpretation of the Jones polynomials [30, 31] from the perspective of physics leading to the construction of a sequence of complex-valued 3-manifold invariants. This led to the field of *quantum topology*, and the construction of a wealth of new link and manifold invariants known as *quantum invariants*. This was first formalized by Reshetikhin and Turaev [48] through the representation theory of quantum groups which gave rise to the colored Jones polynomials. These are a sequence of polynomial invariants of links parameterized by a positive integer n which are a generalization of the Jones polynomial. Additionally, Reshetikhin and Turaev constructed a sequence of 3-manifold invariants calculated from the surgery description of the manifold [35] which correspond to Witten's invariants.

Although the quantum invariants can be used to distinguish links and manifolds, it is conjectured that there are also strong connections between the hyperbolic geometry and quantum topology of 3-manifolds. The most famous example being Kashaev's volume conjecture [32, 33]. Kashaev introduced a sequence of quantum invariants for links in S^3 using quantum dilogarithm functions, and Kashaev also observed in a few examples, as well as conjectured in the general case, that the absolute value of the invariants grows exponentially for hyperbolic links where the growth rate is given by the hyperbolic volume of the complement. Later in [44], Murakami and Murakami showed that the values of the colored Jones polynomials evaluated at a particular root of unity coincide with Kashaev's invariants leading to a reformulation of the volume conjecture. As this conjecture is analogous to numerous topics in this dissertation, we provide its statement here.

Conjecture 1.0.1 ([33, 44])**.** *For a hyperbolic link L in S^3, let $J_n(L;q)$ be the n-th colored Jones polynomial evaluated at q. Then*

$$\lim_{n\to\infty} \frac{2\pi}{n} \log \left| J_n\left(L; e^{\frac{2\pi\sqrt{-1}}{n}}\right)\right| = Vol\left(S^3 \backslash \text{IntNbd}(L)\right)$$

where $Vol\left(S^3\backslash \text{IntNbd}(L)\right)$ is the hyperbolic volume of the complement of L in S^3.

The volume conjecture is one of the many proposed relations between hyperbolic geometry and quantum topology. In this work, we will investigate two other conjectures which further deepen the connection between the fields. Namely, we will explore the Turaev-Viro invariant volume conjecture, stated by Chen and Yang in [13], and the Andersen-Masbaum-Ueno (AMU) conjecture [3]. For the formal statements of the conjectures as well as main results, see Sections 1.2 and 1.3, respectively.

Briefly, the Turaev-Viro invariant volume conjecture is analogous to the original volume conjecture; however, in place of the colored Jones polynomials, the Turaev-Viro invariant volume conjecture relates the exponential growth rate of a sequence of real-valued invariants known as the *Turaev-Viro invariants* [57] to the volume of the hyperbolic manifold. As opposed to the original volume conjecture which was stated for link complements in S^3, the Turaev-Viro invariant is a 3-manifold invariant defined on a triangulation of the 3-manifold. Because of this, the Turaev-Viro invariant version of the volume conjecture can be stated for more classes of hyperbolic 3-manifolds.

For the latter, the AMU conjecture asserts that the geometric properties of the elements of the surface mapping class groups given by the Nielsen-Thurston classification [23, Theorem 13.2] are detected by objects arising from the Witten-Reshetikhin-Turaev topological quantum field theories known as the *quantum representations* [48, 56]. More explicitly, the Nielsen-Thurston classification splits the mapping class group into either *periodic*, *reducible*, or *pseudo-Anosov* elements, and in the reducible case, the elements may be further reduced to smaller parts on which the Nielsen-Thurston classification again applies. The AMU con-

jecture states that there is a quantum representation of infinite order if and only if the associated mapping class group element contains any parts that are pseudo-Anosov.

Notably, we will see in Subsection 2.2.3 that it is natural to study the two conjectures jointly. This is due to the Turaev-Viro invariant volume conjecture implying the AMU conjecture as shown by Detcherry and Kalfagianni in [18].

1.1 Organization of Dissertation

The main results of this dissertation along with the statements of the Turaev-Viro invariant volume conjecture and the AMU conjecture can be found in Sections 1.2 and 1.3, respectively. In Chapter 2, we will present necessary preliminary material involving the definition of the Turaev-Viro invariant [57], an introduction to surface mapping class groups [23], an introduction to Turaev's shadow theory approach to 3-manifolds [56], and the construction of a family of links known as the *fundamental shadow links* which were originally introduced by Constantino and Thurston in [15]. In Chapter 3, we consider the Turaev-Viro invariants of the once-punctured torus bundles and their possible relationship to quantities in hyperbolic geometry. Lastly, in Chapters 4 and 5, we demonstrate positive results towards the Turaev-Viro invariant volume conjecture and the AMU conjecture, respectively, through applications of the fundamental shadow links.

1.2 The Turaev-Viro Invariant Volume Conjecture

In this section, we will write the statement of the Turaev-Viro invariant volume conjecture followed by the main results found in Chapters 3 and 4.

The $SO(3)$-version of the Turaev-Viro invariants $TV_r(M, q)$ [21, 57] of a compact 3-manifold M are real-valued invariants of M that depend on an odd integer $r \geq 3$ and a $2r$-th root of unity q. For a precise definition of the Turaev-Viro invariant, see Section 2.1. Similar in form to the original volume conjecture, Chen and Yang proposed the following which

relates the exponential growth rate of $TV_r(M,q)$ to the hyperbolic volume of the manifold M, denoted by $Vol(M)$.

Conjecture 1.2.1 ([13]). *Let M be a hyperbolic 3-manifold and $q = \exp\left(\frac{2\pi\sqrt{-1}}{r}\right)$. Then*

$$\lim_{r\to\infty} \frac{2\pi}{r} \log|TV_r(M,q)| = Vol(M)$$

as r ranges along the odd natural numbers.

Additionally in [13], Chen and Yang provided numerous computations supporting the exponential growth rate of the Turaev-Viro invariant at this particular root of unity. It is notable that this conjecture is in contrast to the evaluation of the invariant at $q = \exp\left(\frac{\pi\sqrt{-1}}{r}\right)$ where the growth rate is expected to only be polynomial.

Currently, Conjecture 1.2.1, which we call the *Turaev-Viro invariant volume conjecture*, has been proven for multiple 3-manifolds. It has been shown for the complement of the Borromean rings and the complement of the figure-eight knot by Detcherry, Kalfagianni, and Yang in [21]. It was verified by Ohtsuki that the closed hyperbolic 3-manifolds arising from integral Dehn surgeries on the figure-eight knot satisfy the conjecture in [45] which was extended by Wong and Yang to rational surgeries in [62]. In [7], Belletti, Detcherry, Kalfagianni, and Yang verified the conjecture for the complements of the fundamental shadow links which are a family of links in connected sums of $S^2 \times S^1$. Additionally in [6], Belletti proved Conjecture 1.2.1 for families of links in connected sums of $S^2 \times S^1$ which contain examples that are not fundamental shadow links. Lastly in [61], Wong proved Conjecture 1.2.1 for the twisted Whitehead links as well as certain subfamilies of Whitehead chains originally introduced by Roland van der Veen in [58].

Additionally in this work, it will be useful for us to generalize the Turaev-Viro invariant volume conjecture for the cases when the manifold is not necessarily hyperbolic. For this, we will write the Turaev-Viro invariant volume conjecture in terms of the *simplicial volume*. We will only state the relationship between the simplicial volume and the hyperbolic volume

of a manifold; however, more details may be found in [27] by Gromov and in [54, Section 6.5] by Thurston.

We will denote the simplicial volume for a manifold M by $\|M\|$. If M is a hyperbolic manifold of finite volume, then

$$Vol\,(M) = v_4\,\|M\|$$

where $v_4 \approx 1.0149$ is the volume of a regular ideal tetrahedron. For manifolds which are not hyperbolic, the simplicial volume can be thought of as measuring the sum of the volumes of the hyperbolic pieces. Because of this, the following conjecture, which is formally stated by Detcherry and Kalfagianni in [19], is a natural extension of the Turaev-Viro invariant volume conjecture.

Conjecture 1.2.2 ([13])**.** *Let M be a compact and orientable 3-manifold with empty or toroidal boundary. Then for $q = \exp\left(\frac{2\pi\sqrt{-1}}{r}\right)$,*

$$LTV\,(M) = \limsup_{r\to\infty} \frac{2\pi}{r} \log\left|TV_r\,(M,q)\right| = v_4\,\|M\|$$

as r ranges along the odd natural numbers.

In [19], the authors show that the extended Turaev-Viro invariant volume conjecture holds for certain manifolds of simplicial volume zero. In addition, the authors show that the extended Turaev-Viro invariant volume conjecture is preserved under gluings by manifolds known as the *invertible cabling spaces*. Furthermore, Detcherry shows that the conjecture is preserved under $(p, 2)$-cabling for p odd in [17].

In the following subsections, we provide results from this work in relation to the Turaev-Viro invariant volume conjecture.

1.2.1 Main Results From Chapter 3

In Chapter 3, we consider the Turaev-Viro invariants of once-punctured torus bundles. Briefly, the *mapping class group* $Mod(\Sigma_1^1)$ is the group of isotopy classes of orientation-preserving self-homeomorphisms of the surface. More information on mapping class groups may be found in Section 2.2. From the elements of $Mod(\Sigma_1^1)$, we may form the once-punctured torus bundles. For $\phi \in Mod(\Sigma_1^1)$, the once-punctured torus bundle is constructed as the *mapping torus* $M(\phi) = \Sigma_1^1 \times [0,1]/(x,0) \sim (\phi(x),1)$ such that $M(\phi)$ has *monodromy* ϕ. In the case of hyperbolic once-punctured torus bundles, the monodromy ϕ admits a canonical presentation in terms of generators R and L which is related to the canonical triangulation of the bundle. From this canonical triangulation, we construct a closed formula for the Turaev-Viro invariants which depends, in a trivial way, on the form of the canonical presentation of the monodromy $\phi \in Mod(\Sigma_1^1)$. For more details on either the mapping tori or the canonical triangulations, see Subsections 2.2.1 and 3.1.1, respectively.

We will now proceed with the closed formula for the Turaev-Viro invariants of the hyperbolic once-punctured torus bundles. Although understanding the formula involves the introduction of additional notation found in Section 3.2, we will still first state the formula here as follows. We remark that an *admissible coloring* is a set of criteria, dependent on the odd and positive integer r, which the terms $E^{N_k}_{i_{k-1},j_{k-1}}$ known as the *quantum* $6j$*-symbols* will have to satisfy. See Section 2.1 for the precise definition.

Theorem 3.2.1. *Let* $\phi = R^{N_1}L^{N_2}\cdots R^{N_{2n-1}}L^{N_{2n}} \in Mod(\Sigma_1^1)$ *where* $n, N_i > 0$ *for* $1 \leq i \leq 2n$*, and let* $N = \left(\sum_{i=1}^{2n} N_i\right)$*. Then the mapping torus* $M(\phi)$ *has Turaev-Viro invariant*

$$TV_r(M(\phi), q) = 2^{b_2-b_0} \sum_{adm} \left[\left(\prod_{k=4}^{N+3} |a_k| \right) \left(E^{N_1}_{i_0,j_0} \cdot E^{N_2}_{i_1,j_1} \cdot \ldots \cdot E^{N_{2n}}_{i_{2n-1},j_{2n-1}} \right) \right]$$

where the sum is over all admissible colorings, $a_1 = a_{(N+2)}$*,* $a_2 = a_{(N-N_{2n}+2)}$*, and* $a_3 = a_{(N+3)}$*. Additionally, the indices* i_k *and* j_k *may be computed inductively from* $(i_0, j_0) = (2, 3)$ *where*

$i_k \notin \{i_{k-1}, j_{k-1}\}$ *and with*

$$j_k = \begin{cases} i_{k-1} & \textit{For } N_k \textit{ odd} \\ \\ j_{k-1} & \textit{For } N_k \textit{ even} \end{cases}.$$

In Subsection 3.2.1, we provide examples of explicit calculations of the Turaev-Viro invariants for once-punctured torus bundles using Theorem 3.2.1.

Lastly, we end Chapter 3 with a conjecture relating the Turaev-Viro invariants of hyperbolic manifolds to a geometric quantity of the mapping class group known as the *stretch factor*. The conjecture is stated in the following where pseudo-Anosov elements are defined in Subsection 2.2.1.

Conjecture 3.3.3. *Let $\phi \in Mod(\Sigma_1^1)$ be a pseudo-Anosov element with stretch factor λ_ϕ. Then*

$$LTV\,(M) = \limsup_{r\to\infty} \frac{2\pi}{r} \log |TV_r\,(M(\phi), q)| \leq 2\pi \log\,(\lambda_\phi)$$

where r runs along the odd integers and $q = \exp\left(\frac{2\pi\sqrt{-1}}{r}\right)$.

As the goal of the Turaev-Viro invariant volume conjecture is to relate quantum topology to hyperbolic geometry, Conjecture 3.3.3 further supports the claim. As we will discuss in Section 3.3, a similar bound involving the hyperbolic volume and the stretch factor is known.

1.2.2 Main Results From Chapter 4

We first note that a large part of the results stated here are based on the work found in [36] by the author of this dissertation. An important observation is that the Turaev-Viro invariant volume conjecture is preserved under homeomorphisms of manifolds. This is due to the Turaev-Viro invariant being a 3-manifold invariant as well as the hyperbolic volume being a topological invariant by Mostow-Prasad rigidity [43, 46]. By utilizing this property, we are able to prove the Turaev-Viro invariant volume conjecture for many link complements in S^3 through explicit homeomorphisms to the complements of the fundamental shadow links. In this sense, we say that the fundamental shadow links are *realized* as links in S^3.

The precise definition of the fundamental shadow links may be found in Subsection 2.3.1; however, in summary, the fundamental shadow links are a family of links in connected sums of $S^2 \times S^1$ with useful properties. More specifically, they are hyperbolic links with explicit hyperbolic volumes constructed from even multiples of regular ideal hyperbolic octahedra along with relatively simple Turaev-Viro invariants from which the Turaev-Viro invariant volume conjecture can be directly verified [7]. Additionally, they are "universal" in the sense that every orientable 3-manifold with empty or toroidal boundary can be realized as the manifold obtained from *Dehn fillings* along some subset of the boundary components for the complement of some fundamental shadow link. See Subsection 4.1.3 for more details on Dehn fillings.

Using *LinkInfo* [39] by Livingston and Moore, we begin by classifying links up to 11-crossings in S^3 with complements homeomorphic to the complement of a fundamental shadow link. Here, we denote $v_8 \approx 3.6639$ as the volume of a regular ideal hyperbolic octahedron.

L_{6a4}	L_{8n5}	L_{8n7}	L_{9n25}	L_{9n26}	L_{10n32}
L_{10n36}	L_{10n70}	L_{10n84}	L_{10n87}	L_{10n97}	L_{10n105}
L_{10n108}	L_{11n287}	L_{11n376}	L_{11n378}	L_{11n385}	

Table 1.1: The links up to 11-crossings in S^3 which satisfy the Turaev-Viro invariant volume conjecture with volume $2v_8$.

Theorem 1.2.3. *Each of the links in Table 1.1 is hyperbolic with volume $2v_8$ and satisfies the Turaev-Viro invariant volume conjecture.*

The given notation L_{***} is such that the first index indicates the minimum number of crossings, the second index indicates whether it is alternating or non-alternating, and the last index indicates that it is the k-th link with the same first two indices. We note that in Section 4.3, we compile a list of all possible links in *LinkInfo* which could be a fundamental shadow link with hyperbolic volume $2v_8$. With the exception of the link L_{10n59}, all of the possible links are fundamental shadow links realized in S^3. For the case of L_{10n59}, our method gave an inconclusive result; however, we believe that the link does not have complement

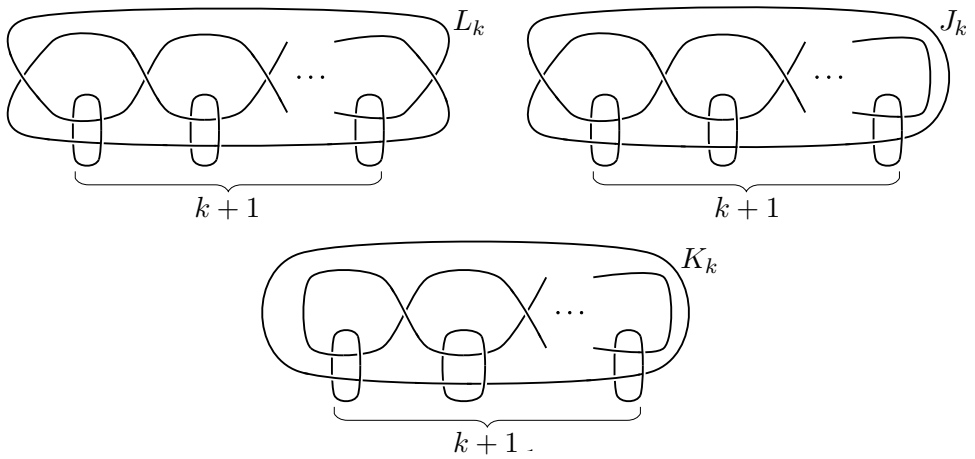

Figure 1.1: The defined link families L_k, J_k, and K_k in S^3. For the link family $\{L_k\}$ with $(5k+6)$ crossings, the number of components is $(k+2)$ for k odd and $(k+3)$ for k even. For the link family $\{J_k\}$ and $\{K_k\}$ with $(5k+5)$ and $(5k+4)$ crossings, the number of components is $(k+2)$ and $(k+3)$, respectively.

homeomorphic to the complement of a fundamental shadow link.

Additionally, we construct infinite link families in S^3 which satisfy the Turaev-Viro invariant volume conjecture.

Theorem 4.4.2. *Given an integer $k \geq 1$, let L_k, J_k, and K_k be the links in S^3 shown in Figure 1.1. The complement of each L_k, J_k, and K_k is a hyperbolic manifold with volume $2kv_8$ and satisfies the Turaev-Viro invariant volume conjecture.*

In the sense that they correspond to $k = 1$, the complements of these links should be seen as a generalization of the complements of the Borromean rings and the Borromean twisted sisters. For an illustration of the Borromean rings and the Borromean twisted sisters, see Figure 4.3.

As we will see in Subsection 2.3.2, the fundamental shadow links may be constructed from planar 4-valent graphs. In Section 4.5, we show that at least one of the fundamental shadow links corresponding to a planar 4-valent graph can be realized as a link in S^3. Here, the *complexity* is the number of vertices of the graph. We remark that the following theorem is a generalization of Theorem 4.1 first appearing in [36].

Theorem 4.5.1. *For any G, a planar 4-valent graph of complexity k, there exists a corre-*

sponding fundamental shadow link realized in S^3 with hyperbolic volume $2kv_8$.

Now as an immediate corollary, we obtain the result that every link in S^3 may be augmented by adding additional link components such that the resultant link satisfies the Turaev-Viro invariant volume conjecture.

Corollary 4.5.2. *Every link $J \subset S^3$ is a sublink of a link $L \subset S^3$ such that the link complement $S^3 \backslash \text{IntNbd}(L)$ is homeomorphic to a fundamental shadow link complement and satisfies the Turaev-Viro invariant volume conjecture.*

We note that Corollary 4.5.2 should be compared to a result of Baker [5, Theorem 1] and Roland van der Veen [59, Corollary 3] which states that all links are sublinks of arithmetic links. In particular, Corollary 4.5.2 is similar in application to Corollary 1 in [59]. By using augmented knotted trivalent graphs, the author showed that any link may be augmented to satisfy an $SO(3)$-version of the original volume conjecture.

At the end of Chapter 4, we note that the augmentations of the links can be described explicitly. We outline the general method for augmenting a link in S^3, and we provide a specific example of the augmentation for an unknot.

1.3 The Andersen-Masbaum-Ueno (AMU) Conjecture

In this section, we will write the statement of the Andersen-Masbaum-Ueno conjecture in addition to the main results regarding the conjecture found in Chapter 5.

We will begin with a brief introduction to the quantum representations. We first fix an odd integer $r \geq 3$ which we refer to as the *level*. We now let $\Sigma_{g,n}$ be a surface with genus g and n boundary components, and we let $Mod(\Sigma_{g,n})$ be its mapping class group which fixes the boundaries. For a more in-depth discussion of surface mapping class groups, see Section 2.2. Now let $|\partial(\Sigma_{g,n})|$ denote the set of boundary components of $\Sigma_{g,n}$, and we define $I_r = \{0, 1, \ldots, \frac{r-5}{2}, \frac{r-3}{2}\}$ to be the set of non-negative integers less than or equal to

$\frac{r-3}{2}$. Lastly, given a primitive $2r$-th root of unity and an assignment $c : |\partial\Sigma_{g,n}| \to I_r$, the $SO(3)$-Witten-Reshetikhin-Turaev TQFT [10, 48, 56] gives a projective representation

$$\rho_{r,c} : Mod(\Sigma_{g,n}) \to PGL_{d_{r,c}}(\mathbb{C})$$

called the $SO(3)$-*quantum representation* where $PGL_{d_{r,c}}(\mathbb{C})$ is the projective general linear group with $d_{r,c}$ an integer dependent on the level r and the choice of c. Here, we will often refer to the assignment c as a *coloring* of the boundaries. More intuitively, for a choice of r and c, we can associate a matrix to every element of $Mod(\Sigma_{g,n})$.

Now the AMU conjecture relates the Nielsen-Thurston classification of elements of the mapping class group for a compact surface $\Sigma_{g,n}$ to its quantum representations. For more details on the Nielsen-Thurston classification, see Subsection 2.2.1. Under the Nielsen-Thurston classification, there are two types of infinite order elements in the mapping class group. These are the reducible and pseudo-Anosov elements. For the reducible case, a power of the element fixes a collection of disjoint curves on the surface such that we may consider the induced self-homeomorphisms on the individual components obtained from cutting the surface along the fixed curves. If at least one of the induced self-homeomorphisms is pseudo-Anosov, we say that the mapping class group element contains *pseudo-Anosov parts*.

As we will see in the following statement, the AMU conjecture asserts that the asymptotics of the quantum representations detect the pseudo-Anosov parts in the mapping class group.

Conjecture 1.3.1 ([3], AMU conjecture)**.** *An element $f \in Mod(\Sigma_{g,n})$ has pseudo-Anosov parts if and only if, for any big enough level r, there is a choice of coloring c of the elements of $\partial\Sigma_{g,n}$ such that $\rho_{r,c}(f)$ has infinite order.*

We remark that one direction of the AMU conjecture is already known. If there exists a $\rho_{r,c}(f)$ with infinite order, then f has pseudo-Anosov parts. Because of this, whenever we find a $\rho_{r,c}(f)$ with infinite order, then we know that the associated element f satisfies the

conclusion of the AMU conjecture. Although, in this work, we still consider cases where the elements can additionally be shown to be pseudo-Anosov and not reducible.

The AMU conjecture was first stated in [3] where Andersen, Masbaum, and Ueno proved the conjecture for the mapping class group of the four-holed sphere. Using a similar method, Santharoubane also proved the conjecture for the one-holed torus in [51]. Although for the following surfaces the AMU conjecture is still unknown, certain elements in the mapping class group have been shown to satisfy the conjecture. Egsgaard and Jorgensen in [22] and Santharoubane in [52], by using different approaches, produced elements of $Mod(\Sigma_{0,2n})$ satisfying Conjecture 1.3.1.

For the higher genus cases, there have also been results. Marché and Santharoubane in [40] construct finitely many conjugacy classes of pseudo-Anosov elements for $Mod(\Sigma_{g,1})$, and Detcherry and Kalfagianni construct cosets of $Mod(\Sigma_{g,1})$, for sufficiently large g, that satisfy the AMU conjecture in [20]. Additionally, Detcherry and Kalfagianni in [18] find infinitely many pseudo-Anosov elements in $Mod(\Sigma_{g,2})$ for $g \geq 3$ and in $Mod(\Sigma_{g,n})$ where $g \geq n \geq 3$.

In the following subsection, we provide results from this work which further progress the Andersen-Masbaum-Ueno conjecture.

1.3.1 Main Results From Chapter 5

Similar to Subsection 1.2.2, we remark that a large part of the results stated here are also based on the work found in [36] by the author of this dissertation. As we will see in Subsection 2.2.3, the asymptotics of the Turaev-Viro invariants can be utilized in proving the AMU conjecture. Our results in Chapter 5 are a consequence of this correlation. We first begin with the following definition.

Definition 1.3.2. We say that two elements $f, g \in Mod(\Sigma_{g,n})$ are *independent* if there is no $h \in Mod(\Sigma_{g,n})$ such that both f and g are conjugate to non-trivial powers of h.

As explained in [20], the motivation behind the definition of independent is if f and g are not independent, then f satisfies the AMU conjecture if and only if g does. Because

of this, we need a less trivial definition for having infinitely many elements in the mapping class group which satisfy the AMU conjecture. We now state the following theorem which is based on techniques developed by Detcherry and Kalfagianni in [18].

Theorem 5.2.1. *Given $g \geq 0$, there exists a pseudo-Anosov element in $Mod(\Sigma_{g,4})$ that satisfies the AMU conjecture. Furthermore, for $g \geq 3$, there are infinitely many pairwise independent pseudo-Anosov elements in $Mod(\Sigma_{g,4})$ that satisfy the AMU conjecture.*

As a byproduct of the proof of Theorem 5.2.1, we also construct examples in $Mod(\Sigma_{n-1,n})$ and $Mod(\Sigma_{n-2,n})$, for $n \geq 5$, as well as examples in $Mod(\Sigma_{1,3})$ and $Mod(\Sigma_{3,3})$ which satisfy the AMU conjecture.

For our next result, we construct explicit elements in the mapping class group for a genus zero surface with boundary components that satisfy the AMU conjecture. In particular, to the author's knowledge, we obtain the first known examples of pseudo-Anosov elements satisfying the AMU conjecture in the mapping class group for a genus zero surface with an odd number of boundary components. We will now state the result as follows where the elements $\omega_n \in Mod(\Sigma_{0,n})$ are defined in Subsection 5.2.3.

Corollary 5.2.9. *For $n \geq 4$, the element $\omega_n \in Mod(\Sigma_{0,n})$ satisfies the AMU conjecture. Additionally, if $n \notin \{5, 7\}$, then ω_n is a pseudo-Anosov element.*

We note that the elements $\omega_n \in Mod(\Sigma_{0,n})$ can be written explicitly as elements in the pure braid group. For a summary of the braid group, see Subsection 2.2.2. Moreover, we remark that the elements appearing in Corollary 5.2.9 have corresponding 3-manifolds which also satisfy the Turaev-Viro invariant volume conjecture for when $n \notin \{5, 7\}$. In the case when $n \in \{5, 7\}$, the corresponding 3-manifolds satisfy the extended Turaev-Viro invariant volume conjecture.

At the end of Chapter 5, we discuss a method, originally stated in [18, Remark 5.7], to construct cosets of the pure braid group which satisfy the AMU conjecture. The general idea utilizes Artin's normal form for the pure braid group [4]. Artin demonstrates that every

pure braid group of n-strands, denoted by PB_n, can be realized as the semidirect product of a subgroup W_n in PB_n with PB_k where $k < n$. In particular, every element in PB_n may be written as a product $\beta \cdot \omega$ for $\beta \in PB_k$ and $\omega \in W_n$. By a method stated in Section 5.3, we show, for certain β, that any pure braid group element of the form $\beta \cdot \omega$ satisfies the AMU conjecture. In the following statement, the set of elements $\mathcal{P}$ is explicitly defined in Section 5.3; however, they are the collection of pure braids obtained from the links in Theorem 1.2.3 as well as the elements of Corollary 5.2.9.

Corollary 5.3.2. *For a fixed n, let $\beta \in PB_s$ be an element of $\mathcal{P}$ with $n > s$. Now for any $b \in PB_n$ with normal form $b = \beta \cdot \omega$ where $\omega \in W_n$, the corresponding element b in $Mod(\Sigma_{0,n+1})$ satisfies the AMU conjecture.*

Chapter 2

Preliminaries

In this chapter, we will detail relevant material that will be used throughout this work. In Section 2.1, we introduce definitions for the particular version of the Turaev-Viro invariant studied in this dissertation. In Section 2.2, we introduce definitions for the mapping class groups, the statement of the Nielsen-Thurston classification, an introduction to braid groups, and relations between the quantum representations and the Turaev-Viro invariants. Lastly, in Section 2.3, we introduce the shadow theory approach towards studying 3-manifolds as well as the construction of the fundamental shadow links.

2.1 The Turaev-Viro Invariants

In this section, we will recall the basic definitions of the $SO(3)$-version of the Turaev-Viro invariants [21, 57].

For the remainder of this section, we fix an odd $r \geq 3$, and we let $I_r = \{0, 1, \ldots, \frac{r-5}{2}, \frac{r-3}{2}\}$ be the set of non-negative integers less than or equal to $\frac{r-3}{2}$ where the set I_r is commonly referred to as the *coloring set*. As mentioned in Section 1.2, the Turaev-Viro invariant $TV_r(M, q)$ is a real-valued invariant defined on a triangulation of the 3-manifold M which depends on a $2r$-th root of unity q. In order to construct the invariant, we will first need to define additional sets of complex numbers.

Let $q \in \mathbb{C}$ be a root of unity such that q^2 is a primitive root of unity of order r. For an

integer n, we let the *quantum integer* $[n]$ be the number defined by

$$[n] = \frac{q^n - q^{-n}}{q - q^{-1}} = \frac{2\sin\left(\frac{2n\pi}{r}\right)}{2\sin\left(\frac{2\pi}{r}\right)}.$$

Analogous to the factorial for integers, we can also define a *quantum factorial* by $[n]! = \prod_{i=1}^{n}[i]$ where we define $[0]! = 1$. Using the quantum integers, we can build the necessary data set for the invariant.

Definition 2.1.1. We say that a triple $(i, j, k) \in I_r^3$ is *admissible* if

- $i + j + k \leq (r - 2)$,
- $i \leq j + k$, $j \leq i + k$, and $k \leq i + j$.

Given an admissible triple $(i, j, k) \in I_r^3$, we define the number $\Delta(i, j, k)$ by

$$\Delta(i, j, k) = \left(\frac{[i + j - k]![j + k - i]![k + i - j]!}{[i + j + k + 1]!}\right)^{\frac{1}{2}}$$

with the convention that $\sqrt{x} = \sqrt{|x|}\sqrt{-1}$ when the real number x is negative.

Additionally, we say that a 6-tuple $(i, j, k, l, m, n) \in I_r^6$ is *admissible* if each of the triples (i, j, k), (j, l, n), (i, m, n), and (k, l, m) are admissible.

Definition 2.1.2. For a given admissible 6-tuple $(i, j, k, l, m, n) \in I_r^6$, we define the *quantum* $6j$*-symbol* by

$$\left|\begin{array}{ccc} i & j & k \\ l & m & n \end{array}\right| = \left(\sqrt{-1}\right)^{2(i+j+k+l+m+n)} \Delta(i, j, k)\Delta(j, l, n)\Delta(i, m, n)\Delta(k, l, m)$$
$$\sum_{z=\max\{T_1,T_2,T_3,T_4\}}^{\min\{Q_1,Q_2,Q_3\}} \frac{(-1)^z\,[z + 1]!}{[z - T_1]![z - T_2]![z - T_3]![z - T_4]![Q_1 - z]![Q_2 - z]![Q_3 - z]!}$$

where $T_1 = i + j + k$, $T_2 = j + l + n$, $T_3 = i + m + n$, $T_4 = k + l + m$, $Q_1 = i + j + l + m$, $Q_2 = i + k + l + n$, and $Q_3 = j + k + m + n$. Furthermore, the quantum $6j$-symbol has the

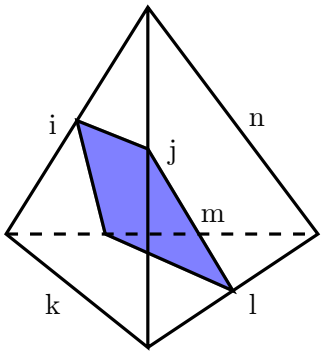

Figure 2.1: The correspondence of an admissible colored tetrahedron to the quantum $6j$-symbol. The edges of the tetrahedron are labeled by the 6-tuple (i, j, k, l, m, n), and the blue shaded region is a quadrilateral which corresponds to Q_1.

following symmetry relations

$$\left|\begin{array}{ccc} i & j & k \\ l & m & n \end{array}\right| = \left|\begin{array}{ccc} j & i & k \\ m & l & n \end{array}\right| = \left|\begin{array}{ccc} i & k & j \\ l & n & m \end{array}\right| = \left|\begin{array}{ccc} i & m & n \\ l & j & k \end{array}\right| = \left|\begin{array}{ccc} l & m & k \\ i & j & n \end{array}\right| = \left|\begin{array}{ccc} l & j & n \\ i & m & k \end{array}\right|.$$

Although the definition of the quantum $6j$-symbol is quite complicated, it is easier to memorize using the geometric association described in Definition 2.1.3.

Definition 2.1.3. An *admissible coloring* of a tetrahedron is an assignment, or *coloring*, of the six colors of an admissible 6-tuple $(i, j, k, l, m, n) \in I_r^6$ to the edges of the tetrahedron such that the three colorings assigned to the edges of each face form the corresponding admissible triples of the admissible 6-tuple.

As a memory aid, we will construct an admissible coloring of a tetrahedron from a given admissible 6-tuple (i, j, k, l, m, n). We begin by coloring the edges of an arbitrary face of the tetrahedron with i, j, and k, and we also color the edges on the opposite sides of i, j, and k with l, m, and n, respectively. Now each of the T_1, T_2, T_3, and T_4 corresponds to a face of the tetrahedron, and each of the Q_1, Q_2, and Q_3 corresponds to a quadrilateral separating two pairs of vertices of the tetrahedron. This labeling can be seen in Figure 2.1 where the blue shaded area is a quadrilateral which corresponds to Q_1. Notice that for a given admissible

coloring of a tetrahedron, there are multiple associated quantum $6j$-symbols which accounts for the symmetry relations.

Lastly, in order to define our invariant, we need a triangulation of our manifold M. If M is a closed manifold, we consider triangulations in the usual sense where a triangulation is a finite collection of tetrahedra and a collection of homeomorphisms between pairs of faces such that the space obtained from gluing along the homeomorphisms is homeomorphic to M.

For compact manifolds M with boundary, we allow (partially) ideal triangulations where some of the vertices are truncated such that the truncated faces triangulate the boundary of M by triangles. When defining the invariant on a triangulation of M, we will need to additionally consider the sets V and E. The set V is the collection of vertices not lying on ∂M, and the set E are the collection of edges of the triangulation excluding the edges coming from the truncation of the vertices.

Definition 2.1.4. For a triangulation τ of a manifold M, an *admissible coloring c at level r* of the pair (M, τ) is an assignment of colors by c to the edges of τ such that each tetrahedron has an admissible coloring. Furthermore, we will consider $A_r(\tau)$ to be the set of all possible admissible colorings at level r.

Now for a given coloring c at level r of the pair (M, τ), an edge $e \in E$, and a tetrahedron $\Delta \in \tau$, we consider the numbers

$$|e|_c = (-1)^{2c(e)} [2c(e) + 1]$$

and $|\Delta|_c$ where $|\Delta|_c$ is the quantum $6j$-symbol associated to the admissible coloring of the tetrahedron Δ obtained by the assignment of c.

We are now ready to define the Turaev-Viro invariant as a state-sum.

Theorem 2.1.5 ([57])**.** *Let M be a compact and orientable manifold that is either closed or with boundary. Let b_2 and b_0 denote the $\mathbb{Z}_2$-Betti number and the number of closed connected*

components in M, respectively. Then for $\eta_r = \frac{2\sin\left(\frac{2\pi}{r}\right)}{\sqrt{r}}$, the following state-sum

$$TV_r(M,q) = 2^{b_2-b_0}\eta_r^{2|V|}\sum_{c\in A_r(\tau)}\left[\left(\prod_{e\in E}|e|_c\right)\left(\prod_{\Delta\in\tau}|\Delta|_c\right)\right]$$

is a topological invariant independent of the partially ideal triangulation.

Now lastly, we will end the section with two propositions both appearing in [19] by Detcherry and Kalfagianni which relate to the changes of the asymptotics of the Turaev-Viro invariant under the drilling and gluing of tori.

Proposition 2.1.6 ([19], Corollary 5.3)**.** *Let M' be a compact and oriented 3-manifold with (possibly empty) toroidal boundary, and let M be a manifold obtained from M' by drilling out tori. Then*

$$lTV(M') \leq lTV(M)$$

where

$$lTV(M) = \liminf_{r\to\infty}\frac{2\pi}{r}\log|TV_r(M,q)|$$

for r running over odd integers and $q = \exp\left(\frac{2\pi\sqrt{-1}}{r}\right)$.

Proposition 2.1.6 states that drilling out tori from our manifold does not decrease the growth rate of the Turaev-Viro invariants. This will be a particularly useful property when dealing with the AMU conjecture in Chapter 5.

Now for the second proposition, we will first define a family of manifolds known as the invertible cabling spaces. Although the invertible cabling spaces have a more general definition [19, Definition 8.3], we will only be concerned with the one provided.

Definition 2.1.7. We define an *invertible cabling space* T_p to be the complement in the solid torus of $p \geq 2$ parallel copies of the core. Here, we note that there is a distinguished outer boundary component arising from the original solid torus.

A key property of the invertible cabling spaces is that they all have simplicial volume zero. As the following proposition states, gluings of these manifolds will preserve the extended Turaev-Viro invariant volume conjecture.

Proposition 2.1.8 ([19], Corollary 8.4)**.** *Let M be a 3-manifold with toroidal boundary such that the extended Turaev-Viro invariant volume conjecture holds, and let T_p be an invertible cabling space with distinguished torus boundary T. Now the manifold M' obtained by gluing a component of $\partial(T_p)\backslash T$ to a component of ∂M satisfies the extended Turaev-Viro invariant volume conjecture such that*

$$\lim_{r\to\infty} \frac{2\pi}{r} \log |TV_r(M,q)| = \lim_{r\to\infty} \frac{2\pi}{r} \log |TV_r(M',q)| = v_4\|M\| = v_4\|M'\|$$

where r runs over the odd integers and $q = \exp\left(\frac{2\pi\sqrt{-1}}{r}\right)$.

Given a manifold which satisfies the extended Turaev-Viro invariant volume conjecture, Proposition 2.1.8 may be used to generate additional examples satisfying the conjecture. We will see an application of this using Theorem 5.2.5 towards both the extended Turaev-Viro invariant volume conjecture and the AMU conjecture.

2.2 Surface Mapping Class Groups

In this section, we will introduce the necessary definitions and concepts from surface mapping class groups. Although the mapping class groups for surfaces can be defined for non-compact surfaces, we will mostly be concerned with the compact and oriented case with the exception of the once-punctured torus.

Definition 2.2.1. For a compact and oriented surface $\Sigma_{g,n}$ of genus g with n removed open disks, we define the *mapping class group of* $\Sigma_{g,n}$, denoted by $Mod(\Sigma_{g,n})$, to be the group of isotopy classes of orientation-preserving homeomorphisms of $\Sigma_{g,n}$ that fix the boundary

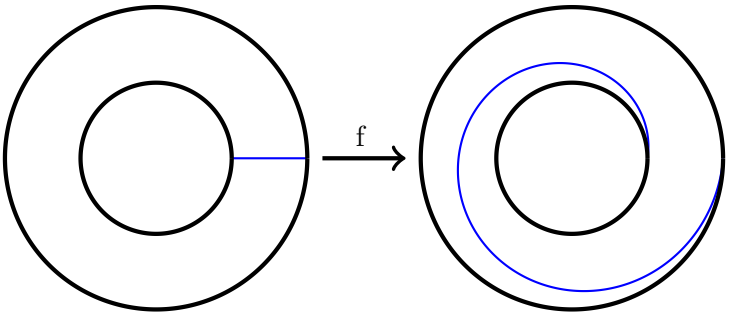

Figure 2.2: The image of the blue curve under a Dehn twist of the annulus.

components where the group operation is composition of homeomorphisms. Additionally, elements of $Mod(\Sigma_{g,n})$ are called *mapping classes*.

Example 2.2.2. As a quick introductory example, we consider the mapping class group of the sphere $\Sigma_{0,0}$. Notice that any self-homeomorphism of $\Sigma_{0,0}$ may be isotoped to fix a single point $x \in \Sigma_{0,0}$. We may identify the space $\Sigma_{0,0} \backslash \{x\}$ with the plane $\mathbb{R}^2$. In $\mathbb{R}^2$, every homeomorphism may be isotoped to the identity by considering the straight line homotopy, therefore, every self-homeomorphism of $\Sigma_{0,0}$ is isotopic to the identity map. This implies that $Mod(\Sigma_{0,0})$ is isomorphic to the trivial group.

In order to understand more complicated examples, it is useful to consider the mapping class group of the annulus $\Sigma_{0,2}$.

Definition 2.2.3. For an annulus $A = S^1 \times [0,1]$ where we identify S^1 as a circle of radius 1 about the origin in $\mathbb{C}$, we define a *Dehn twist* to be the self-homeomorphism

$$f : S^1 \times [0,1] \to S^1 \times [0,1]$$

such that $f\left(\exp\left(\pi\sqrt{-1}\theta\right), t\right) = \left(\exp\left(\pi\sqrt{-1}\left(\theta + 2\pi t\right)\right), t\right)$. See Figure 2.2 for an illustration of the Dehn Twist.

Now the Dehn twist of the annulus generates the mapping class group with $Mod(\Sigma_{0,2}) = \langle [f] \rangle \cong \mathbb{Z}$.

Remark 2.2.4. In general, every surface contains an annulus where we can perform a Dehn twist. Oftentimes, we describe the annulus by a curve on the surface which is its core. The Dehn twists are particularly useful because they can be used to generate the mapping class group of surfaces. In this work, an important example is the mapping class group of the once-punctured torus which we cover in Chapter 3. The surface is not compact; however, we can treat the mapping class group of the once-punctured torus as the mapping class group of the one-holed torus where we define a Dehn twist t_δ on a curve δ parallel to the boundary to be trivial. In this case, the mapping class group is generated by Dehn twists along the meridian curve α and the longitude curve β. Additionally, the mapping class group is isomorphic to the group $SL_2(\mathbb{Z})$ with

$$t_\alpha \to \begin{bmatrix} 1 & 1 \\ 0 & 1 \end{bmatrix}$$

and

$$t_\beta \to \begin{bmatrix} 1 & 0 \\ -1 & 1 \end{bmatrix}$$

where t_α and t_β are the Dehn twists along the curves α and β, respectively. As a supplementary remark, the trivial Dehn twist t_δ can be realized as $(t_\alpha t_\beta)^6$. This can be seen as the identity matrix under the identification with $SL_2(\mathbb{Z})$.

2.2.1 The Nielsen-Thurston Classification

In this subsection, we give a brief introduction into the Nielsen-Thurston classification which, as the name suggests, classifies the elements of the surface mapping class groups.

Definition 2.2.5. We consider three characterizations of elements in $Mod(\Sigma_{g,n})$.

i. An element $f \in Mod(\Sigma_{g,n})$ is *periodic* if there exists some power of f which is isotopic to the identity.

ii. An element $f \in Mod(\Sigma_{g,n})$ is reducible if there exists a finite nonempty set of simple closed curves in $\Sigma_{g,n}$ which are fixed under f. In this case, we may cut our surface $\Sigma_{g,n}$ along the collection of simple closed curves, and we can consider the induced self-homeomorphisms on the resulting parts.

iii. An element $f \in Mod(\Sigma_{g,n})$ is pseudo-Anosov if it has infinite order and is not reducible.

As stated in the following theorem, we see that the three characterizations of the elements in the surface mapping class groups are a complete classification.

Theorem 2.2.6 (Nielsen-Thurston classification)**.** *For any $g, n \geq 0$, each $f \in Mod(\Sigma_{g,n})$ is either periodic, reducible, or pseudo-Anosov.*

An important motivation for the Nielsen-Thurston classification is the relationship with the geometric structures of the following family of 3-manifolds.

Definition 2.2.7. For any $f \in Mod(\Sigma_{g,n})$, we consider the *mapping torus* $M(f)$ to be the 3-manifold defined as

$$M(f) = \Sigma_{g,n} \times [0,1]/(x,0) \sim (f(x),1)$$

where f is called the *monodromy* of $M(f)$.

In [55], Thurston showed the following deep connection between the Nielsen-Thurston classification of surface mapping class groups and the geometric structures of the mapping torus.

Theorem 2.2.8 ([55])**.** *An element $f \in Mod(\Sigma_{g,n})$ is pseudo-Anosov if and only if the mapping torus $M(f)$ is hyperbolic.*

2.2.2 Braid Groups

In this subsection, we introduce briefly the braid groups as well as their relationship with the surface mapping class groups. For a more comprehensive survey, one may refer to [23, Chapter 9] by Farb and Margalit.

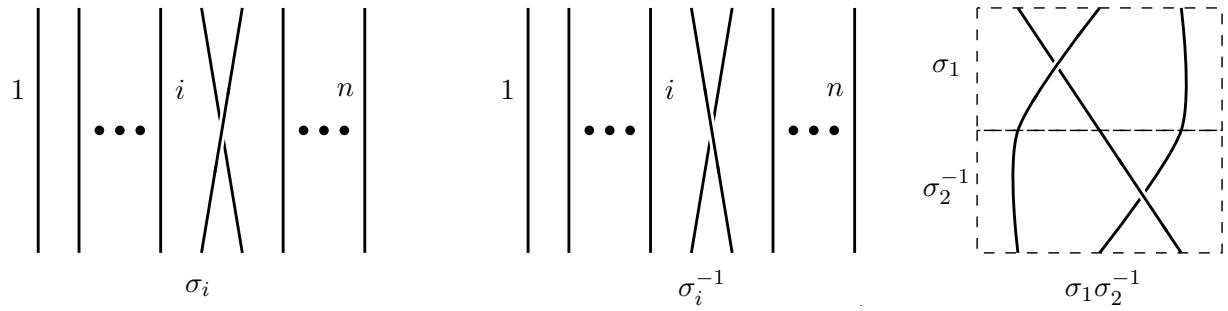

Figure 2.3: For the two leftmost diagrams, we have the generator σ_i and its inverse σ_i^{-1}, respectively, for the braid group B_n where $i \in \{1, \ldots, n-1\}$. On the rightmost diagram, we show the composition with the example $\sigma_1\sigma_2^{-1}$.

The braid group was first rigorously defined by Artin in [4]. There are multiple equivalent ways to define the braid group; however, we will first choose the intuitive definition of braids as a composition of n-strands.

Definition 2.2.9. For a given integer $n \geq 2$, a *braid* of n-strands is a composition by vertical stackings of *standard generators* σ_i for $1 \leq i \leq n-1$ and their inverses σ_i^{-1}. The standard generators, their inverses, and the order of the compositions are shown in Figure 2.3. In the cases for $b \in B_n$ where each strand begins and ends in the same position, we call b a *pure braid*.

Definition 2.2.10. The *braid group* of n-strands, denoted by B_n, is the group of isotopy classes of all n-stranded braids where the group operation is stacking. Similarly, we define the *pure braid group* of n-strands, denoted by PB_n, to be the subgroup of B_n comprised of n-stranded pure braids.

Now for a given $b \in B_n$, we can define two operations on b such that we obtain a link in S^3.

Definition 2.2.11. For $b \in B_n$, we define the *braid closure* of b, denoted by $\hat{b}$, to be the link in S^3 obtained from connecting the endpoints of the strands as in the left diagram of Figure 2.4. Additionally, we may define a *braided link*, denoted by $\overline{b}$, to be the link in S^3 obtained from the braid closure with the addition of an unknotted component which bounds an n-punctured disk called the *braid axis* as shown on the right diagram of Figure 2.4.

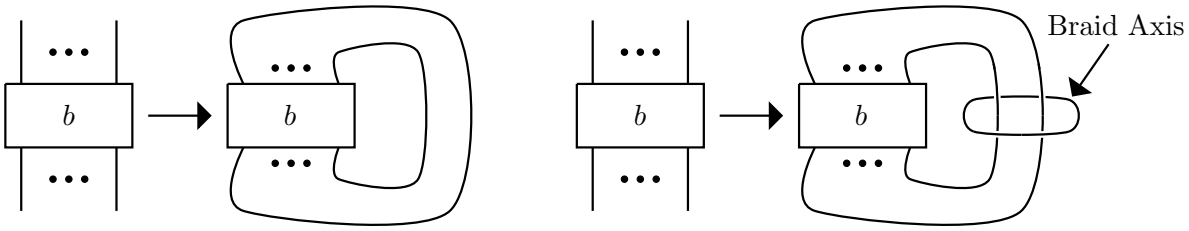

Figure 2.4: On the left diagram, we show the braid closure of an arbitrary braid $b \in B_n$. On the right diagram, we show the diagram of the associated braided link where we labeled the braid axis.

The braided links will be of particular use to us in this work. Our braided links in S^3 will always fiber over S^1 where the fiber surface is the n-punctured disk bounded by the braid axis. We will see that this is closely related to the mapping class group of a genus zero surface which we will utilize in finding elements which satisfy the AMU conjecture.

Definition 2.2.12. For a surface with punctures Σ, we will define $MCG(\Sigma)$ to be the group of isotopy classes of orientation-preserving self-homeomorphisms of Σ where the group operation is composition of homeomorphisms.

Now for a given n, there exists a surjective homomorphism Γ from the braid group of n-strands to the mapping class group of the n-punctured disk $MCG(D_n)$ such that

$$\Gamma : B_n \to MCG(D_n).$$

This map can be defined explicitly as sending the standard generators $\sigma_i \in B_n$, for $i \in \{1, \ldots, n-1\}$, to a positive half-twist on an arc between the i-th puncture to the $(i+1)$-th puncture of D_n. Furthermore, the kernel of the map Γ is generated by the element $(\sigma_1\sigma_2 \ldots \sigma_{n-1})^n$ which corresponds to a full-twist along the boundary of D_n.

For a given $\Gamma(b) \in MCG(D_n)$, we can construct the associated mapping torus $M(\Gamma(b)) = D_n \times [0,1]/(x,0) \sim (\Gamma(b)(x),1)$ with monodromy $\Gamma(b)$. This mapping torus is homeomorphic to the complement of the braided link $\overline{b}$. Now from our setup, we can note that every braid $b \in B_n$ corresponds to a braided link $\overline{b}$ which, up to homeomorphism, can be realized as the

mapping torus $M(\Gamma(b))$ with monodromy $\Gamma(b)$.

Lastly, we may use this correspondence with the pure braid group to study the mapping tori for genus zero surfaces with boundary. By replacing the boundary of D_n by an additional puncture, we induce an injective homomorphism from $MCG(D_n)$ to $MCG(S^2_{n+1})$ where S^2_{n+1} is the $(n+1)$-punctured sphere. Under this homomorphism, we may identify every element of $MCG(D_n)$ as an element in $MCG(S^2_{n+1})$. Now consider the case for an element b in the pure braid group PB_n. The element $\Gamma(b) \in MCG(D_n)$ fixes the n punctured points of D_n which corresponds to fixing the associated punctures in S^2_{n+1}. Because of this, we may also realize the element $\Gamma(b)$ as an element in $Mod(\Sigma_{0,n+1})$ in which we defined the boundary components to be fixed. From the induced injective homomorphism, the complement of the mapping torus $M(\Gamma(b))$ is homeomorphic to the mapping torus of the corresponding element in $Mod(\Sigma_{0,n+1})$. Since our mapping torus $M(\Gamma(b))$ may be understood in terms of the braided link $\overline{b}$, we can similarly approach the corresponding mapping torus of $Mod(\Sigma_{0,n+1})$ with the complement of the braided link.

2.2.3 Quantum Representations and the Turaev-Viro Invariants

In this subsection, we will write necessary properties of the quantum representations. In particular, we will see that the quantum representations of a surface mapping class group are closely related to the Turaev-Viro invariants of the corresponding mapping tori. Because of this connection, it can be shown that the Turaev-Viro invariant volume conjecture implies the AMU conjecture.

As noted in Section 1.3, for a given surface $\Sigma_{g,n}$, an odd $r \geq 3$, and a coloring c of $\partial(\Sigma_{g,n})$ by elements in $I_r = \{0, 1, \ldots, \frac{r-5}{2}, \frac{r-3}{2}\}$, we have an associated $SO(3)$ quantum representation

$$\rho_{r,c} : Mod(\Sigma_{g,n}) \to \mathrm{PGL}_{d_{r,c}}(\mathbb{C}).$$

Although it is not focused on in this work, we will briefly mention that the traces of the

individual quantum representations themselves are significant in that they are related to another well-known quantum invariant. We denote the *Reshetikhin-Turaev invariant* for closed manifolds with an embedded colored link (L, c) by $RT_r(M, (L, c))$ where c is a coloring of the components of L with elements of I_r. For more information on the Reshetikhin-Turaev invariant, one may refer to [9, 48]. Now the traces of the quantum representations of the mapping class groups are related to the Reshetikhin-Turaev invariant in the following way.

Theorem 2.2.13 ([10]). *For $r \geq 3$ and odd, let $\Sigma_{g,n}$ be a compact and oriented surface with a coloring of the boundary from elements of I_r. Define $\overline{\Sigma_{g,n}}$ to be the surface obtained from $\Sigma_{g,n}$ by capping the components of $\partial\Sigma_{g,n}$ by disks. For $f \in Mod(\Sigma_{g,n})$, let $\overline{f} \in Mod(\overline{\Sigma_{g,n}})$ be the mapping class group element of the extension of f from capping the disks by the identity. Now let $L \subset M(\overline{f})$ whose components consists of the cores of the tori in $M(\overline{f})$ arising from the capping disks on the surface. Then*

$$Tr(\rho_{r,c}(f)) = RT_r(M(\overline{f}), (L, c))$$

where $Tr(\rho_{r,c}(f))$ is the trace of the quantum representation.

From Theorem 2.2.13, we can see that we can study quantum invariants through the traces of the quantum representations. Although we omit the details here, the Reshetikhin-Turaev invariant for closed manifolds are part of a larger set of compatible invariants for compact 3-manifolds known as a TQFT [9, 10]. In this sense, the Reshetikhin-Turaev invariant may be defined for manifolds M with toroidal boundary; however, in these cases, $RT_r(M)$ is a vector.

Now the Turaev-Viro invariant can be recovered from the Reshetikhin-Turaev invariant which was originally shown for closed 3-manifolds by Roberts in [49] and extended to manifolds with boundary by Benedetti and Petronio in [8]. Although Benedetti and Petronio state their result for the $SU(2)$-version of the Turaev-Viro invariant, Detcherry and Kalfagianni adapt the proof in the setting of the $SO(3)$-version in [21]. The relation is as follows.

Theorem 2.2.14 ([8], Theorem 3.2)**.** *Fix $r \geq 3$ and odd. For M an oriented and compact 3-manifold with either empty or toroidal boundary, we have*

$$TV_r(M, e^{\frac{2\pi\sqrt{-1}}{r}}) = \|RT_r(M, e^{\frac{\pi\sqrt{-1}}{r}})\|^2.$$

As a consequence of Theorems 2.2.13 and 2.2.14, we can similarly study the Turaev-Viro invariant in terms of quantum representations. In the proof of Theorem 1.2 in [18], Detcherry and Kalfagianni show the following relation.

Proposition 2.2.15 ([18], Theorem 1.2)**.** *Let $f \in Mod(\Sigma_{g,n})$ and $M(f)$ the mapping torus of f, then*

$$TV_r(M(f), q) = \sum_c |Tr(\rho_{r,c}(f))|^2$$

where c runs over all possible colorings of the boundary components of $\Sigma_{g,n}$ by I_r.

Although our definition of the Turaev-Viro invariant in Section 2.1 follows the original construction, we can equally calculate the invariant in terms of the quantum representations. This is especially advantageous when dealing with the Turaev-Viro invariant of mapping tori. Even though $\rho_{r,c}$ are projective representations, we note that the scaling coefficients are roots of unity such that the magnitude of the trace is well-defined.

We end this subsection by showing that the Turaev-Viro invariant volume conjecture implies the AMU conjecture. This result was first shown by Detcherry and Kalfagianni in [18].

Theorem 2.2.16 ([18], Theorem 1.2)**.** *For a compact and oriented surface $\Sigma_{g,n}$, let f be an element in $Mod(\Sigma_{g,n})$ with pseudo-Anosov parts. For the mapping torus $M(f)$ of the element f, if $lTV(M(f)) > 0$, then f satisfies the AMU conjecture where*

$$lTV(M) = \liminf_{r\to\infty} \frac{2\pi}{r} \log |TV_r(M, q)|$$

for r running over odd integers and $q = e^{\left(\frac{2\pi\sqrt{-1}}{r}\right)}$.

Proof. Let $f \in Mod(\Sigma_{g,n})$ such that it contains pseudo-Anosov parts where we define $M(f)$ to be its corresponding mapping torus. Now suppose that

$$lTV(M) = \liminf_{r\to\infty} \frac{2\pi}{r} \log |TV_r(M,q)| > 0.$$

Therefore, our sequence of Turaev-Viro invariants with respect to r is growing exponentially. Now from [10], it is known that the dimensions of the vector spaces of the quantum representations for these surface mapping class groups grow at most polynomially. By Proposition 2.2.15, we note that

$$TV_r(M(f),q) = \sum_c |Tr(\rho_{r,c}(f))|^2 .$$

Here, the left-hand side grows exponentially with r, and the dimensions of the quantum representations on the right-hand side grow at most polynomially. This implies that for a large enough r, there exists at least one coloring c with quantum representation $\rho_{r,c}(f)$ such that the modulus of $Tr(\rho_{r,c}(f))$ exceeds the dimension of $\rho_{r,c}(f)$.

Now since the modulus of the trace exceeds the dimension, then there must exist at least one eigenvalue whose modulus is strictly larger than 1. This implies that the quantum representation $\rho_{r,c}(f)$ is infinite order which is the conclusion of the AMU conjecture for the given f. □

Notice if $TV_r(M(f),q)$ has exponential growth rate, then $lTV(M(f)) > 0$. This is a more general condition; however, it states that the Turaev-Viro invariant volume conjecture implies the AMU conjecture for mapping tori. Theorem 2.2.16 shows that as long as we can represent our manifold as a mapping torus, we can study the Turaev-Viro invariant volume conjecture and the AMU conjecture simultaneously by looking at the asymptotics of the Turaev-Viro invariant.

Lastly, in conjunction with Theorem 2.2.16, we consider Proposition 2.1.6. Proposition 2.1.6 states that drilling out tori from our manifold does not decrease the growth rate of our Turaev-Viro invariants. Together with Theorem 2.2.16, once we have a mapping torus

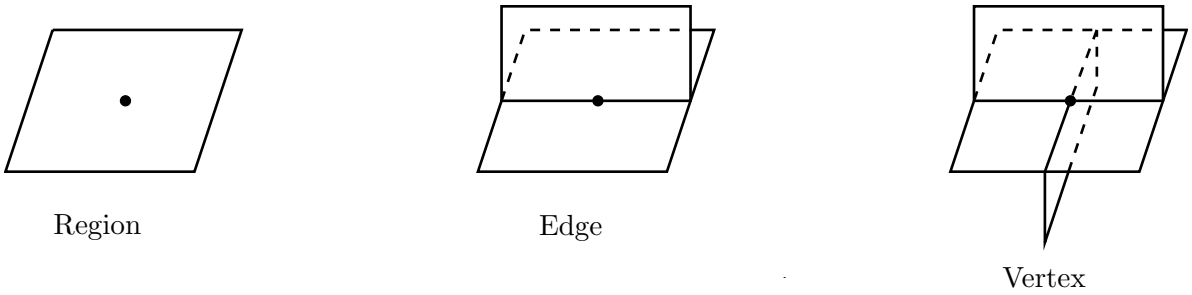

Figure 2.5: The local models of the simple polyhedron.

with exponential growth rate, we can continue to drill out tori to obtain new manifolds with exponential growth rate from which Theorem 2.2.16 applies again. In general, the new manifolds we obtain may not be hyperbolic; however, as we will see in Proposition 5.2.3, it may be clear in certain circumstances which tori we may drill out such that the resulting manifold is a hyperbolic mapping torus. By Theorem 2.2.8, our corresponding element in the mapping class group will be pseudo-Anosov, and we know that it will also satisfy the AMU conjecture.

2.3 Shadows of 3-Manifolds

In this section, we introduce Turaev's shadow theory approach towards 3-manifolds [56]. Briefly, shadows are a way to study 3- and 4-manifolds using 2-dimensional polyhedra endowed with topological data. We will use the theory to construct the family of fundamental shadow links which will have direct applications towards the Turaev-Viro invariant volume conjecture and the AMU conjecture.

We will begin by defining the theory for oriented, closed, and connected 3-manifolds.

Definition 2.3.1. A *simple polyhedron* P is a compact topological space which locally is homeomorphic to one of the models in Figure 2.5. The set of points with local models of the right two types form a graph called the *singular set*, denoted by $Sing(P)$. Additionally, the set of points locally homeomorphic to the third model are known as *vertices*, and the number of vertices of P is called the *complexity* of P. The set of points locally homeomorphic to the

second model are known as *edges*, and we define the *regions* of P to be the set of connected components of $P \backslash Sing(P)$. Lastly, the set of points with local models corresponding to the boundaries of Figure 2.5 are known as the *boundary* of P, denoted by ∂P, and if P has no boundary components, then we say P is *closed*.

Definition 2.3.2. Let W be a piecewise linear, compact, and oriented 4-manifold, and let P be a closed simple polyhedron. We say that $P \subset W$ is a *shadow* of W if the following two conditions are satisfied.

i. W *collapses* onto P as a deformation retract.

ii. Every point x in P has a neighborhood $U_x \subset W$ which can be piecewise-linearly embedded in $\mathbb{R}^4$ such that $U_x \cap P \subset \mathbb{R}^3 \subset \mathbb{R}^4$. This condition will be referred to as $P \subset W$ being *locally flat*.

Definition 2.3.3. A closed simple polyhedron P is a *shadow* of an oriented 3-manifold M if $\partial(W) = M$ where P is the shadow of the 4-manifold W.

Theorem 2.3.4 ([56], Theorem IX.2.1.1)**.** *Every closed, oriented, and connected* 3*-manifold has a shadow.*

We can see from Theorem 2.3.4 that every closed, oriented, and connected 3-manifold has a shadow; however, the simple polyhedron P may not be unique. There could possibly be non-homeomorphic 3-manifolds with the same shadow.

In order to uniquely describe the 3-manifolds with a shadow, we need to endow the shadow with the additional topological information known as the gleam. In this work, we will define the gleam of a region in its simplest case where the closure of the region is embedded in the simple polyhedron; however, one can refer to [56] for a more detailed discussion.

Definition 2.3.5. Let D be an embedded region in P where the closure $\overline{D}$ is embedded with $\partial\overline{D} \subset Sing(P)$, and let $N(D)$ be a regular neighborhood of $\partial\overline{D} \subset P \backslash Int(D)$. We say that the $\mathbb{Z}_2$-gleam of the region D is 1 if $N(D)$ collapses over a Möbius strip, otherwise, the $\mathbb{Z}_2$-gleam is 0.

Definition 2.3.6. We define the *gleam* of a simple polyhedron to be an assignment of $\frac{1}{2}\mathbb{Z}$ to all regions of the polyhedron such that the assignment is an integer if and only if the $\mathbb{Z}_2$-gleam is 0. Now a simple polyhedron equipped with a gleam will be called a *shadowed polyhedron*.

The idea behind the gleam is the following. When we thicken our polyhedron to a 4-manifold, the regions of the polyhedron thicken to copies of $B^2 \times B^2$ where B^2 is a disk. These copies of $B^2 \times B^2$ may be glued to the rest of the thickened polyhedron in different ways resulting in possibly non-homeomorphic manifolds. The gleam of the region is the topological data necessary to convey the gluing information.

Now we will extend our definitions to include shadows for manifolds M containing links where M possibly has toroidal boundary components. In order to achieve this, we will consider *decorations* of the boundary components for non-closed simple polyhedron.

Definition 2.3.7. A *boundary-decorated simple polyhedron* P is a simple polyhedron such that each boundary component is either labeled as *internal*, *external*, or *false*. Respectively, we will denote these subsets as $\partial_{int}(P)$, $\partial_{ext}(P)$, and $\partial_f(P)$.

The intuition behind these labelings can be thought of as follows. We consider the internal labeled boundaries to be components of the link in the manifold, the external labeled boundaries correspond to drilling out solid tori contributing to the toroidal boundary components of the manifold, and the false labeled boundaries are to be ignored.

Now we can define the boundary-decorated simple polyhedron acting as a shadow for the pair (M, L) where M is an oriented 3-manifold, possibly with toroidal boundary components, and L is a link embedded in M.

Definition 2.3.8. For a 4-manifold W with $\partial W = M$, a boundary-decorated simple polyhedron P is a *shadow* for the pair (M, L) if the following three conditions are satisfied.

i. W collapses onto P.

ii. $P \subset W$ is locally flat.

iii. $(M, L) = (\partial W \backslash \text{IntNbd}(\partial_{ext}(P), \partial W), \partial_{int}(P))$ where $\text{IntNbd}(\partial_{ext}(P), \partial W)$ is an interior neighborhood of the subset $\partial_{ext}(P)$ in ∂W.

Similar to before, we need to assign a gleam to the regions of the boundary-decorated simple polyhedron in order to distinguish non-homeomorphic thickenings of the polyhedron.

Definition 2.3.9. For a boundary-decorated simple polyhedron P, an assignment by half-integers of the regions of P which do not touch $\partial_f(P) \cup \partial_{ext}(P)$ is called a *gleam*. A boundary-decorated simple polyhedron equipped with a gleam is called a *boundary-decorated shadowed polyhedron*.

Now in [56], Turaev showed that if a simple polyhedron embedded in a compact oriented smooth 4-manifold W is a shadow of ∂W, then there is an induced gleam of the regions of the polyhedron. Otherwise stated, every shadow P of a manifold M inherits a gleam such that P may be identified with a shadowed polyhedron of M. Conversely, Turaev showed that given a boundary-decorated shadowed polyhedron P, one can construct a compact and oriented 4-manifold W with an embedding of P such that the induced gleam of the embedding corresponds to the initial gleam of P. This correspondence allows us to study 3-manifolds from the viewpoint of the boundary-decorated shadowed polyhedron.

In the following, we will show a general sketch of constructing a 3-manifold from a boundary-decorated shadowed polyhedron. For a more in-depth discussion, one may consult Turaev's proof in [56].

Theorem 2.3.10 ([56], Section IX.6.1)**.** *For a given boundary-decorated shadowed polyhedron P, there exists a pair (W_P, P) such that W_P is a smooth, compact, and oriented 4-manifold, and P is embedded such that P is a boundary-decorated shadowed polyhedron of the 3-manifold ∂W_P. Additionally, the induced gleam of the regions from the embedding coincides with the initial gleam of P.*

Proof. We begin with the case when P is a shadowed polyhedron constructed from a closed simple polyhedron. For when $Sing(P)$ is empty, W_P is simply a 2-disk bundle over P with Euler class equal to the gleam of the region. Now let us consider the case when the singular set $Sing(P)$ is non-empty. We first take a neighborhood of the singular set in P, denoted by $S(P) = Nbd(Sing(P), P)$. The set $S(P)$ can be viewed as a collection of compositions of the edge and vertex local models. We will now proceed to thicken this set to a 3-manifold N such that $S(P)$ is properly embedded in N where the gluing of the components is induced from the shadowed polyhedron P. Next, we further thicken the manifold N to an orientable 4-manifold W_0.

The previous steps explained how to thicken the composition of the edge and vertex local models to a 4-manifold. In the following, we will also thicken the regions of the shadowed polyhedron to a 4-manifold, and we will glue the resulting collections together. We will only consider one region R since adding additional regions follows similarly. As in the W_0 case, we may thicken the region R into a manifold W_R. When R is an orientable surface, $W_R = R \times B^2$ where B^2 is a disk. In order to discuss the gluing of the manifolds W_R and W_0, notice the following. From the intersection of $R \cap \partial(S(P))$, we obtain a simple closed curve C. In the 3-dimensional thickening of the collection R and $S(P)$, the curve C will be either the core of an annulus or a Möbius band. Our topological data of the gleam from P is used as the framing of the core when identifying the components of the annuli and Möbius bands together.

Lastly, we will consider the case when P has boundary. For the results in this work, we will assume that the boundaries are copies of S^1. We let $\{L_i\}$ be the collection of boundary components such that L is their union. We now thicken L to be the framed link $L \times [-1, 1]$ such that $L \times \{0\} = \partial(P)$. This results in a new polyhedron $\overline{P}$ where $Sing(\overline{P}) = Sing(P) \cup \partial(P)$, and we may follow the same construction as before using $Sing(\overline{P})$ to obtain a 3-manifold containing the framed link $L \times [-1, 1]$. Now by repeating the rest of the construction, we end with a 4-manifold W_P such that $L \times [-1, 1] \subset \partial(W_P)$. $\square$

2.3.1 Fundamental Shadow Links

In this subsection, we will construct the fundamental shadow links. The family was originally introduced and discussed by Constantino and Thurston in [15, Section 3.6]. The fundamental shadow links are a family of links in connected sums of $S^2 \times S^1$ with certain advantageous properties. In particular, the Turaev-Viro invariants of the family are relatively simple, and the hyperbolic volumes of the complements are well-understood. These two properties were utilized to prove the following theorem in [7] by Belletti, Detcherry, Kalfagianni, and Yang.

Theorem 2.3.11 ([7], Theorem 1.1)**.** *For any fundamental shadow link L, the link complement of L satisfies the Turaev-Viro invariant volume conjecture.*

Additionally, these links are "universal" in the sense that every orientable 3-manifold with empty or toroidal boundary can be realized as the manifold obtained from Dehn fillings along some subset of the boundary components for the complement of some fundamental shadow link. For the definition of a Dehn filling, see Subsection 4.1.3. As a consequence, it may be possible to prove the Turaev-Viro invariant volume conjecture by showing that the conjecture is preserved under Dehn fillings of the boundary tori for the complements of the fundamental shadow links.

Now as discussed in Subsection 1.2.2, the Turaev-Viro invariant volume conjecture is preserved under homeomorphisms. This implies that if two manifolds are homeomorphic where ones satisfies the Turaev-Viro invariant volume conjecture, then both manifolds satisfy the conjecture. This will be our main motivation in considering the fundamental shadow link complements.

In order to construct this family, we will be using Theorem 2.3.10 on a particular family of boundary-decorated shadowed polyhedron. We will begin by considering a closed simple polyhedron P which contains at least one vertex in the singular set $Sing(P)$ where $Sing(P)$ is also connected. Now let $S(P)$ be a regular neighborhood of $Sing(P)$ in P such that $S(P)$ can be viewed as a composition of the edge and vertex local models. From $S(P)$, we define

P' to be the boundary-decorated shadowed polyhedron such that $S(P)$ is the 2-dimensional simple polyhedron with the boundary components of P' decorated as external boundaries.

We will now build a 3-manifold $M_{P'}$ with boundary by applying Theorem 2.3.10 on P'. We can better understand the manifold $M_{P'}$ by studying the equipped collapsing map $\pi : M_{P'} \to P'$ obtained from the construction. As shown in Proposition 3.32 from [15], the preimages of the edge local models will be a product of a pair of pants with $[-1, 1]$, and the preimages of the vertex local models are genus 3 handlebodies. The components glue along pairs of pants, and the resulting manifold $M_{P'}$ has boundary a union of tori. In Subsection 2.3.2, we will show an explicit representation of the manifold in terms of the complement of a surgery presentation of a link.

Now in the following, we can see that the manifold $M_{P'}$ has a decomposition into regular ideal hyperbolic octahedra, therefore, an explicit hyperbolic volume.

Proposition 2.3.12 ([15], Proposition 3.33)**.** *For a given P' as above, the manifold $M_{P'}$ can be equipped with a complete hyperbolic metric with volume $2kv_8$. Here, k is the number of vertices of P', and $v_8 \approx 3.6639$ is the volume of a regular ideal hyperbolic octahedron.*

Moreover, the manifold $M_{P'}$ can be realized as the complement of a link embedded in connected sums of $S^2 \times S^1$. This can be achieved using the same simple polyhedron $S(P)$; however, instead of decorating the boundary components as external boundaries, we choose to decorate the boundary components as internal boundaries.

Definition 2.3.13. Let P'' be the boundary-decorated shadowed polyhedron with simple polyhedron $S(P)$ of complexity k and with boundary components decorated as internal boundaries. Using Theorem 2.3.10, the 4-manifold $W_{P''}$ obtained from P'' corresponds to the pair

$$(M_{P''}, L_{P''}) = (\partial(W_{P''}), \partial_{int}(P'')) = (\#^{k+1}(S^2 \times S^1), L_{P''}).$$

These pairs of links and 3-manifolds are known as the *fundamental shadow links*. In addition, the 3-manifold $M_{P'}$ is homeomorphic to the link complement of $L_{P''}$ in the manifold $M_{P''}$.

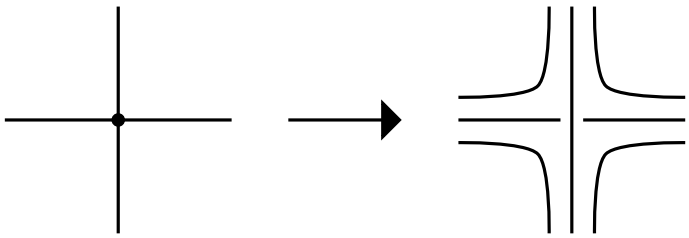

Vertex

Figure 2.6: The procedure to replace the vertices of the graph.

2.3.2 Planar Graph Constructions of Fundamental Shadow Links

Although the fundamental shadow links can be constructed using boundary-decorated shadowed polyhedron, it is more intuitive to build them from planar 4-valent graphs. In particular, the fundamental shadow links of complexity k can be defined in terms of 0-surgeries on a set of $(k+1)$ unknotted link components of a link in S^3 obtained from the planar 4-valent graphs. For a brief summary of a 0-surgery on a link component, see Subsection 4.1.3.

Before we begin, we will first define the following.

Definition 2.3.14. We define a *planar 4-valent graph* G to be a connected graph embedded on the plane in S^3 such that each vertex is incident to 4 edges where loops are edges which are counted twice. Additionally, the *complexity* of G is the number of vertices of the graph.

Definition 2.3.15. For a graph G, a *tree* is a connected subgraph without any cycles. Furthermore, a *maximal tree* is a tree with a maximal set of edges, or equivalently, a tree which includes all vertices of G.

We will now state the construction which was first discussed as Proposition 3.35 in [15] and written explicitly in terms of the planar 4-valent graphs in [14, Section 2.3].

- Let G be a planar 4-valent graph of complexity k embedded in S^3, and let T be a maximal tree of the graph G.
- We replace each edge of G by any 3-braid, and we replace each vertex of G by the 6 strands in Figure 2.6 or its mirror.

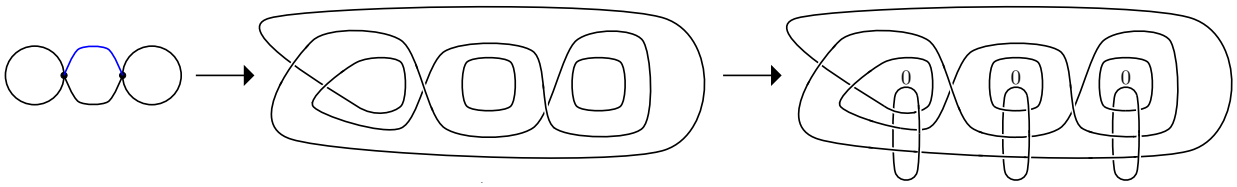

Figure 2.7: An example of constructing a fundamental shadow link from a planar 4-valent graph G. On the left, we begin with a planar 4-valent graph of complexity 2 where the maximal tree T is colored blue. We obtain the middle illustration by replacing the edges and vertices by 3-braids and the 6 strands described in Figure 2.6, respectively. The right illustration is obtained by encircling the 3-braids corresponding to the edges $G\backslash T$ by 0-framed unknotted components.

- Next, for each 3-braid corresponding to an edge of $G\backslash T$, we encircle the 3-braid by a 0-framed unknotted component.

- Lastly, the union of the 3-braids, the 6 strands obtained from Figure 2.6, and the 0-framed unknotted link give a surgery presentation in S^3 of a fundamental shadow link.

As in the case of the boundary-decorated shadowed polyhedron, the hyperbolic volume of the resulting fundamental shadow link from a graph of complexity k is given by $2kv_8$.

In Figure 2.7, we provide an explicit example of constructing a fundamental shadow link given a graph G of complexity 2. In this case, our maximal tree consists of a single edge which is colored blue in the leftmost diagram of Figure 2.7. Shown in the middle diagram of Figure 2.7, we decide to replace three of the four edges with the identity 3-braid and the fourth edge with a non-trivial 3-braid. On the rightmost diagram of Figure 2.7, we encircle by 0-framed unknotted components the 3-braid components which correspond to $G\backslash T$.

Remark 2.3.16. For a given planar 4-valent graph G, we have multiple choices of 3-braids for each edge of the graph. The choice of 3-braids may result in different non-homeomorphic fundamental shadow link complements such that the graph G does not have a unique associated fundamental shadow link. However, it is to be noted that 3-braids which induce the same permutation on the 3-strands result in homeomorphic fundamental shadow link

complements. Therefore, there are only finitely many fundamental shadow links for each given complexity k. Because there are only finitely many hyperbolic manifolds of the same given volume [54, Chapters 5 and 6], this is consistent with the fact that the fundamental shadow links are hyperbolic links.

Remark 2.3.17. From the viewpoint of constructing a fundamental shadow link from a boundary-decorated shadowed polyhedron, we can see that the strands of the 3-braids are the boundary of a simple polyhedron $S(P)$. For the simple polyhedron $S(P)$, the singular set $Sing(P)$ is the planar 4-valent graph. It is from this correspondence that we obtain the planar 4-valent graph construction from the boundary-decorated shadowed polyhedron construction.

Chapter 3

The Turaev-Viro Invariants for Once-Punctured Torus Bundles

In this chapter, we define a closed formula for the Turaev-Viro invariants of hyperbolic once-punctured torus bundles which depends, in a trivial way, on the monodromy. Additionally, we introduce a conjecture which relates the Turaev-Viro invariants of the mapping torus to the stretch factor of the corresponding pseudo-Anosov element in the mapping class group.

3.1 Background

In this section, we introduce the canonical triangulations for hyperbolic once-punctured torus bundles.

3.1.1 Canonical Triangulations

For a reference, see [24] by Floyd and Hatcher as well as [25, Section 3] by Futer and Guéritaud. Given a pseudo-Anosov element in the mapping class group of the once-punctured torus, we will highlight the construction of the canonical triangulation for the corresponding mapping torus.

From the isomorphism between $Mod(\Sigma_1^1)$ and $SL_2(\mathbb{Z})$ described in Section 2.2, we define the following matrices

$$R = \begin{bmatrix} 1 & 1 \\ 0 & 1 \end{bmatrix}$$

and

$$L = \begin{bmatrix} 1 & 0 \\ 1 & 1 \end{bmatrix}.$$

Now consider the following well-known proposition. For a sketch of the proof, we refer to [25, Proposition 2.1].

Proposition 3.1.1. *Let ϕ be an element in $SL_2(\mathbb{Z})$ with two distinct positive eigenvalues. Then the conjugacy class of $\phi \in SL_2(\mathbb{Z})$ contains an element of the form*

$$R^{N_1}L^{N_2}R^{N_3}L^{N_4}\dots R^{N_{2n-1}}L^{N_{2n}}$$

where $n, N_i > 0$ for all i. Conversely, any product of such form is an element in $SL_2(\mathbb{Z})$ with two distinct positive eigenvalues.

Since mapping tori constructed with conjugate monodromies are homeomorphic, we may always consider our element in the mapping class group to be represented in this form. We now begin with an arbitrary matrix

$$R^{N_1}L^{N_2}R^{N_3}L^{N_4}\dots R^{N_{2n-1}}L^{N_{2n}} = \begin{bmatrix} a & b \\ c & d \end{bmatrix}.$$

From the given monodromy, we consider the following vectors

$$\begin{bmatrix} a \\ c \end{bmatrix}, \quad \begin{bmatrix} b \\ d \end{bmatrix}, \quad \text{and} \quad \begin{bmatrix} a+b \\ c+d \end{bmatrix}.$$

When viewing the once-punctured torus Σ_1^1 as the quotient of the space $\mathbb{R}^2\backslash\mathbb{Z}^2$, we can form a triangulation of the space by lines connecting the punctures where the slopes of the lines are the rational slopes of the vectors. Now note that when we multiply our monodromy on the right by either R or L, one of the corresponding vectors will be fixed by either the

column

$$\begin{bmatrix} 1 \\ 0 \end{bmatrix}$$

of R or the column

$$\begin{bmatrix} 0 \\ 1 \end{bmatrix}$$

of L. This implies that after multiplication, we will have a new triangulation of Σ_1^1 using the slopes associated to the fixed vector, the vector

$$\begin{bmatrix} a+b \\ c+d \end{bmatrix},$$

and a new vector which is the sum of the other two vectors. Because of this, the new triangulation will always switch exactly one edge. This principle will be known as a *diagonal exchange*.

Now given a sequence of triangulations of Σ_1^1 related by diagonal exchanges, we can form a collection of ideal tetrahedra in the sense that the vertices are removed by the puncture in the triangulation of Σ_1^1. This is obtained by considering the 2-dimensional triangulation formed by pairwise gluing edges with identical slopes from two consecutive triangulations of Σ_1^1. The resultant figure will bound our desired tetrahedron where two opposite pairs of edges are identified together. The remaining two edges which are not identified correspond to the diagonal exchange.

Now lastly, our collection of tetrahedra are stacked on top of each other from the previous gluings such that the bottommost and topmost triangulations of Σ_1^1 are unaffected. These final two triangulations are glued together by the self-homeomorphism from the mapping class group. The resulting 3-dimensional triangulation is homeomorphic to the mapping torus obtained from the corresponding mapping class group element.

3.2 A Closed Formula for the Turaev-Viro Invariants

In this section, we calculate a closed formula for the Turaev-Viro invariants of the hyperbolic once-punctured torus bundles as well as compute explicit examples. This will be achieved by considering the canonical triangulations of the manifolds along with the original definition of the Turaev-Viro invariant stated in Section 2.1.

As mentioned in Subsection 3.1.1, for a given monodromy which is pseudo-Anosov, we can construct a triangulation of the manifold through diagonal exchanges. Now notice the following. Every tetrahedron of the manifold is constructed from a diagonal exchange on a triangulation of the once-punctured torus where each diagonal exchange corresponds to either the element R or L. Because of this, for a given monodromy $\phi = R^{N_1}L^{N_2}\cdots R^{N_{2n-1}}L^{N_{2n}}$ in $Mod(\Sigma_1^1)$, the number of tetrahedra for the mapping torus $M(\phi)$ is $N = \left(\sum_{i=1}^{2n} N_i\right)$. On the triangulations of the once-punctured torus, we have two pairs of opposite sides that are identified, and the sides corresponding to the diagonal exchange will be opposite of each other on the formed tetrahedron. Therefore, every $6j$-symbol is of the following form.

$$E_1 = \begin{vmatrix} a_1 & a_2 & a_3 \\ a_4 & a_2 & a_3 \end{vmatrix}, \quad E_2 = \begin{vmatrix} a_1 & a_2 & a_3 \\ a_1 & a_4 & a_3 \end{vmatrix}, \quad \text{or } E_3 = \begin{vmatrix} a_1 & a_2 & a_3 \\ a_1 & a_2 & a_4 \end{vmatrix}$$

where E_i is the $6j$-symbol such that the side opposite of the side associated to the color a_i is the side of the diagonal exchange. In this case, we chose to color the new side obtained from the diagonal exchange with a_4. For an illustration of the triangulation of the once-punctured torus bundles, see Figure 3.1 where we demonstrate the first tetrahedron obtained from the diagonal exchanges. In this example, as the quotient of $\mathbb{R}^2\backslash\mathbb{Z}^2$, the once-punctured torus may be triangulated by edges with slopes 1, 0, and ∞, shown on the leftmost diagram, which

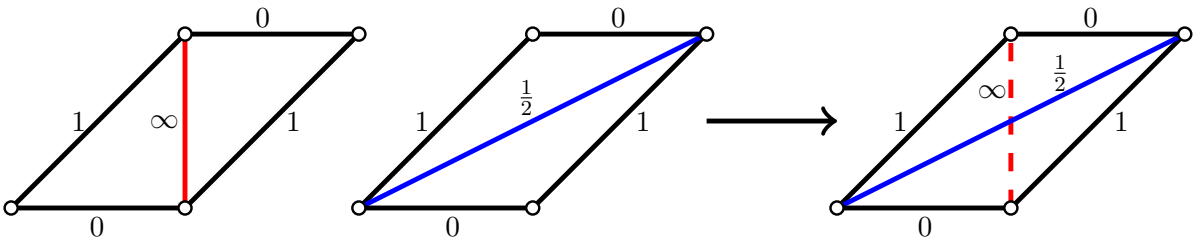

Figure 3.1: On the left, we have two triangulations of the once-punctured torus as the quotient of $\mathbb{R}^2\backslash\mathbb{Z}^2$. On the right, we have the tetrahedron obtained from stacking the triangulations by identifying the edges with the same slope. Here, the slopes of the triangulations are given in the illustrations, the white vertices are the puncture, and the red and blue edges correspond to the edges of the diagonal exchange.

corresponds to the vectors given by the identity matrix

$$\begin{bmatrix} 1 & 0 \\ 0 & 1 \end{bmatrix}$$

as well as edges with slopes 1, 0, and $\frac{1}{2}$, shown on the second diagram, which corresponds to vectors given by the matrix

$$R = \begin{bmatrix} 1 & 1 \\ 0 & 1 \end{bmatrix}.$$

The two resulting triangulations may then be identified to obtain the tetrahedron of the rightmost diagram where each edge of the same slope is glued together. Since every tetrahedron of the triangulation is formed in a similar way, we see more directly that, depending on the monodromy, each tetrahedron will correspond to one of the defined $6j$-symbols E_1, E_2, and E_3.

To simplify the notation, we will now define a specific product, denoted by $\cdot$, on the $6j$-symbols E_i. We will think of the operation $E_i \cdot E_j$ as the standard product of the $6j$-symbols where we additionally "glue" the bottom row of E_i to the top row of E_j. Because of this, we refer to the product as a *gluing* of $6j$-symbols. This is best illustrated with an example

such as

$$E_1 \cdot E_2 \cdot E_2 \cdot E_3 = \left| \begin{array}{ccc} a_1 & a_2 & a_3 \\ a_4 & a_2 & a_3 \end{array} \right| \left| \begin{array}{ccc} a_4 & a_2 & a_3 \\ a_4 & a_5 & a_3 \end{array} \right| \left| \begin{array}{ccc} a_4 & a_5 & a_3 \\ a_4 & a_6 & a_3 \end{array} \right| \left| \begin{array}{ccc} a_4 & a_6 & a_3 \\ a_4 & a_6 & a_7 \end{array} \right|.$$

This product corresponds with the general principle of obtaining the triangulation of the once-punctured torus bundles where we stack the tetrahedra on top of each other. For convenience, we will take the convention of labeling the $6j$-symbols such that the first $6j$-symbol in the product has the first row labeled as

$$\left| \begin{array}{ccc} a_1 & a_2 & a_3 \end{array} \right|,$$

and we label any edge obtained from the diagonal exchange with the subsequent index such as in the example of $E_1 \cdot E_2 \cdot E_2 \cdot E_3$. Additionally, it is worth noting that any gluing of k $6j$-symbols will have $(k+3)$ labelings by colors a_i.

Before we state the closed formula, we will introduce more useful notation using the monodromy R^{N_1} as our example. By nature of the construction, the triangulation associated to R^{N_1} will always fix one of the edges. As mentioned in Subsection 3.1.1, this is due to the first column of R being the vector

$$\begin{bmatrix} 1 \\ 0 \end{bmatrix}.$$

Now because of this, the diagonal exchanges are going to alternately occur on the other two non-fixed edges. In terms of the E_i's, this corresponds to N_1 alternating gluings of E_{i_0} and E_{j_0} where $i_0 \neq j_0$. We will denote this alternating gluing as $E_{i_0,j_0}^{N_1}$ where we note that the column which is not either i_0 nor j_0 will always remain a fixed color under the gluings. Additionally, we can see that depending on whether N_1 is odd or even, the final E_i in the alternating gluings of $E_{i_0,j_0}^{N_1}$ will either be E_{i_0} or E_{j_0}, respectively. We will denote this final

index by j_1 such that

$$j_1 = \begin{cases} i_0 & \text{For } N_1 \text{ odd} \\ j_0 & \text{For } N_1 \text{ even} \end{cases}.$$

Furthermore, we can generalize this notation to all R^{N_k} such that for any alternating gluing $E^{N_k}_{i_{k-1},j_{k-1}}$, the final index is

$$j_k = \begin{cases} i_{k-1} & \text{For } N_k \text{ odd} \\ j_{k-1} & \text{For } N_k \text{ even} \end{cases}.$$

Analogously for L^{N_k}, we can define the same alternating gluing $E^{N_k}_{i_{k-1},j_{k-1}}$ with j_k defined in the same manner.

For the once-punctured torus Σ^1_1, we will now state the closed formula for the corresponding mapping torus of a pseudo-Anosov element where we define $|a_i| = (-1)^{2a_i}[2a_i + 1]$ for a color a_i.

Theorem 3.2.1. *Let $\phi = R^{N_1}L^{N_2}\cdots R^{N_{2n-1}}L^{N_{2n}} \in Mod(\Sigma^1_1)$ where $n, N_i > 0$ for $1 \leq i \leq 2n$, and let $N = \left(\sum_{i=1}^{2n} N_i\right)$. Then the mapping torus $M(\phi)$ has Turaev-Viro invariant*

$$TV_r(M(\phi), q) = 2^{b_2 - b_0} \sum_{adm} \left[\left(\prod_{k=4}^{N+3} |a_k| \right) \left(E^{N_1}_{i_0,j_0} \cdot E^{N_2}_{i_1,j_1} \cdot \ldots \cdot E^{N_{2n}}_{i_{2n-1},j_{2n-1}} \right) \right]$$

where the sum is over all admissible colorings, $a_1 = a_{(N+2)}$, $a_2 = a_{(N-N_{2n}+2)}$, and $a_3 = a_{(N+3)}$. Additionally, the indices i_k and j_k may be computed inductively from $(i_0, j_0) = (2, 3)$ where $i_k \notin \{i_{k-1}, j_{k-1}\}$ and with

$$j_k = \begin{cases} i_{k-1} & \textit{For } N_k \textit{ odd} \\ j_{k-1} & \textit{For } N_k \textit{ even} \end{cases}.$$

Proof. From Theorem 2.1.5, the Turaev-Viro invariant may be defined as

$$TV_r(M,q) = 2^{b_2-b_0}\eta_r^{2|V|}\sum_{c\in A_r(\tau)}\left[\left(\prod_{e\in E}|e|_c\right)\left(\prod_{\Delta\in\tau}|\Delta|_c\right)\right]$$

where c runs over all admissible colorings of the edges. Since our triangulation is ideal, then $|V| = 0$ such that

$$TV_r(M,q) = 2^{b_2-b_0}\sum_{c\in A_r(\tau)}\left[\left(\prod_{e\in E}|e|_c\right)\left(\prod_{\Delta\in\tau}|\Delta|_c\right)\right].$$

Notice that our triangulation will have N distinct edges such that each edge is colored by a_k where $4 \leq k \leq N+3$. The edges corresponding to the colors a_1, a_2, and a_3 are not included since they will be identified to other edges under the homeomorphism ϕ. We now obtain

$$TV_r(M(\phi),q) = 2^{b_2-b_0}\sum_{adm}\left[\left(\prod_{k=4}^{N+3}|a_k|\right)\left(\prod_{\Delta\in\tau}|\Delta|_c\right)\right].$$

Next, to obtain the $6j$-symbols, we need to consider the triangulations of the manifold. As mentioned previously, each R^{N_k} and $L^{N_{k'}}$ corresponds to the alternating gluings of $6j$-symbols $E^{N_k}_{i_{k-1},j_{k-1}}$ and $E^{N_{k'}}_{i_{k'-1},j_{k'-1}}$. We consider the case when we multiply R^{N_k} on the right by L where the case for multiplying $L^{N_{k'}}$ on the right by R is similar. This corresponds to a diagonal exchange on the edge that is fixed by R^{N_k} such that we introduce a gluing on the right by the $6j$-symbol E_{i_k} where $i_k \notin \{i_{k-1}, j_{k-1}\}$. Now if we continue multiplying on the right by L, we will once again have an edge which is fixed such that we have an alternating gluing of $6j$-symbols $E^{N_{k+1}}_{i_k,j_k}$ for some j_k. This j_k will correspond to the column of the final diagonal exchange of $E^{N_k}_{i_{k-1},j_{k-1}}$ such that

$$j_k = \begin{cases} i_{k-1} & \text{For } N_k \text{ odd} \\ \\ j_{k-1} & \text{For } N_k \text{ even} \end{cases}.$$

This implies that we can rewrite $\left(\prod_{\Delta\in\tau}|\Delta|_c\right)$ in terms of alternating gluings of $6j$-symbols such that

$$TV_r(M(\phi),q)=2^{b_2-b_0}\sum_{adm}\left[\left(\prod_{k=4}^{N+3}|a_k|\right)\left(E^{N_1}_{i_0,j_0}\cdot E^{N_2}_{i_1,j_1}\cdot\ldots\cdot E^{N_{2n}}_{i_{2n-1},j_{2n-1}}\right)\right].$$

Lastly, we will consider the identification of the colors under the gluing of the edges by the map ϕ. We will note that each once-punctured torus is triangulated by lines with rational slopes between the punctures. For any given monodromy conjugated to the form $R^{N_1}L^{N_2}\cdots R^{N_{2n-1}}L^{N_{2n}}$ with matrix

$$\begin{bmatrix}a' & b'\\ c' & d'\end{bmatrix},$$

the slopes of the lines are determined by the slopes of the vectors

$$\begin{bmatrix}a'\\ c'\end{bmatrix},\quad \begin{bmatrix}b'\\ d'\end{bmatrix},\quad \text{and}\quad \begin{bmatrix}a'+b'\\ c'+d'\end{bmatrix}.$$

Here, the vector

$$\begin{bmatrix}a'+b'\\ c'+d'\end{bmatrix}$$

corresponds to the new edge obtained from the diagonal exchange. From this viewpoint, it is more clear to understand the alternating gluings. For example, for ϕR^n, we have that

$$\phi R^n=\begin{bmatrix}a' & b'\\ c' & d'\end{bmatrix}\begin{bmatrix}1 & n\\ 0 & 1\end{bmatrix}=\begin{bmatrix}a' & a'n+b'\\ c' & c'n+d'\end{bmatrix}$$

such that the edge corresponding to the vector

$$\begin{bmatrix}a'\\ c'\end{bmatrix}$$

is always fixed. Now if we multiply ϕR^n by L^m, then we have

$$\phi R^n L^m = \begin{bmatrix} a' & a'n+b' \\ c' & c'n+d' \end{bmatrix} \begin{bmatrix} 1 & 0 \\ m & 1 \end{bmatrix} = \begin{bmatrix} a'+m(a'n+b') & a'n+b' \\ c'+m(c'n+d') & c'n+d' \end{bmatrix}$$

such that the new fixed edge corresponds to the vector

$$\begin{bmatrix} a'n+b' \\ c'n+d' \end{bmatrix}.$$

Notice that when $m=1$, then the first column of $\phi R^n L$ is

$$\begin{bmatrix} a'(n+1)+b' \\ c'(n+1)+d' \end{bmatrix}$$

which corresponds to the edge obtained by the final diagonal exchange of ϕR^n. This implies that by gluing the tetrahedra corresponding to L^m, our gluings of $6j$-symbols are alternating between the E_i's associated to the previously fixed column of ϕR^n and the E_j's associated to the final diagonal exchange of ϕR^n .

We will now continue with our consideration of gluing the edges of the top and bottom tetrahedra. If we consider the triangulation of the once-punctured torus by

$$\begin{bmatrix} 1 & 0 \\ 0 & 1 \end{bmatrix},$$

then our slopes are determined by the vectors

$$v_1 = \begin{bmatrix} 1 \\ 0 \end{bmatrix}, \quad v_2 = \begin{bmatrix} 0 \\ 1 \end{bmatrix}, \quad \text{and } v_3 = \begin{bmatrix} 1 \\ 1 \end{bmatrix}.$$

In order to see which edges are identified, we only need to check the mapping of the vectors

v_1, v_2, and v_3 under ϕ.

Let us consider the final multiplication of the monodromy $R^{N_1}L^{N_2}\cdots R^{N_{2n-1}}L^{N_{2n}-1}$ by L. This may be viewed as the matrix

$$\phi = R^{N_1}L^{N_2}\cdots R^{N_{2n-1}}L^{N_{2n}-1}L = \begin{bmatrix} a & b \\ c & d \end{bmatrix}\begin{bmatrix} 1 & 0 \\ 1 & 1 \end{bmatrix} = \begin{bmatrix} a+b & b \\ c+d & d \end{bmatrix}$$

such that we have the vectors

$$w_1 = \begin{bmatrix} a+b \\ c+d \end{bmatrix}, \quad w_2 = \begin{bmatrix} b \\ d \end{bmatrix}, \quad \text{and } w_3 = \begin{bmatrix} a+2b \\ c+2d \end{bmatrix}.$$

First, we note that $\phi(v_3) = w_3$ where w_3 corresponds to our final diagonal exchange. Since v_3 is associated to the color a_3, then we are identifying a_3 with $a_{(N+3)}$ which is the color of the final edge added by the diagonal exchange.

Next, we note that $\phi(v_1) = w_1$ where w_1 corresponds to the previous diagonal exchange. Similar to before, since v_1 is associated to the color a_1, then we are identifying a_1 with $a_{(N+2)}$ which is the color of the edge added by the previous diagonal exchange.

In the last case, $\phi(v_2) = w_2$ where w_2 corresponds to the fixed edge under $L^{N_{2n}}$. Here, v_2 is associated to the color a_2 which we are identifying to the color of the fixed column of the alternating gluing $E^{N_{2n}}_{i_{2n-1},j_{2n-1}}$. This edge is obtained from the gluing of $R^{(N_{2n-1})-1}$ which has the color $a_{(N-N_{2n}+2)}$. □

Although the following is not reliant on Theorem 3.2.1, it is still worth noting to demonstrate the similarities between the hyperbolic volume of the manifold and the asymptotics of the Turaev-Viro invariants. In [7], Belletti, Detcherry, Kalfagianni, and Yang showed a relationship between the hyperbolic volume of a regular ideal octahedron and the asymptotics of the $6j$-symbols at $q = \exp\left(\frac{2\pi\sqrt{-1}}{r}\right)$.

Theorem 3.2.2 ([7], Theorem 1.2)**.** *For* $q = \exp\left(\frac{2\pi\sqrt{-1}}{r}\right)$ *and any admissible* 6*-tuple*

$(i, j, k, l, m, n) \in I_r^6$, *we have that*

$$\limsup_{r\to\infty} \frac{2\pi}{r} \log \left\| \begin{array}{ccc} i & j & k \\ & & \\ l & m & n \end{array} \right\| \leq v_8$$

where r *runs over the odd integers and with* v_8 *the volume of a regular ideal octahedron.*

Using Theorem 3.2.2, we have the direct calculation that

$$LTV(M(\phi)) = \limsup_{r\to\infty} \frac{2\pi}{r} \log |TV_r\left(M(\phi), q\right)| \leq N v_8$$

where $\phi = R^{N_1} L^{N_2} \cdots R^{N_{2n-1}} L^{N_{2n}}$, $N = \left(\sum_{i=1}^{2n} N_i\right)$, and $q = \exp\left(\frac{2\pi\sqrt{-1}}{r}\right)$. For the steps involved in the calculation, see the proof of Theorem 1.3 in [19] by Detcherry and Kalfagianni.

On the hyperbolic geometry side, a similar, although more precise, inequality has been obtained by Agol in [1, Theorem 2.4], and separately by Futer and Guéritaud in [25, Theorem B.1], where the inequality is given by

$$Vol(M(\phi)) < 2n v_8.$$

The similarities of the two results further support the claim of the Turaev-Viro invariant volume conjecture. Furthermore, it also suggests that much sharper bounds on the asymptotics of the Turaev-Viro invariants for the once-punctured torus bundles can be obtained through closer analysis.

3.2.1 Calculations of Turaev-Viro Invariants

In this subsection, we will calculate some examples of the Turaev-Viro invariants for once-punctured torus bundles using Theorem 3.2.1.

Example 3.2.3. We will begin with the small example of $RL \in Mod(\Sigma_1^1)$. For context, the complement of the mapping torus is homeomorphic to the complement of the figure-eight

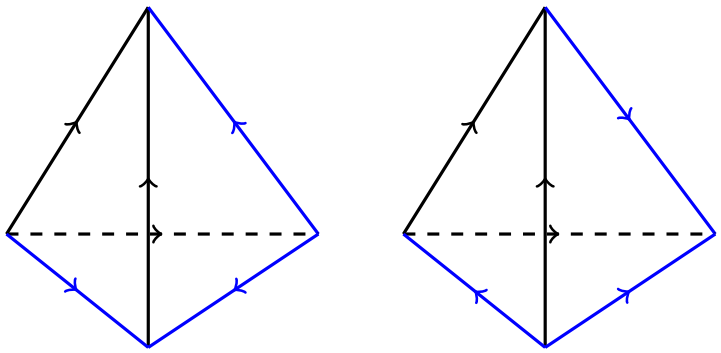

Figure 3.2: An ideal triangulation of the figure-eight knot. Here, we identify the black edges together, and we identify the blue edges together.

knot in S^3 with hyperbolic volume $2v_4 \approx 2.0299$.

By Theorem 3.2.1, we have that $\phi = R^{N_1}L^{N_2}$ where $N_1 = N_2 = 1$ such that $N = N_1 + N_2 = 2$. Now the indices i_k and j_k may be computed inductively from $(i_0, j_0) = (2, 3)$. Since $i_1 \notin \{i_0, j_0\}$, then $i_1 = 1$, and since $N_1 = 1$ is odd, then $j_1 = i_0 = 2$. This implies that

$$\begin{aligned} TV_r(M(\phi), q) &= 2^{b_2-b_0} \sum_{adm} \left[(|a_4||a_5|) \left(E^1_{2,3} \cdot E^1_{1,2} \right) \right] = 2^{b_2-b_0} \sum_{adm} \left[(|a_4||a_5|) \left(E_2 \cdot E_1 \right) \right] \\ &= 2^{b_2-b_0} \sum_{adm} \left[(|a_4||a_5|) \begin{vmatrix} a_1 & a_2 & a_3 \\ a_1 & a_4 & a_3 \end{vmatrix} \begin{vmatrix} a_1 & a_4 & a_3 \\ a_5 & a_4 & a_3 \end{vmatrix} \right]. \end{aligned}$$

Additionally, we can compute that $a_1 = a_4$, $a_2 = a_3$, and $a_3 = a_5$. Using the symmetry relations of the $6j$-symbols in Section 2.1, we have that

$$\begin{aligned} TV_r(M(\phi), q) &= 2^{b_2-b_0} \sum_{adm} \left[(|a_4||a_5|) \begin{vmatrix} a_4 & a_5 & a_5 \\ a_4 & a_4 & a_5 \end{vmatrix} \begin{vmatrix} a_4 & a_4 & a_5 \\ a_5 & a_4 & a_5 \end{vmatrix} \right] \\ &= 2^{b_2-b_0} \sum_{adm} \left[(|a_4||a_5|) \begin{vmatrix} a_4 & a_4 & a_5 \\ a_4 & a_5 & a_5 \end{vmatrix}^2 \right]. \end{aligned}$$

This Turaev-Viro invariant corresponds with the known ideal triangulation of the figure-eight knot given in Figure 3.2.

Example 3.2.4. In this example, we will consider the element $R^{N_1}L^{N_2} \in Mod(\Sigma_1^1)$. In this case, we have that $N = N_1 + N_2$, and the indices change depending on the parity of N_1. We still have that $i_0 = 2$, $j_0 = 3$, and $i_1 = 1$; however, we will either have that $j_1 = 2$ or $j_1 = 3$ for N_1 odd or even, respectively. For the gluings of the edges, we have that $a_1 = a_{N+2}$, $a_2 = a_{N_1+2}$, and $a_3 = a_{N+3}$. This gives us either

$$TV_r(M(\phi), q) = 2^{b_2-b_0} \sum_{adm} \left[\left(\prod_{k=4}^{N+3} |a_k| \right) \left(E_{2,3}^{N_1} \cdot E_{1,2}^{N_2} \right) \right]$$

for N_1 odd, or

$$TV_r(M(\phi), q) = 2^{b_2-b_0} \sum_{adm} \left[\left(\prod_{k=4}^{N+3} |a_k| \right) \left(E_{2,3}^{N_1} \cdot E_{1,3}^{N_2} \right) \right]$$

for N_1 even.

Example 3.2.5. As our last example, we will consider the element $(RL)^n \in Mod(\Sigma_1^1)$. The mapping torus of this element has complement homeomorphic to the complement of the n-fold cyclic cover of the figure-eight knot. Because of this, the complement has hyperbolic volume $2nv_4$.

We consider $\phi = R^{N_1}L^{N_2}R^{N_3}L^{N_4} \dots R^{N_{2n-1}}L^{N_{2n}}$ such that each $N_i = 1$ with $N = 2n$. Now for the indices, notice the following. Since every N_i is odd, then $j_k = i_{k-1}$ for every k. Also notice that $i_k \notin \{i_{k-1}, j_{k-1}\} = \{i_{k-1}, i_{k-2}\}$. Since initially $i_0 = 2$ and $i_1 = 1$, then $i_2 = 3$. Inductively, this implies that i_k cycles between the numbers 2, 1, and 3 starting at $i_0 = 2$. For the gluings, we have that $a_1 = a_{2n+2}$, $a_2 = a_{2n+1}$ and $a_3 = a_{2n+3}$.

Now our Turaev-Viro invariants will be $2n$ gluings of $6j$-symbols and fall into one of the three following cases:

$$TV_r(M(\phi), q) = 2^{b_2-b_0} \sum_{adm} \left[\left(\prod_{k=4}^{2n+3} |a_k| \right) (E_2 \cdot E_1 \cdot E_3 \cdot \ldots \cdot E_2 \cdot E_1 \cdot E_3) \right]$$

for $n \equiv 0 \mod 3$.

$$TV_r(M(\phi), q) = 2^{b_2 - b_0} \sum_{adm} \left[\left(\prod_{k=4}^{2n+3} |a_k| \right) (E_2 \cdot E_1 \cdot E_3 \cdot \ldots \cdot E_3 \cdot E_2 \cdot E_1) \right]$$

for $n \equiv 1 \mod 3$.

$$TV_r(M(\phi), q) = 2^{b_2 - b_0} \sum_{adm} \left[\left(\prod_{k=4}^{2n+3} |a_k| \right) (E_2 \cdot E_1 \cdot E_3 \cdot \ldots \cdot E_1 \cdot E_3 \cdot E_2) \right]$$

for $n \equiv 2 \mod 3$.

Remark 3.2.6. The Turaev-Viro invariant volume conjecture is known for the complement of the figure-eight knot [21]; however, the proof utilized the relationship between the Turaev-Viro invariants and the colored Jones polynomials. This relationship is a special case of Theorem 2.2.15 which related the traces of the quantum representations to the Turaev-Viro invariants. It would be of interest to prove the Turaev-Viro invariant volume conjecture for the figure-eight knot from the viewpoint of the triangulation given in Example 3.2.3. This may give further insight on proving the Turaev-Viro invariant volume conjecture for the n-fold cyclic cover of the figure-eight knot using the triangulation given in Example 3.2.5.

3.3 A Conjecture in Relation to the Stretch Factor

In this section, we will state a conjecture which relates the asymptotics of the Turaev-Viro invariants of a mapping torus with its stretch factor. This conjecture is supported by known results in hyperbolic geometry.

Briefly, we will introduce the stretch factor for the example of the once-punctured torus. For more details, see Chapter 14 in [23]. Now for the once-punctured torus Σ_1^1, the mapping class group $Mod(\Sigma_1^1)$ is generated by the Dehn twists t_α and t_β along the canonical meridian and longitude, respectively. As stated in Section 2.2, there is also an isomorphism between

$Mod(\Sigma_1^1)$ and $SL_2(\mathbb{Z})$ which sends

$$t_\alpha \to \begin{bmatrix} 1 & 1 \\ 0 & 1 \end{bmatrix} = R$$

and

$$t_\beta \to \begin{bmatrix} 1 & 0 \\ -1 & 1 \end{bmatrix} = L^{-1}$$

where R and L^{-1} are the generators of $SL_2(\mathbb{Z})$. Now for certain elements in $Mod(\Sigma_1^1)$, we can define the stretch factor.

Definition 3.3.1. For a given element $\phi \in Mod(\Sigma_1^1) \cong SL_2(\mathbb{Z})$ with $|Trace(\phi)| > 2$, the unique real-valued eigenvalue $\lambda > 1$ is defined as the *stretch factor*. Furthermore, ϕ is pseudo-Anosov if and only if $|Trace(\phi)| > 2$.

It is easier to understand the stretch factor when viewing the once-punctured torus as a quotient of $\mathbb{R}^2\backslash\mathbb{Z}^2$. Homeomorphisms of Σ_1^1 may be viewed as the corresponding matrices of $SL_2(\mathbb{Z})$ acting on $\mathbb{R}^2\backslash\mathbb{Z}^2$ followed by the quotient of the space. Because we have that $|Trace(\phi)| > 2$, any curve in Σ_1^1 will be stretched by λ along parallel copies of one eigenvector and will contract by $\frac{1}{\lambda}$ along parallel copies of the other eigenvector. These dilations and contractions are the geometric interpretation of the stretch factor. In fact, a pseudo-Anosov map is more accurately defined as a generalization of this principle.

Now we will discuss the following open question posed by Andersen, Masbaum, and Ueno in [3].

Question 3.3.2 ([3], Question 1.1)**.** *Can one compute the stretch factor for pseudo-Anosov mapping classes from the quantum representations?*

In [3], the authors show that this is true for the four-punctured sphere with certain colorings of the punctures. In regards to Question 3.3.2, we consider the case for the once-punctured torus where there is only one puncture to color. In [51], Santharoubane showed

that, for any dimension N, the sequence of quantum representations for a fixed dimension converge to a matrix with known eigenvalues. In particular, the eigenvalues of the convergent matrix are powers of the stretch factor which implies that Question 3.3.2 is also true for the once-punctured torus.

Now the following is not rigorous and only supported through small computational examples. For a fixed $r \geq 3$ with r odd, there is one quantum representation $\rho^N_{r,c(N,r)}$ of dimension N for $1 \leq N \leq \frac{r-1}{2}$ where $c(N,r)$ is a chosen coloring of the puncture such that the quantum representation has dimension N. For an explicit formulation of the quantum representations, one may refer to [26] by Gilmer and Masbaum as well as [51] by Santharoubane. Now given a pseudo-Anosov element ϕ with stretch factor λ_ϕ, we make the assumption that, for any N, the eigenvalues $\lambda_{i,N}$ of the quantum representation $\rho^N_{r,c(N,r)}(\phi)$ has the property that $|\lambda_{i,N}| \leq \lambda_\phi^{\frac{r-3}{2}}$. The motivation behind assuming this property is that it appears that the eigenvalues of the quantum representations converge to the eigenvalues of the convergent matrix from below. By Proposition 2.2.15, we have the following calculation which would imply the subsequent conjecture.

$$\begin{aligned} TV_r(M(\phi)) &= \sum_{N=1}^{\frac{r-1}{2}} \left|Tr(\rho^N_{r,c(N,r)}(\phi))\right|^2 = \sum_{N=1}^{\frac{r-1}{2}} \left|\lambda_{1,N} + \cdots + \lambda_{N,N}\right|^2 \\ &\leq \sum_{N=1}^{\frac{r-1}{2}} \left[N\left(|\lambda_{1,N}|^2 + \cdots + |\lambda_{N,N}|^2\right)\right] \leq \sum_{N=1}^{\frac{r-1}{2}} \left[N\left(\sum_{i=1}^{N} \lambda_\phi^{r-3}\right)\right] \\ &= \sum_{N=1}^{\frac{r-1}{2}} \left[N^2\left(\lambda_\phi^{r-3}\right)\right] = \left(\lambda_\phi^{r-3}\right) \sum_{N=1}^{\frac{r-1}{2}} \left[N^2\right] = \frac{\lambda_\phi^{r-3}(r^3-r)}{24}. \end{aligned}$$

Conjecture 3.3.3. *Let $\phi \in Mod(\Sigma_1^1)$ be a pseudo-Anosov element with stretch factor λ_ϕ. Then*

$$LTV(M) = \limsup_{r\to\infty} \frac{2\pi}{r} \log\left|TV_r\left(M(\phi), q\right)\right| \leq 2\pi \log\left(\lambda_\phi\right)$$

where r runs along the odd integers and $q = \exp\left(\frac{2\pi\sqrt{-1}}{r}\right)$.

Although we could write a more general conjecture for all surface mapping class groups,

the arguments for the four-punctured sphere and the once-punctured torus depended on exploiting their convergence to the homological representation which does not generalize to other cases. Because of this, it is not known to what extent the quantum representations determine the stretch factors of the mapping class group.

The main motivation of Conjecture 3.3.3 is still to relate the asymptotics of the Turaev-Viro invariants to the hyperbolic volume of the manifold. The term $\log(\lambda_\phi)$, known as the *entropy*, has significance in hyperbolic geometry. By the works of Brock, Mazur, and Minsky in [11, 12, 42] and Kin, Kojima, and Takasawa in [34], the authors have shown a relationship between the hyperbolic volume of the mapping torus for a pseudo-Anosov element and the corresponding entropy. In particular, it is known that the volume of a hyperbolic manifold is bounded by a constant multiplied by the entropy where the constant depends on the surface of the mapping class group. Because of this, Conjecture 3.3.3 would further support that the Turaev-Viro invariant volume conjecture is true. Additionally, it may provide another method in calculating the constants for the bounds.

Chapter 4

Realizing Fundamental Shadow Links in S^3

In this chapter, we construct infinite families of links in S^3 whose complements satisfy the Turaev-Viro invariant volume conjecture. Additionally, we provide a general method in augmenting a link such that the resultant link also has complement which satisfies the Turaev-Viro invariant volume conjecture. The method involves finding a homeomorphism of the complement of the link with the complement of a fundamental shadow link where the conjecture is already known. Since the Turaev-Viro invariant and the hyperbolic volume are preserved under homeomorphisms, this provides link complements in S^3 which satisfy the conjecture. We note that the results for Sections 4.3, 4.4, and 4.5 first appeared in [36] by the author of this dissertation; however, in Section 4.5, we consider a more general approach.

4.1 Background

In this section, we will introduce the Stein factorization of stable maps of links followed by their connection with shadows of links in S^3. Under this correspondence, we are able to understand the collapsing map given by Turaev's shadow theory approach to 3-manifolds through the explicit map given by the Stein factorization. Additionally, we briefly discuss Kirby calculus which we will use in an alternate proof of Theorem 4.5.1. The method involving Kirby calculus provides a direct approach based purely on the surgery presentation.

4.1.1 The Stein Factorization of Stable Maps of Links

In this subsection, we will introduce the Stein factorization of stable maps. We remark that the definitions stated here are written formally; however, it is only necessary to have a loose conceptual understanding of this subsection in order to follow the results appearing later in Chapter 4. As discussed in Subsection 2.3.2, the fundamental shadow links may be viewed as a surgery presentation in S^3. In this case, one can realize the fundamental shadow links in S^3 through the widely used Kirby calculus. An alternate proof using this technique will be provided in this work; however, by Constantino and Thurston [15], we will also see that there is a close connection between the Stein factorization of stable maps of links and boundary-decorated shadowed polyhedron. Through the explicit maps, we have a more natural approach to studying the complements of the fundamental shadow links.

We will begin with a brief outline. For a 3-manifold M, the Stein factorization of a stable map $f = g \circ h : M \to \mathbb{R}^2$ decomposes f into a map $h : M \to W_f$ of connected fibers and a map $g : W_f \to \mathbb{R}^2$ which is finite-to-one where W_f is a 2-dimensional polyhedron. For our cases, W_f will be a simple polyhedron in the same manner as the shadows in Section 2.3. Analogous to the 3-manifolds obtained from Turaev's shadow construction, the generic points of W_f have preimages under the map h which are circle bundles inside a 3-manifold. At these circle bundles, we can glue disks which is similar to the 4-thickening process. This results in a 4-manifold which collapses onto the simple polyhedron along the disks where the boundary is given by the 3-manifold M.

Much of this construction is close to the boundary-decorated shadowed polyhedron viewpoint of a manifold. The main difference is that we do not state the topological data of the gleam explicitly in the Stein factorization. We will proceed with the basic definitions of the Stein surface. One can find more detailed information in [37] by Levine and in [50] by Saeki.

We will now begin to define the Stein factorization for a map on a 3-manifold with (possibly empty) boundary of tori.

Definition 4.1.1. Let M be a closed 3-manifold and f a smooth map from M to an orientable 2-manifold Σ. Now suppose that f satisfies the following conditions. For every $p \in M$ and $f(p)$, there exist local coordinates centered at p such that f can be described as one of the following:

i. $(u, x, y) \mapsto (u, x)$.

ii. $(u, x, y) \mapsto (u, x^2 + y^2)$.

iii. $(u, x, y) \mapsto (u, x^2 - y^2)$.

iv. $(u, x, y) \mapsto (u, y^2 + ux - x^3)$.

For the previous conditions $(i), (ii), (iii)$, and (iv) at a point p, we say p is a *regular point*, a *definite fold point*, an *indefinite fold point*, or a *cusp point*, respectively. Furthermore, if $S(f)$ are the singular points of f, then suppose f also satisfies these global conditions:

v. $f^{-1} \circ f(p) \cap S(f) = \{p\}$ for a cusp point.

vi. The restriction of f to the singular points which are not cusp points is an immersion with normal crossings.

We say that a map f satisfying all of the conditions is a *stable map*.

Definition 4.1.2. Suppose that M is a compact and orientable 3-manifold with (possibly empty) boundary of tori. We say that a smooth map f of M into an orientable 2-manifold Σ is an *S-map* if the restriction to the interior of M is a stable map, and each $p \in \partial M$ can be described locally by the map $(u, x, y) \mapsto (u, x)$ such that $x = 0$ corresponds to points on the boundary.

Definition 4.1.3. For a given S-map, we define the space W_f to be the quotient of the space M along the connected fibers of f with map $h : M \to W_f$. Now we let $g : W_f \to \Sigma$ be the map such that $f = g \circ h$. This factorization of the map f is the *Stein factorization* with corresponding *Stein surface* W_f.

Lastly, we can further extend this definition such that M contains a link L.

Definition 4.1.4. Let M be a compact and orientable 3-manifold M with (possibly empty) boundary of tori and a (possibly empty) link L. Let f be an S-map of the manifold M into an orientable 2-manifold Σ. We define f to be an *S-map* of the pair (M, L) if the link L is contained in the set of definite fold points of f. In the case when M is a closed 3-manifold, the map f is called a *stable map* of the pair (M, L).

4.1.2 Stein Surfaces and Shadows of 3-Manifolds

In this subsection, we will construct a boundary-decorated shadowed polyhedron for the manifold pair (S^3, L). We will then see that the collapsing map in Turaev's construction from shadows can be realized as an explicit map given by the Stein factorization of the pair.

We let D be a flat oriented disk in the 4-ball B^4, and we define the closure of D minus a neighborhood of the boundary to be the set D'. Now we have a clear map $\pi : S^3 \to D$ given by collapsing B^4 onto the disk D. From this collapsing map, we can assume that the preimage of D' under the map π is a solid torus T, and additionally, the remaining $T' = S^3 \backslash Int(T)$ is also a solid torus.

Now in order to consider a link L in S^3 of n-components, we proceed in the following way. We begin by isotoping the link L such that it is contained in $D' \times [-\epsilon, \epsilon]$ for some ϵ where the projection under the collapsing map $\pi|_T$ is generic with respect to the link L. Here, we define generic in the usual sense where the projection contains no cusps, no crossings contain more than two strands, and there are no self-tangencies of the projection. This property can always be obtained through small isotopies of the link.

Now we will begin to define the boundary-decorated shadowed polyhedron for the pair (S^3, L). Consider the mapping cylinder obtained from the quotient

$$P'_L = (L \times [0, 1] \sqcup D')/((x, 0) \sim \pi(x)).$$

From P'_L, we define the boundary-decorated shadowed polyhedron P_L as having the simple polyhedron obtained from collapsing the region touching the boundary $\partial(D')$ onto the components of $\pi(L)$. Here, we decorate the boundary $\partial(P_L) = L \times \{1\}$ as internal components where the gleam is explained as follows. For the regions not touching the boundary of P_L, there is a choice of gleam such that P_L is a boundary-decorated shadowed polyhedron corresponding to the pair (S^3, L). In this work, the gleam for such regions R will be $\frac{V_R}{2}$ where V_R denotes the number of vertices touching R. More details can be found in Section 3.2 of [15].

Now given the boundary-decorated shadowed polyhedron P_L, we can construct a stable map $f : (S^3, L) \to \mathbb{R}^2$ such that the corresponding Stein surface W_f with map $h : (S^3, L) \to W_f$ can be identified in a natural way to P_L. In [29], Ishikawa and Koda discuss the explicit map h in terms of preimages of points in W_f for links inside compact and orientable 3-manifolds with (possibly empty) toroidal boundary. Additionally, in Section 4 of [29], the authors construct the map h for the specific case of the pair (S^3, L). Their result is provided as follows where the details are discussed in-depth in the proof of Theorem 3.5 in [29].

Proposition 4.1.5 ([29], Theorem 3.5)**.** *Let L be a link in S^3. There exists a stable map $f : (S^3, L) \to \mathbb{R}^2$ with Stein surface W_f and Stein factorization $f = g \circ h$ such that the preimage of a point in W_f can be viewed as one of the five following:*

i). If x_1 is a point on $P_L \backslash (L \times [0, 1])$, then $h^{-1}(x_1)$ is the regular fiber $\{x_1\} \times S^1 \subset T$.

ii). If x_2 is a point on $L \times (0, 1)$, then $h^{-1}(x_2)$ is a meridian of the corresponding link component of $L \times \{1\}$.

iii). If x_3 is a point on $L \times \{1\}$, then $h^{-1}(x_3)$ is a point on the corresponding link in S^3.

iv). Let x_4 be a point from the singular set $S(P)$ which are not vertices. Locally around x_4, there are three regions separated by the singular set. There exists a triple of points, one from each region, such that their preimages are circles which are the boundary to a pair of pants with $h^{-1}(x_4)$ as its spine.

v). Let x_5 be a point from the set of vertices of the singular set $S(P)$. As in case iv), there exist preimages of points from the regions around the vertex which pullback to circles such that they bound a surface with spine $h^{-1}(x_5)$.

4.1.3 Kirby Calculus

In this subsection, we give a brief summary of Kirby calculus. For an introduction, one may refer to Chapter VI in [47] by Prasolov and Sossinsky.

Similar to how isotopic links in S^3 may be realized through Reidemeister moves of the link diagrams, Kirby calculus gives a method for studying homeomorphic 3-manifolds from their surgery presentation.

We recall that a 3-manifold may be viewed as an integer framing of a link in S^3. Here, the framed link carries the topological data to construct the 3-manifold through Dehn surgeries.

Definition 4.1.6. A *Dehn surgery* is the procedure of removing a toroidal neighborhood of the link component followed by a *Dehn filling* where we glue back the meridian of the removed solid torus to the boundary torus. For a given integer framing n, the gluing sends the meridian of the removed torus to a simple closed curve γ in the homology class of $[n\alpha+\beta]$ where α and β, respectively, are the standard generating meridian and longitude curves of the first homology group of the torus.

The Dehn surgery operation may be defined for rational surgeries; however, we will mostly only see either 0-framed surgeries or ∞-framed surgeries in this work. For the 0-framed surgeries, the solid torus is removed and glued back such that the meridian of the removed torus is glued as the longitude of the boundary torus. For the ∞-framed surgeries, we consider this case to be the identity Dehn surgery. The removed solid torus is glued back to the boundary torus such that the meridian is still identified with the meridian.

Now given a surgery presentation of a 3-manifold, we consider the two moves shown in Figure 4.1. In this work, we will often refer to the Kirby II move as a *handleslide*. Now

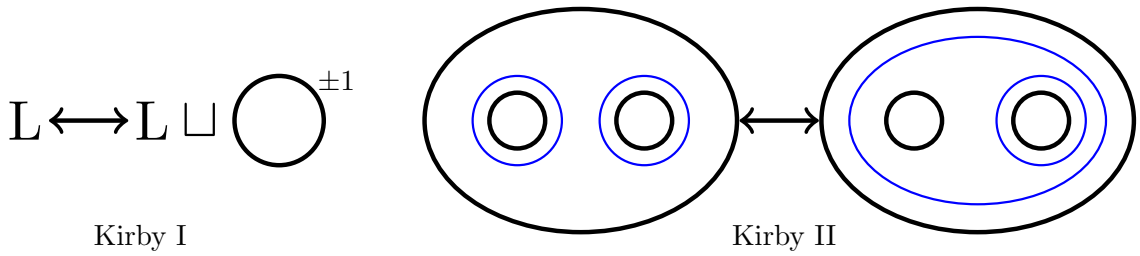

Figure 4.1: On the left, the Kirby I move which adds or removes an unlinked component with framing ± 1. On the right, the Kirby II move where any two components with their framing curves contained in a possibly knotted two-holed disk in S^3 can be changed as shown. Here, the framed link is colored blue, the two-holed disk may be linked with other components, and the new framing curves are still on the two-holed disk.

by the following theorem, the Kirby moves may be used to relate surgery presentations of homeomorphic manifolds.

Theorem 4.1.7 ([35])**.** *Two framed links in S^3 represent the same oriented 3-manifold by surgery if and only if they are related by a sequence of Kirby I and Kirby II moves.*

Theorem 4.1.7 will be essential in our alternate proof of Theorem 4.5.1. By using the handleslides on the surgery presentation of the fundamental shadow links given in Subsection 2.3.2, we can obtain a simpler surgery presentation for a homeomorphic manifold. From this new surgery presentation, we can explicitly find a link in S^3 with a complement homeomorphic to the complement of a fundamental shadow link.

4.2 An Obstruction to Knots in S^3

In the following sections of the chapter, we will see that every obtained hyperbolic link in S^3 which satisfies the Turaev-Viro invariant volume conjecture contains at least two components. In this section, we provide an explanation by showing that, up to homeomorphisms of the knot complements, there are only finitely many knots in S^3 that can have complement homeomorphic to the complement of a fundamental shadow link with one component.

Proposition 4.2.1. *Let K be a knot in S^3, and let $K^c \subset \#^{c+1}(S^2 \times S^1)$ be a complexity*

c fundamental shadow link with one link component. For any $c \geq 2$, the complements of K and K^c are not homeomorphic.

Proof. This proof is a simple consequence of the Mayer–Vietoris sequence. For more information, see Hatcher [28, Section 2.2]. For a knot K in S^3, it is well-known through a quick application of the Mayer–Vietoris sequence that the first homology group $H_1(S^3 \backslash \mathrm{IntNbd}(K))$ is isomorphic to $\mathbb{Z}$ [38, Theorem 1.5]. In a similar way, we will use the Mayer–Vietoris sequence for the first homology group of the complement of the fundamental shadow link. We will first define the spaces

$$X = \#^{c+1} \left(S^2 \times S^1\right), \quad A = D^2 \times S^1, \quad B = X \backslash A, \quad \text{and } Y = A \cap B = S^1 \times S^1$$

where D^2 is the two-dimensional closed disk. Now from the Mayer–Vietoris sequence, we have the long exact sequence

$$\begin{aligned} \cdots \to H_1(Y) \to H_1(A) \oplus H_1(B) \xrightarrow{f} H_1(X) \xrightarrow{g} \\ \to H_0(Y) \to H_0(A) \oplus H_0(B) \to H_0(X) \to 0. \end{aligned}$$

The zeroth homology group is generated by the number of path connected components such that we have

$$\begin{aligned} \cdots \to H_1(Y) \to H_1(A) \oplus H_1(B) \xrightarrow{f} H_1(X) \xrightarrow{g} \\ \to \mathbb{Z} \to \mathbb{Z} \oplus \mathbb{Z} \to \mathbb{Z} \to 0. \end{aligned}$$

In this case, from the exactness of the sequence, g is the zero map. Therefore, we can consider the following long exact sequence

$$\cdots \to H_1(Y) \to H_1(A) \oplus H_1(B) \xrightarrow{f} H_1(X) \xrightarrow{g} 0.$$

We will compute the homologies of $H_1(A)$ and $H_1(X)$. For $H_1(A)$, there is a deformation retraction of the space A onto the space S^1 such that $H_1(A) \cong \mathbb{Z}$. Now the manifold X is obtained from the connected sum of closed and oriented 3-manifolds. In the case of finitely generated abelian groups, the first homology group of the connected sum may be computed as the direct sum of the first homology groups shown as

$$H_1\left(\#^{c+1}\left(S^2 \times S^1\right)\right) \cong \bigoplus^{c+1} H_1\left(S^2 \times S^1\right) \cong \mathbb{Z}^{c+1}.$$

Replacing our isomorphisms into the long exact sequence, we obtain

$$\cdots \to H_1(Y) \to \mathbb{Z} \oplus H_1(B) \xrightarrow{f} \mathbb{Z}^{c+1} \xrightarrow{g} 0.$$

Now since g is the zero map, then the kernel of g is the entire set $\mathbb{Z}^{c+1}$. By exactness of the sequence, the kernel of g must be equal to the image of f such that $\mathbb{Z} \oplus H_1(B)$ must have at least $(c+1)$ generators. This implies that $H_1(B)$ will have at least c generators. For the complement of a fundamental shadow link B, in the case when $c \geq 2$, the first homology group $H_1(B)$ has more generators than the first homology group of the knot complement in S^3. This implies that their first homology groups cannot be isomorphic, and the two manifolds must be distinct.

□

4.3 Links in S^3 up to 11-Crossings

In this section, we will classify, up to homeomorphisms of their complements, the hyperbolic links of volume $2v_8$ with at most 11-crossings which are complexity one fundamental shadow links. As discussed in Subsection 1.2.2, since the Turaev-Viro invariant and the hyperbolic volume are preserved under homeomorphisms, this provides new examples of links in S^3 which satisfy the Turaev-Viro invariant volume conjecture. We will obtain the results

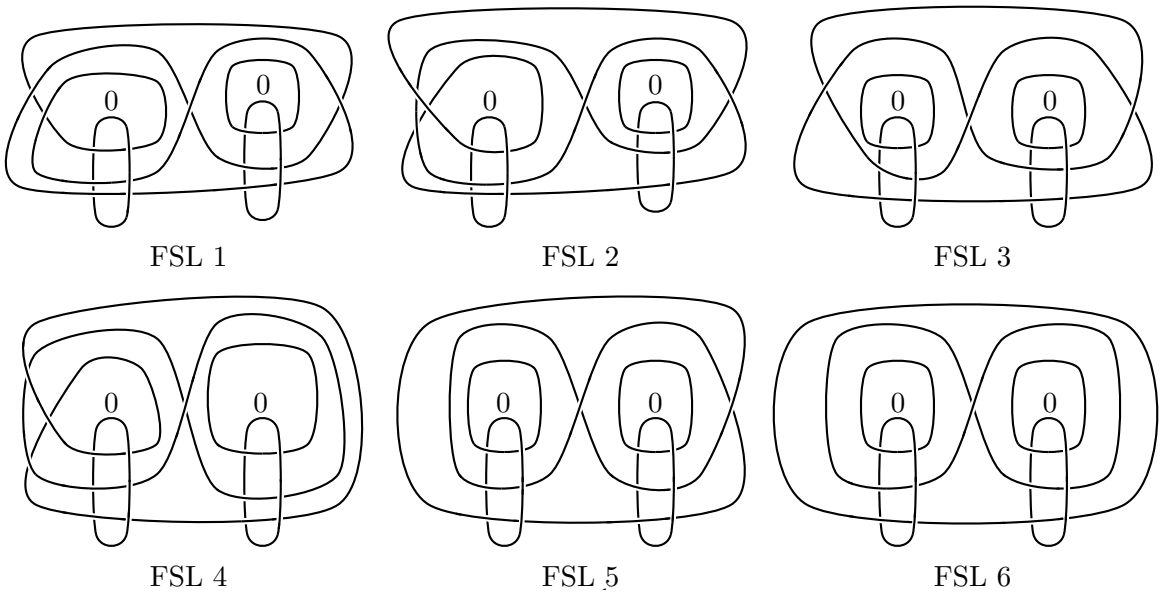

Figure 4.2: The six fundamental shadow links with complements homeomorphic to the complements of links up to 11-crossings.

using the link database of *LinkInfo* [39] in combination with computations from *SnapPy* [16]. In Figure 4.2, we provide the six fundamental shadow links which have complements homeomorphic with at least one of the complements of links up to 11-crossings.

Remark 4.3.1. From our calculations, the only candidate that we were not able to determine was a fundamental shadow link was the link L_{10n59}. Although *SnapPy* determined the link was not a fundamental shadow link, this is not rigorous and may be due to a numerical error. To prove whether or not it is a fundamental shadow link would require a different method.

Fundamental Shadow Link	LinkInfo Name
FSL 1	L_{10n32}
FSL 2	L_{10n36}
FSL 3	L_{6a4}, L_{9n25}, L_{11n287}, L_{11n378}
FSL 4	L_{10n84}, L_{10n87}
FSL 5	L_{8n5}, L_{9n26}, L_{10n70}, L_{11n376}, L_{11n385}
FSL 6	L_{8n7}, L_{10n97}, L_{10n105}, L_{10n108}

Table 4.1: The links with homeomorphic complements to a fundamental shadow link.

Theorem 4.3.2. *The links given in Table 4.1 have volume $2v_8$ and satisfy the Turaev-Viro invariant volume conjecture.*

Proof. We will prove Theorem 4.3.2 using the following procedure:

- Since we know that we are looking for complexity one fundamental shadow links, then the volume of all of our links will be $2v_8 \approx 7.3277$. From using *LinkInfo*, this will allow us to narrow down all links up to 11-crossings whose volume is approximately $2v_8$.

- The previous step gives us the list of links: L_{6a4}, L_{8n5}, L_{8n7}, L_{9n25}, L_{L9n26}, L_{10n32}, L_{10n36}, L_{10n59}, L_{10n70}, L_{10n84}, L_{10n87}, L_{10n97}, L_{10n105}, L_{10n108}, L_{11n287}, L_{11n376}, L_{11n378}, and L_{11n385} where, as a reminder, the first number indicates the number of crossings, the letter indicates whether it is alternating or non-alternating, and the second number indicates it is the n-th link with the same first two parameters.

- As mentioned in Remark 2.3.16, the complements of the fundamental shadow links obtained by replacing edges by 3-braids of single vertex planar 4-valent graphs are homeomorphic if they induce the same permutation on the 3-strands, therefore, there are only finitely many fundamental shadow links with volume $2v_8$. This implies that we can compare the finite list of links up to 11-crossings with the finite list of fundamental shadow links of volume $2v_8$.

- As demonstrated in Subsection 2.3.2, the complements of the fundamental shadow links in connected sums of $S^2 \times S^1$ can be realized as the complement of a surgery presentation of a link in S^3. From this, we define each of the surgery presentations of the fundamental shadow links into *SnapPy* as well as our candidates from the list of links up to 11-crossings.

- Lastly, we use *SnapPy* to test the finitely many cases to see which manifolds are homeomorphic to each other. Of the possible fundamental shadow links, the links in Figure 4.2 are the only fundamental shadow links which *SnapPy* recognizes as having homeomorphic complements with a link of at most 11-crossings.

□

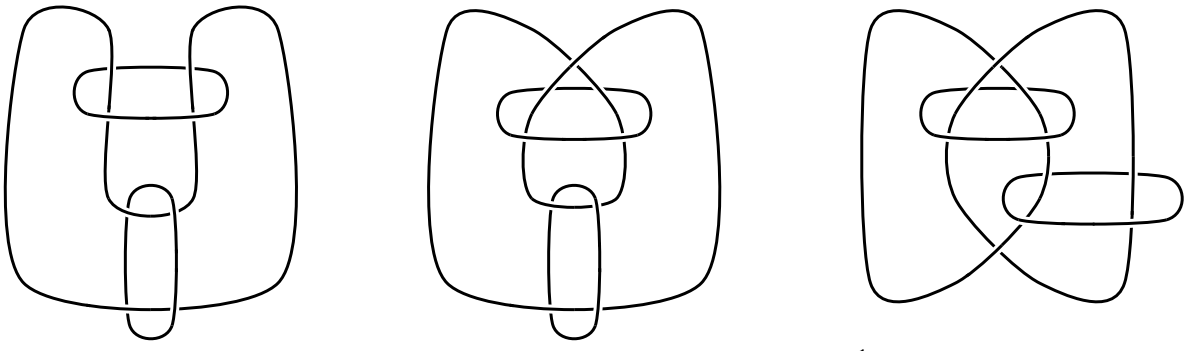

Figure 4.3: The Borromean rings are the leftmost link, and the Borromean twisted sisters are the two rightmost links.

Remark 4.3.3. From *LinkInfo*, all links up to 11-crossings have volume strictly less than $6v_8$. This implies that the only other links in this set that have homeomorphic complements with the fundamental shadow links must have complexity two. Similar to the proof of Theorem 4.3.2, we could also look for candidates by looking for links with volume $4v_8$ in *LinkInfo*. From doing this, the only possible links are the links L_{11n387} and L_{11n388}; however, currently, it has not been shown that if either of the links have complements homeomorphic to the complement of a complexity two fundamental shadow link.

4.4 Families of Links in S^3

In this section, we will construct infinite families of links which satisfy the Turaev-Viro invariant volume conjecture. The motivation for this comes from the Borromean rings and the Borromean twisted sisters depicted in Figure 4.3. These are links with non-homeomorphic complements; however, they each have the same hyperbolic volume of $2v_8$. Although the conjecture is already known for the Borromean rings, it was not previously verified for both of the Borromean twisted sisters. In pursuing a positive result for these links, we generalize the link complements to infinite families where each link complement satisfies the conjecture.

Before the statement of the main theorem in this section, we will need the following technical lemma.

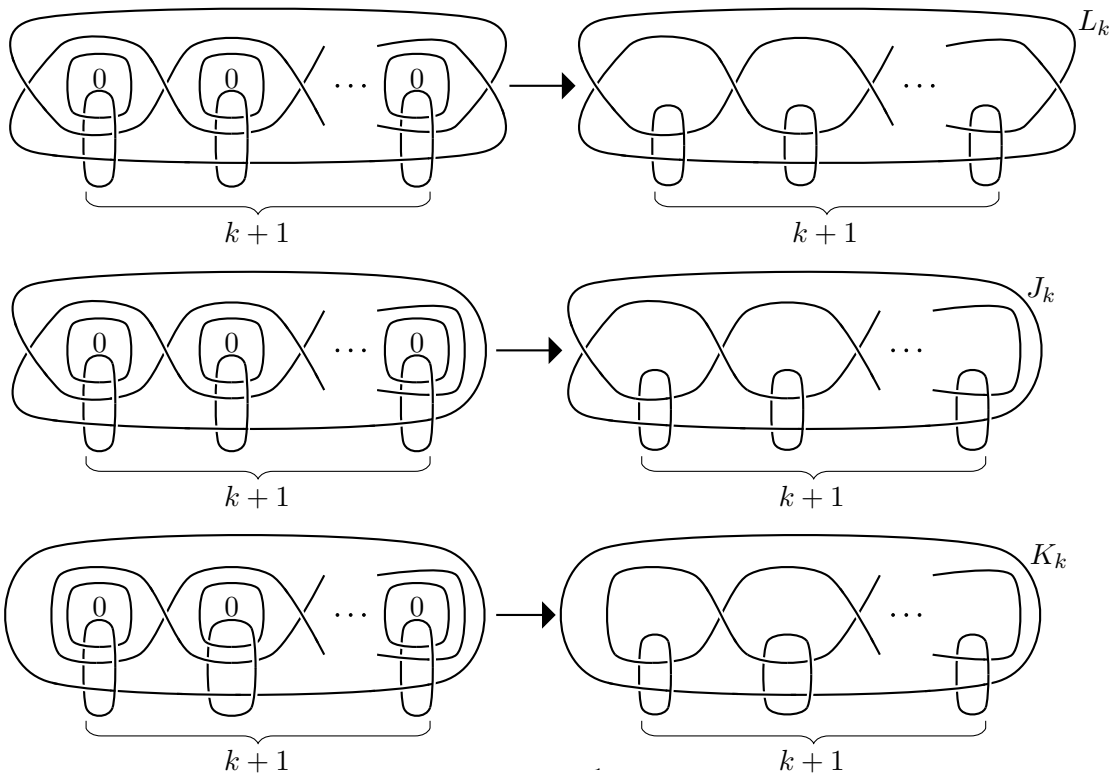

Figure 4.4: On the left are the complexity k fundamental shadow links embedded in connected sums of $S^2 \times S^1$, and on the right are their associated links in S^3.

Lemma 4.4.1 ([15], Lemma 3.25)**.** *Let P be a boundary-decorated shadowed polyhedron of (M, L) where L is a framed link and with M an oriented 3-manifold. Then the manifold M' obtained from Dehn filling L has a shadow P' given by capping components of ∂P by disks.*

Proof. We will begin by letting P be a boundary-decorated shadowed polyhedron of a 4-dimensional manifold W with the boundary $\partial(W) = M$ and the link $L = \partial_{int}(P)$. Performing a Dehn filling along L in the manifold $\partial(W)$ corresponds to gluing 2-handles $B^2 \times B^2$ to W. Without loss of generality, we can assume that the copies of $B^2 \times B^2$ collapse onto the disks $B^2 \times \{pt\}$ such that the boundary of each disk $S^1 \times \{pt\}$ is a link component of $\partial_{int}(P)$. After the gluings, we obtain a new simple polyhedron P' which is the result of the disk components $B^2 \times \{pt\}$ being attached to the original P. On the simple polyhedron P', the gleam of the new regions are determined by the framing of the link L. □

Now with Lemma 4.4.1, we will proceed to state and prove the main result of the section.

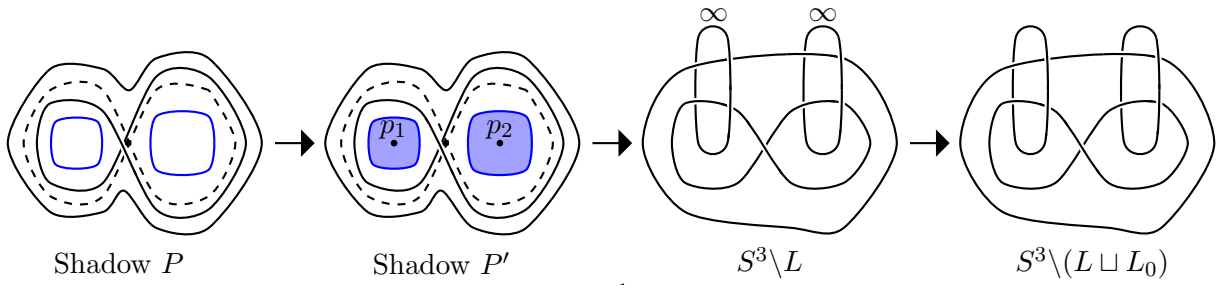

Figure 4.5: On the leftmost diagram, we have the shadow P with $Sing(P)$ the dashed lines, $\partial_{int}(P)$ colored blue, and $\partial_{ext}(P)$ colored black. We cap $\partial_{int}(P)$ with disks to obtain regions R_j shaded blue, and we mark their centers with p_1 and p_2 to recover a new shadow P'. In this case, the gleam of the new regions are both $\frac{1}{2}$. P' is the shadow of a link complement in S^3 such that the preimages of the points p_1 and p_2 are the cores of the ∞-framed link in S^3. Drilling out the ∞-framed link gives a link complement in S^3 homeomorphic to the complement of the original fundamental shadow link.

First, we will define the generalizations of the complements of the Borromean rings and the Borromean twisted sisters as the complements of the link families appearing in Figure 4.4, denoted by L_k, J_k, and K_k. The links in S^3 on the right of Figure 4.4 are the same as the families in S^3 appearing in Figure 1.1.

Theorem 4.4.2. *Given an integer $k \geq 1$, let L_k, J_k, and K_k be the links in S^3 shown in Figure 1.1. The complement of each L_k, J_k, and K_k is a hyperbolic manifold with volume $2kv_8$ and satisfies the Turaev-Viro invariant volume conjecture.*

Proof. Each of the links shown on the right of Figure 4.4 can be constructed using the following steps. As an example, one can reference Figure 4.5 which demonstrates the case for K_1. As a quick note, in Remark 4.4.4, we discuss a proof using Hopf link pairs which are sublinks of the surgery presentation. Although this approach leads to a more immediate discovery of the homeomorphisms, the method we choose to highlight here allows us to consider a more general case stated later in this work.

From the procedure of constructing a fundamental shadow link from a graph in Subsection 2.3.2, we let $S(P)$ be the simple polyhedron of the fundamental shadow link of complexity k which corresponds to the planar 4-valent graph of Figure 4.6. Here, we choose the construction such that the link can be represented as one of the links in connected sums

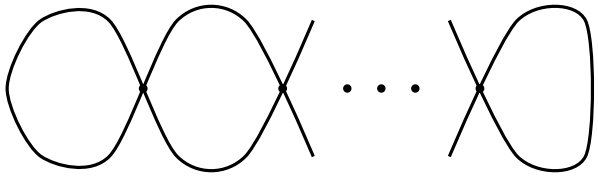

Figure 4.6: The planar 4-valent graph of complexity k used in the construction of the link families L_k, J_k, and K_k.

of $S^2 \times S^1$ illustrated by the surgery presentations on the left side of Figure 4.4.

We now consider P to be the boundary-decorated shadowed polyhedron obtained from $S(P)$ by decorating the innermost $(k+1)$ boundaries of $S(P)$ as internal boundaries with the remaining boundary components decorated as external boundaries. In the leftmost diagram of our example of Figure 4.5, this is demonstrated as the boundary-decorated shadowed polyhedron with singular set the dashed lines, with internal boundaries colored blue, and with external boundaries colored as black.

Now we consider the boundary-decorated shadowed polyhedron P' with newly introduced regions and gleam obtained by capping the internal boundaries with disks. We will label this set of regions by R_j. From Lemma 4.4.1, gluing disks to P corresponds to performing Dehn fillings along the internal boundary components where the new gleam is determined by the initial framing of the link. In order for P' to be a boundary-decorated shadowed polyhedron for the link complement in S^3, we can choose a framing such that the gleam of R_j is $\frac{V_{R_j}}{2}$ where V_{R_j} is the number of vertices of the singular set touching R_j.

In the second diagram from the left of Figure 4.5, this is shown by capping the blue colored boundary components by blue shaded disks with gleam $\frac{1}{2}$. As shown in Subsection 4.1.2, P' is of the form of a boundary-decorated shadowed polyhedron which can be used in constructing a link complement $S^3 \backslash \text{IntNbd}(L)$ where the link L corresponds to the boundary components of P'. Note that in Subsection 4.1.2, we constructed a pair (S^3, L) from a boundary-decorated shadowed polyhedron; however, in this case, the link complement comes from decorating the boundary of P' as external as opposed to internal.

Now from Proposition 4.1.5, we have a map f with a Stein surface W_f and Stein factor-

ization $f = g \circ h$ such that W_f can be identified with P' where the preimages of the points are as described in Proposition 4.1.5. Now by using the map h, we can find a homeomorphism between the fundamental shadow link and a specific link in S^3.

Previously, the Dehn fillings corresponded to gluing copies of the 2-handles $B^2 \times B^2$ to the 4-thickening of our boundary-decorated shadowed polyhedron P. We let $p_j \in R_j$ be the points in the 2-handles which correspond to the center of the capping disks. Under the map h, the preimages of the set of centers $\{p_j\}$ correspond to cores of tori. From Proposition 4.1.5, we can explicitly see that the preimages of $\{p_j\}$ form an unknotted link $\{p_j\} \times S^1$, denoted by L_0, embedded in $S^3 \backslash \text{IntNbd}(L)$ such that L_0 runs parallel to the z-axis. In our manifold $S^3 \backslash \text{IntNbd}(L)$, the link L_0 can be viewed as having framing ∞. In Figure 4.5, the link complement $S^3 \backslash \text{IntNbd}(L)$ with the ∞-framed link is illustrated in the third diagram from the left.

Next, we will remove the 2-handles which contain the ∞-framed link. This will add an additional toroidal boundary for each component of the link L_0. Our resultant manifold is homeomorphic to the link complement $S^3 \backslash \text{IntNbd}(L \sqcup L_0)$ with boundary-decorated shadowed polyhedron P'' where P'' can be obtained from decorating all of the boundary components of the simple polyhedron $S(P)$ as external boundaries.

As stated in Subsection 2.3.1, P'' is a boundary-decorated shadowed polyhedron for the complement of a fundamental shadow link. This implies that the union of the links L and L_0 in S^3 form the realization of the fundamental shadow link in S^3. This is shown as the right diagrams of Figure 4.4 as well as the rightmost diagram in Figure 4.5. Now since the complement of a fundamental shadow link of complexity k is a hyperbolic manifold of volume $2kv_8$ which satisfies the Turaev-Viro invariant volume conjecture, then through homeomorphisms, the complement of the link $L \sqcup L_0$ in S^3 is also a hyperbolic manifold satisfying the Turaev-Viro invariant volume conjecture with volume $2kv_8$.

□

Remark 4.4.3. Notice for the cases of the link families J_k and K_k, we can reduce our

fundamental shadow links of complexity k to one of complexity $(k-1)$ through certain ∞-framed Dehn surgeries. This can be done by performing the Dehn surgery on the rightmost of the $(k+1)$-unknotted components bounding the twice punctured disks.

Remark 4.4.4. For the link families of Figure 4.4, we implicitly used the following property of the surgery presentation of the link in S^3. Notice that each 0-framed unknotted component could be paired with a component of the fundamental shadow link to form a Hopf link pair in the surgery presentation. In the manifold of connected sums of $S^2 \times S^1$, the component of the Hopf link pair coming from a fundamental shadow link component is isotopic to the core of the tori obtained from the 0-framed surgery on the unknot component. This implies that we can isotope the fundamental shadow link component such that the removed torus in the complement corresponds to removing the torus from the 0-framed unknot surgery. In terms of the surgery diagrams on the left of Figure 4.4, we can obtain our link complements represented on the right by simply drilling out tori with cores the 0-framed unknot and deleting their corresponding fundamental shadow link components from the link. This procedure can work for any fundamental shadow link as long as we can pair as Hopf links every 0-framed unknotted component with a fundamental shadow link component such that all of the Hopf link pairs are disjoint.

Using the viewpoint of the Hopf link pairs on the surgery presentation, we immediately obtain the results of Theorem 4.4.2; however, this is generally not the case. As we will see in Theorem 4.5.1, from the surgery presentation, the Hopf link pairs may not always be disjoint from each other. This may be remedied through the use of Kirby calculus which is provided as an alternate proof; however, we can eliminate this technical issue by utilizing the Stein surface approach. Because of this, the Stein surface approach is a more natural method for generalizing our results. From the map equipped to the Stein surface, we are able to see that each capped disk corresponds to a Hopf link pair. Here, the boundary of the disk is the fundamental shadow link component, and the preimage of the center of the disk corresponds to our 0-framed unknotted component. In order to utilize this method, we

only need a boundary-decorated shadowed polyhedron of a fundamental shadow link which can be augmented by capping disks to a boundary-decorated shadowed polyhedron of the form P_L as defined in Subsection 4.1.2. From the explicit map, the 0-framed unknotted components always run parallel to the z-axis, therefore, all of the Hopf links pairs will be disjoint from each other.

By using Theorems 4.3.2 and 4.4.2, we can now provide an alternate proof to the Turaev-Viro invariant volume conjecture for the Borromean rings as well as extend the result to our initial motivation of the Borromean twisted sisters. Additionally, we can see that the complements of the link families L_k, J_k, and K_k are a generalization of the complements of the Borromean rings and the Borromean twisted sisters.

Corollary 4.4.5. *The Borromean rings and the Borromean twisted sisters shown in Figure 4.3 are hyperbolic links with volume $2v_8$ and satisfy the Turaev-Viro invariant volume conjecture.*

Proof. For the case of $k = 1$ for Theorem 4.4.2, we can see that the links L_1, J_1, and K_1 correspond to the links FSL 3, FSL 5, and FSL 6 in Figure 4.2, respectively. Since the Turaev-Viro invariant volume conjecture is preserved under homeomorphisms, then any links from Table 4.1 homeomorphic to the links FSL 3, FSL 5, and FSL 6 also satisfy the conjecture. From this, we can see that L_1, J_1, and K_1 have complements homeomorphic to the complements of the Borromean rings and the Borromean twisted sisters in Figure 4.3, respectively. In this sense, the complements of the link families L_k, J_k, and K_k are a generalization of the complements of the Borromean rings and the Borromean twisted sisters. □

We will end this section by demonstrating that the links in Theorem 4.4.2 provide new examples of links in S^3 which satisfy the Turaev-Viro invariant volume conjecture. Of the known examples of links in S^3 which satisfy the conjecture, the Whitehead chains are the only other infinite family. As detailed by Roland van der Veen in [58], the Whitehead chains

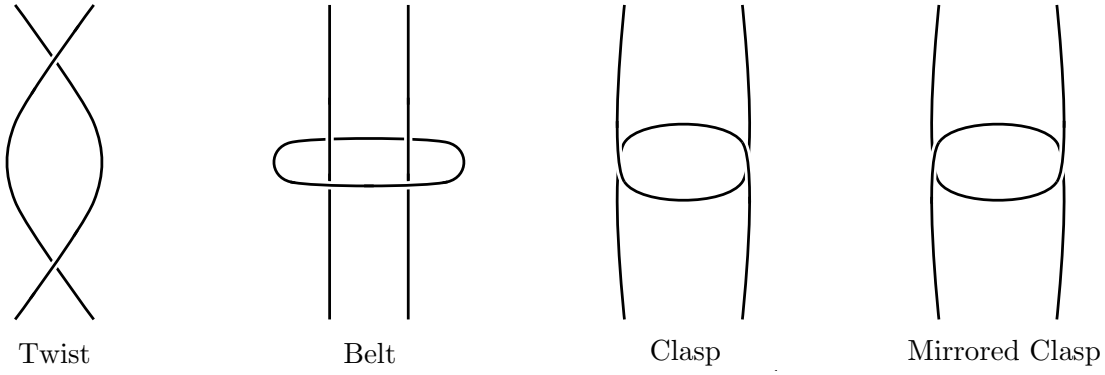

Figure 4.7: The diagrams of the twist, belt, clasp, and mirrored clasp components are illustrated, respectively.

$W_{a,b,c,d}$ are a family of links that can be constructed as the closure of the composition of a-twists, b-belts, c-clasps, and d-mirrored clasps shown in Figure 4.7. The Whitehead chains have the particularly nice property that when $b = 1$, the complement is hyperbolic with $Vol(W_{a,1,c,d}) = (c + d)v_8$. We will let $\mathcal{W}$ be this set of hyperbolic links.

Proposition 4.4.6. *For an integer $k \geq 3$, no link of Theorem 4.4 has complement homeomorphic to the complement of an element of $\mathcal{W}$.*

Proof. For every element in $\mathcal{W}$, the complement has volume $(c + d)v_8$ where c and d are the number of clasps and mirrored clasps, respectively. Since we want to compare the links in $\mathcal{W}$ with the fundamental shadow links, we will always assume that the volume is an even multiple of v_8. Notice that the number of components of the Whitehead chain will be $(c+d+1)$ because the clasps and mirrored clasps each add one component with the addition of the belt component.

Now for a fundamental shadow link of complexity k, the volume of the complement will be $2kv_8$. From the link families in Theorem 4.4.2, the number of components of the link will either be $(k + 2)$ or $(k + 3)$. In order for the Whitehead chains to have the same volume of $2kv_8$, they would need $(2k + 1)$ link components. This implies that when $k \geq 3$, every element of $\mathcal{W}$ with volume $2kv_8$ will have complement with more boundary components than the complements of the links L_k, J_k, and K_k in Theorem 4.4. Therefore, for $k \geq 3$,

no element of $\mathcal{W}$ has complement homeomorphic to the complement of a link appearing in Theorem 4.4. □

As we will see in Section 4.5, we can construct many links in S^3 which satisfy the Turaev-Viro invariant volume conjecture. By following a similar proof to Proposition 4.4.6, many of the links in Section 4.5 can also be shown to be new examples of links in S^3 which satisfy the Turaev-Viro invariant volume conjecture.

4.5 Augmenting Links in S^3

In this section, we will generalize our methodology used in the proof of Theorem 4.4.2 to show that every planar 4-valent graph corresponds to a fundamental shadow link which can be realized as a link in S^3. This is accomplished by considering the fundamental shadow link obtained by replacing each edge by the identity 3-braid. Since every link may be projected as a planar 4-valent graph, we will see that this implies that every link is a sublink of a fundamental shadow link realized in S^3. Therefore, we show that every link in S^3 may be augmented to a link whose complement satisfies the Turaev-Viro invariant volume conjecture.

Theorem 4.5.1. *For any G, a planar 4-valent graph of complexity k, there exists a corresponding fundamental shadow link realized in S^3 with hyperbolic volume $2kv_8$.*

Proof. As noted in Remark 4.4.4, the surgery presentation of a fundamental shadow link generally does not contain disjoint Hopf link pairs. By using the Stein surface approach, we only need to augment our boundary-decorated shadowed polyhedron by capping with disks to one that corresponds to the boundary-decorated shadowed polyhedron P_L in Subsection 4.1.2. By utilizing a particular construction of our graph G to a fundamental shadow link, we can guarantee that such an augmentation is always possible. As stated before, this is an advantage in using the Stein surface method; however, we also provide an alternate proof involving Kirby calculus which remedies the case when the Hopf link pairs are not disjoint.

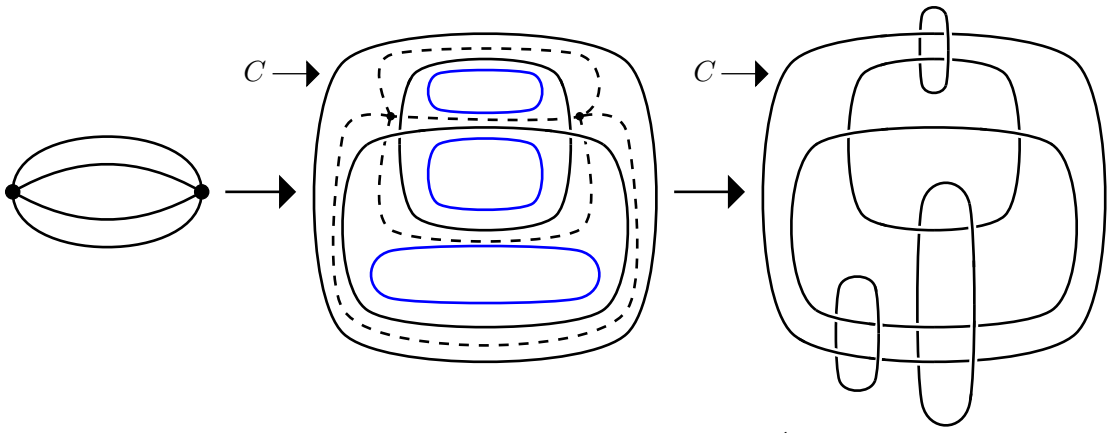

Figure 4.8: On the leftmost diagram, we have a planar 4-valent graph with complexity 2. From the graph, we obtain the boundary-decorated shadowed polyhedron shown in the middle illustration. Here, the edges were replaced by identity 3-braids, the outermost boundary is labeled C, the internal decorated boundaries are blue, the external decorated boundaries are black, and the singular set is dashed. As in Theorem 4.4.2, we cap the blue curves with disks and drill out the corresponding tori to recover the link in the third diagram.

We will begin with the proof where a small example of the general method can be found in Figure 4.8. Let G be a planar 4-valent graph of complexity k. From the graph G, we can consider the boundary-decorated shadowed polyhedron P obtained in the following way. We let P have the simple polyhedron $S(P)$ where the boundary is obtained from replacing all of the edges of G by the identity 3-braid and by replacing the vertices by the 6-stranded figure or its mirror. To recall the 6-stranded figure, see Figure 2.6. Notice that since we have chosen the identity 3-braids, there exists an outermost boundary component C in the sense that it bounds a disk D where $D \times (-\epsilon, \epsilon)$ contains the remaining components of $\partial(S(P))$ for some ϵ.

Now the boundaries of P are decorated such that the outermost boundary component is an external boundary, the boundaries which convey crossing information are external boundaries, and the remaining boundaries are internal boundaries. The decorations are chosen as such since we will be gluing disks onto the internal boundaries. This can be seen as the two leftmost illustrations of Figure 4.8. The leftmost illustration is an arbitrary planar 4-valent graph, and the following illustration shows the associated boundary-decorated shadowed

polyhedron P in S^3. Depicted in the figure, the outermost component is labeled C, the external boundaries are colored black, the internal boundaries are colored blue, and the singular set of P is dashed. It is worth noting that since we chose the identity 3-braids, the internal boundary components are in direct correspondence to all of the initial regions of the graph G excluding the outermost region.

Now since $\partial(P)$ contains an outermost region, we can obtain a boundary-decorated shadowed polyhedron for a link complement in S^3. This can be achieved in the same way as in the proof of Theorem 4.4.2 by gluing disks along the internal boundary components. By our initial choices, this will lead to a boundary-decorated shadowed polyhedron of the form P_L as in Subsection 4.1.2. As mentioned in Remark 4.4.4, from the map arising from the Stein surface of our specific boundary-decorated shadowed polyhedron, we can obtain a collection of Hopf link pairs where one component comes from the fundamental shadow link and the other from a 0-framed unknot component. Again, from the explicit map, the 0-framed unknot component runs parallel to the z-axis such that each Hopf link pair is disjoint, therefore, each capped region corresponds to adding an additional link component.

Finally, the collection of the link components coming from the external decorated boundary components along with the link components arising from the Hopf link pairs give a hyperbolic link in S^3 that is the realization of a fundamental shadow link with volume $2kv_8$. This can be seen in the rightmost illustration of Figure 4.8 where each blue colored internal decorated boundary component from the previous illustration now corresponds to a link component which runs parallel to the z-axis. □

Alternatively, we will provide a proof of Theorem 4.5.1 using a combination of the surgery presentation of the fundamental shadow link along with Kirby calculus.

Alternate proof of Theorem 4.5.1. We will let G be a planar 4-valent graph of k vertices, and we pick a maximal tree T. For convenience, we will consider G as a graph on S^2 such that the *outermost region* is defined to contain the point ∞. We will now define two regions of our graph to be *adjacent* if there exists an edge in $G\backslash T$ which is adjacent to both of them.

Notice that since T is a maximal tree, then T contains no cycles. This implies that any two regions of G are related by a sequence of adjacent regions. In particular, we have that every region is related to the outermost region through a sequence of adjacent regions. We also note that any two adjacent regions are adjacent by exactly one edge of $G\backslash T$.

We will now consider the surgery presentation construction from a planar 4-valent graph given in Subsection 2.3.2. We begin by replacing the edges of the graph by identity 3-braids, replacing the vertices of the graph by the 6-stranded figure or its mirror, and encircling the 3-braids corresponding to the edges of $G\backslash T$ by 0-framed unknots. From this construction, we can see that every region of the graph which is adjacent to an edge $G\backslash T$ will be punctured by at least one 0-framed unknot. Also notice that each region of G will correspond to an unknotted fundamental shadow link component obtained from replacing the edges by the trivial 3-braid. Excluding the component arising from the outermost region which we denote by C, the link components corresponding to the regions will eventually form part of the Hopf link pairs mentioned in Remark 4.4.4. With the exception of the link component C, we will denote the collection of the disks these fundamental shadow link components bound by $\{D_i\}_{i\in I}$ with corresponding regions of G denoted by $\{S_i\}_{i\in I}$.

We will now perform a sequence of handleslides such that each disk D_i is punctured by exactly one 0-framed unknot. This will ensure that our Hopf link pairs will all be disjoint. Now from the construction, given any two adjacent regions, there exists a 0-framed unknot which corresponds to the edge between them. We first consider the collection of regions $\{S_i\}_{i\in I_1}$ of G where I_1 is a subset of I such that the regions are adjacent to the outermost region. As the corresponding 0-framed unknots only puncture the collection of disks $\{D_i\}_{i\in I_1}$, we will leave them alone.

Next, we consider the collection $\{S_i\}_{i\in I_2}$ of regions of G which are adjacent to the collection $\{S_i\}_{i\in I_1}$. Since this collection of corresponding 0-framed unknots also puncture the previous collection $\{D_i\}_{i\in I_1}$, we can see that the Hopf link pairs are currently not disjoint. Now by performing handleslides of the 0-framed unknots arising from the edges between

$\{S_i\}_{i\in I_1}$ and $\{S_i\}_{i\in I_2}$ over the 0-framed unknots corresponding to the edges between $\{S_i\}_{i\in I_1}$ and the outermost region, each $D_{i\in I_1}$ will be punctured by exactly one 0-framed unknot. Additionally, for clarity, we can isotope the two sets of 0-framed unknots such that each 0-framed unknot is parallel to the z-axis and punctures exactly one element of $\{D_i\}_{i\in I_1\cup I_2}$. We can now see that the Hopf link pairs corresponding to the disks $\{D_i\}_{i\in I_1}$ are each disjoint.

Next, we consider the collection of regions $\{S_i\}_{i\in I_3}$ which are adjacent to $\{S_i\}_{i\in I_2}$ with $I_3 \cap I_1 = \emptyset$. Similar to before, the corresponding 0-framed unknots arising from the edges between the regions $\{S_i\}_{i\in I_3}$ and $\{S_i\}_{i\in I_2}$ will puncture the disks $\{D_i\}_{i\in I_3}$ as well as also puncturing the collection $\{D_i\}_{i\in I_2}$. This will create Hopf link pairs which are not disjoint. We can again perform handleslides on the 0-framed unknots which puncture both the disks $\{D_i\}_{i\in I_2}$ and $\{D_i\}_{i\in I_3}$ over the adjacent previous collection of 0-framed unknots. By our isotopy of the previous collection of 0-framed unknots, the 0-framed unknots corresponding to the edges between $\{S_i\}_{i\in I_2}$ and $\{S_i\}_{i\in I_3}$ will also be parallel to the z-axis after the handleslide. Once again, our three sets of 0-framed unknots will each only puncture one element of $\{D_i\}_{i\in I_1\cup I_2\cup I_3}$.

Now lastly, since any two regions are related by a sequence of adjacent regions, we can perform these handleslides until every disk of $\{D_i\}_{i\in I}$ is punctured exactly once by a 0-framed unknot which is parallel to the z-axis. Notice that in the end, we obtain a surgery presentation which is the same as the one obtained from the Stein surface approach. In this case, each of the Hopf link pairs are disjoint from each other, and we can proceed as in Remark 4.4.4. Thus, this concludes the alternate proof of Theorem 4.5.1 using the surgery presentation of the fundamental shadow link along with Kirby calculus.

□

Now as a simple application of Theorem 4.5.1, we obtain the following result.

Corollary 4.5.2. *Every link $J \subset S^3$ is a sublink of a link $L \subset S^3$ such that the link complement $S^3\backslash\mathrm{IntNbd}(L)$ is homeomorphic to a fundamental shadow link complement and satisfies the Turaev-Viro invariant volume conjecture.*

Proof. Let J be a link in S^3. Under isotopies of the link, we can obtain a projection G of J such that G is a planar 4-valent graph where we keep track of the crossing information at each vertex. Note that we may need to introduce crossings of the link through isotopies such that G is connected. Now we follow the same fundamental shadow link construction from Theorem 4.5.1; however, we choose to replace the vertices of our graph by the 6-stranded figure or its mirror such that the crossing information is consistent with the original link J. Notice that since we kept track of the crossing information while replacing the vertices, the link components which correspond to the set $\partial_{ext}(P)\backslash\{C\}$ form our initial link J.

Lastly, we can see that J is now a sublink of the link L which is the realization of the fundamental shadow link in S^3 constructed from Theorem 4.5.1. Therefore, we have that $J \subset L \subset S^3$ such that the link complement $S^3\backslash\text{IntNbd}(L)$ satisfies the Turaev-Viro invariant volume conjecture. □

4.5.1 The Algorithm for Augmentation

Corollary 4.5.2 tells us that we can always augment our link to eventually satisfy the Turaev-Viro invariant volume conjecture. Moreover, the augmentation can be seen explicitly through following the proofs of Theorem 4.5.1 and Corollary 4.5.2; however, for convenience, we will summarize the explicit augmentation in terms of the closure of braids.

Definition 4.5.3. For a braid in the braid group $b \in B_n$, we say b is an *unreduced word* if we do not cancel pairs of elements of the form $\sigma_i\sigma_i^{-1}$ or $\sigma_i^{-1}\sigma_i$. Additionally, we define the *length* of b to be the number of standard generators appearing in the unreduced word b.

The following corollary requires that each generator appears in the braid b at least once; however, since the result is stated in terms of the unreduced word, we can obtain a new unreduced word by adding the elements $\sigma_i\sigma_i^{-1}$ or $\sigma_i^{-1}\sigma_i$ without changing the link in the closure of the braid. By a classical result of Alexander [2] which states that every link is the closure of a braid, Corollary 4.5.4 also implies that every link can be augmented to a link with more components that satisfies the Turaev-Viro invariant volume conjecture.

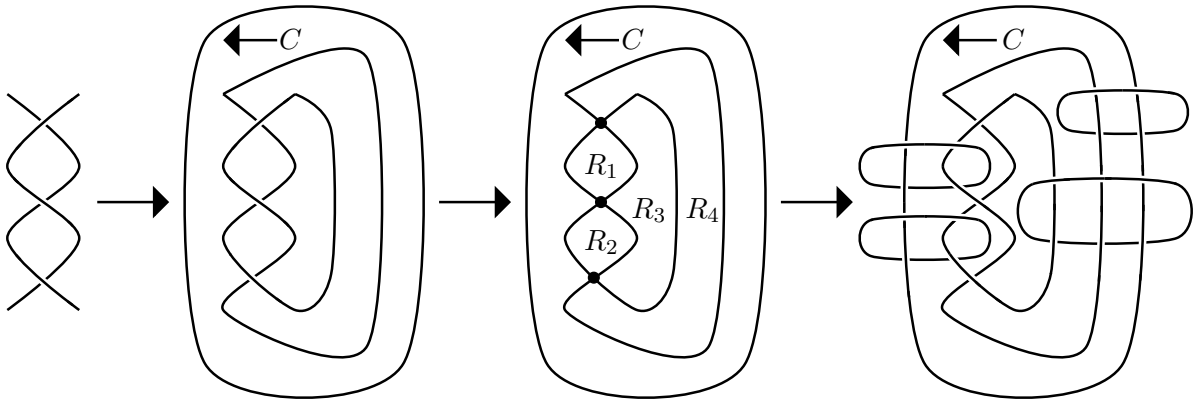

Figure 4.9: As shown in the first two diagrams, we begin with the unreduced word $b = \sigma_1\sigma_1^{-1}\sigma_1^{-1} \in B_2$ which we embed into B_3, and we take the closure of the new braid with outermost component labeled C. The projection of the second diagram onto S^2 gives the third diagram where we label the regions not touching C with R_i. Now each region R_i corresponds to a link component parallel to the z-axis given in the final diagram. The final diagram is of a hyperbolic link that has volume $6v_8$, satisfies the Turaev-Viro invariant volume conjecture, and contains $\hat{b}$ as a sublink.

Corollary 4.5.4. *Let $b \in B_n$ be an unreduced word of length k with each generator appearing at least once. Then the braid closure $\hat{b}$ is a sublink of a link L in S^3 where the complement $S^3\backslash\text{IntNbd}(L)$ satisfies the Turaev-Viro invariant volume conjecture and has volume $2kv_8$.*

Proof. Since $\hat{b}$ is a link in S^3, the result is almost immediate by Corollary 4.5.2; however, we require that each generator appears at least once so that the associated planar 4-valent graph is connected. Additionally, notice that each generator contributes a vertex to the planar 4-valent graph. Therefore, the complexity of the planar 4-valent graph is equal to the length of b. This implies that our resulting hyperbolic manifold has volume $2kv_8$ where k is the length of the unreduced word b. □

We will proceed to wrap up the subsection by summarizing the link augmentation algorithm from a braid group element. A simple example of the augmentation can be seen in Figure 4.9 for the unknot as the closure of the unreduced word $\sigma_1\sigma_1^{-1}\sigma_1^{-1} \in B_2$. Since our initial braid has length 3, then the resulting hyperbolic volume of the link complement will be $6v_8$ by Corollary 4.5.4.

Let L be a link, and let $\hat{b}$ for $b \in B_n$ be its braid closure where b has at least one of every

generator. We begin by embedding b into the larger braid group B_{n+1} which we denote by b' such that each generator σ_i is sent to σ_{i+1}. This can be viewed as adding a new individual strand in front of the original braid b. This new strand will correspond to the outermost component C in the closure.

Now from the braid closure of $\hat{b'}$, we will add new link components to obtain our link L. Consider the projection $p(\hat{b'})$ onto the surface S^2 such that each crossing is now a vertex. Excluding the regions touching C, each region of the projection will correspond to a link component in the augmentation.

We will proceed to count the resulting regions. Since $p(\hat{b'})$ is a graph in S^2, the Euler characteristic $\chi(S^2) = 2 = v - e + r$ where v, e, and r are the number of vertices, edges, and regions, respectively. Now each vertex corresponds to a generator such that $v = k$, and since we have a 4-valent graph, then $e = 2k$. Through a quick calculation which includes the additional region obtained from C, we see that $r = (k + 3)$.

Lastly, since we do not need to add link components to the two regions touching C, we can obtain our link L by adding components parallel to the z-axis in each of the remaining $(k + 1)$ corresponding regions of $\hat{b'}$.

Chapter 5

Applications Towards the AMU Conjecture

In this chapter, we construct elements in the surface mapping class groups which satisfy the AMU conjecture. This is achieved by using the intrinsic relationship between the Turaev-Viro invariant and the quantum representations as stated in Theorem 2.2.16. The links obtained in Chapter 4 can be realized as mapping tori such that the corresponding monodromies satisfy the AMU conjecture. With the exception of Section 5.3, we note that the results of this chapter first appeared in [36] by the author of this dissertation.

5.1 Background

In this section, we will briefly discuss the Stallings fibration which has a useful application in constructing elements of the surface mapping class groups which satisfy the AMU conjecture.

5.1.1 The Stallings Fibration

We will begin with the following definitions.

Definition 5.1.1. An element $b \in B_n$ is a *homogeneous braid* if each standard generator appearing in b always appears with the same sign.

Definition 5.1.2. For an oriented link L in S^3, a *Seifert surface* is a connected, compact, and oriented surface contained in S^3 such that the oriented boundary is the oriented link L.

Seifert showed algorithmically that every oriented link in S^3 has a Seifert surface. A brief introduction of Seifert surfaces may be found in [38, Chapter 2]. Although we will not provide the procedure in this work, we will note that the equation for calculating the genus of the Seifert surface for the closure of a braid $b \in B_s$ constructed with Seifert's algorithm is

$$g = \frac{2 + \#(\text{Crossings}) - \#(\text{Components}) - s}{2}. \tag{5.1}$$

Now in [53], Stallings showed that the complement of the closure of any homogeneous braid is fibered over S^1. In these cases, the fiber surface is $\Sigma_{g,n}$ where the surface is obtained using Seifert's algorithm. In particular, the complement of the closure of the homogeneous braid is a mapping torus of the Seifert surface $\Sigma_{g,n}$ for some $f \in Mod(\Sigma_{g,n})$. In addition, Stallings showed that there is an operation which takes a fibered link and transforms it into another fibered link with the same fiber surface.

Definition 5.1.3. A *Stallings twist* is the operation of performing a $1/m$-surgery on a simple closed curve of the fiber surface where the framing of the curve is induced by the normal vector of the surface.

In general, the Stallings twist may be trivial in the sense that the newly obtained link complement may still be homeomorphic to the complement of the original link. In [18], the authors demonstrate a criterion in obtaining non-trivial Stallings twists. They show that as long as the braid contains either the elements $\sigma_i^2\sigma_{i+1}^{-2}$ or $\sigma_i^{-2}\sigma_{i+1}^2$, then the closure of the braid admits non-trivial Stallings twists on the fiber surface.

As mentioned in Subsection 1.3.1, we recall that two elements $f, g \in Mod(\Sigma_{g,n})$ are independent if there is no $h \in Mod(\Sigma_{g,n})$ such that both f and g are conjugate to non-trivial powers of h. An important utility of the Stallings twist is that we can obtain infinitely many pairwise independent pseudo-Anosov mapping class group elements as stated in the following.

Theorem 5.1.4 ([18], Theorem 5.4)**.** *Let L be a hyperbolic fibered link with fiber Σ and monodromy f. Suppose that L contains a sublink K with $lTV(S^3 \backslash K) > 0$. Suppose, moreover, that the fiber Σ admits a non-trivial Stallings twist along a curve $c \subset \Sigma$ such that the interior of the twisting disc D intersects K at most once geometrically. Let τ_c denote the Dehn twist of Σ along c. Then the family $\{f \circ \tau_c^m\}_m$ of homeomorphisms give infinitely many pairwise independent pseudo-Anosov mapping class group elements in $Mod(\Sigma)$ that satisfy the AMU conjecture.*

Later in Subsection 5.2.1, we will use Theorem 5.1.4 on a particular family of links to construct infinitely many pairwise independent pseudo-Anosov mapping class group elements which satisfy the AMU conjecture.

5.2 Constructions of Pseudo-Anosov Elements

In this section, we construct elements in the mapping class group of the compact and orientable surface $\Sigma_{g,n}$. We will accomplish this using a combination of techniques involving the Stallings fibration, Theorem 4.3.2, and Corollary 4.5.4. At the end of the section, we will define an explicit family of pure braids all of which satisfy the AMU conjecture.

5.2.1 Applications of the Stallings Fibration

In this subsection, we will provide new results of pseudo-Anosov elements in surfaces $\Sigma_{g,n}$ which satisfy the AMU conjecture. The main result of the subsection can be stated as follows.

Theorem 5.2.1. *Given $g \geq 0$, there exists a pseudo-Anosov element in $Mod(\Sigma_{g,4})$ that satisfies the AMU conjecture. Furthermore, for $g \geq 3$, there are infinitely many pairwise independent pseudo-Anosov elements in $Mod(\Sigma_{g,4})$ that satisfy the AMU conjecture.*

The consequence of Theorem 5.2.1 is that we can find a pseudo-Anosov element for every surface with four boundary components such that it satisfies the AMU conjecture. As it

is a direct consequence of the other results of this subsection, we will reserve the proof of Theorem 5.2.1 until the end.

We will begin with a simple application of the Stallings fibration to the links in S^3 up to 11-crossings which are the realization of the fundamental shadow links of complexity one.

LinkInfo Name	Braid Group B_s	Homogeneous Braid	Fiber Surface
L_{6a4}	$s=3$	$(\sigma_1\sigma_2^{-1})^3$	$\Sigma_{1,3}$
L_{6a4}	$s=3$	$(\sigma_1^{-1}\sigma_2)^3$	$\Sigma_{1,3}$
L_{8n7}	$s=4$	$\sigma_1\sigma_2^{-2}\sigma_1\sigma_3^{-1}\sigma_2^{-2}\sigma_3^{-1}$	$\Sigma_{1,4}$
L_{10n87}	$s=3$	$\sigma_1^3\sigma_2^2\sigma_1^2\sigma_2^2\sigma_1$	$\Sigma_{3,3}$
L_{10n97}	$s=4$	$\sigma_1^{-3}\sigma_2^{-2}\sigma_1^{-1}\sigma_3^{-1}\sigma_2^{-2}\sigma_3^{-1}$	$\Sigma_{2,4}$
L_{10n108}	$s=4$	$(\sigma_1^{-1}\sigma_2^{-1})^3\sigma_3\sigma_2^{-2}\sigma_3$	$\Sigma_{2,4}$
L_{11n385}	$s=4$	$(\sigma_1^{-1}\sigma_2^{-1})^3\sigma_3\sigma_2^{-2}\sigma_3\sigma_2^{-1}$	$\Sigma_{3,3}$

Table 5.1: The fundamental shadow links up to 11-crossings written as the closure of a homogeneous braid such that the fiber surface is given by the Stallings fibration.

Corollary 5.2.2. *The monodromy of the closure of the braids in Table 5.1 obtained from the Stallings fibration is pseudo-Anosov and satisfies the AMU conjecture.*

Proof. From Theorem 4.3.2, the link complements appearing in Table 5.1 are homeomorphic to the complement of a fundamental shadow link. Therefore, they all are hyperbolic and satisfy the Turaev-Viro invariant volume conjecture. Since they are hyperbolic and by Theorem 2.2.8, any corresponding monodromy as a mapping torus will be pseudo-Anosov. Since they satisfy the Turaev-Viro invariant volume conjecture and by Theorem 2.2.16, then their monodromies will also satisfy the AMU conjecture.

To end the proof, we will compute the fiber surfaces of the links in Table 5.1. Because the fiber surface is obtained from Seifert's algorithm on a braid closure, Equation (5.1) will allow us to compute the genus as

$$g = \frac{2 + \#(\text{Crossings}) - \#(\text{Components}) - s}{2}.$$

Here, #(Crossings) is the length of the homogeneous braid, and #(Components) is the

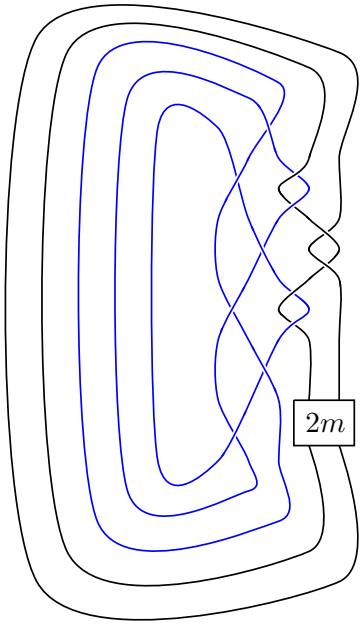

Figure 5.1: The link $L_{5,m}$ where the box indicates $2m$ negative crossings. Here, the Borromean rings are the blue colored sublink.

number of components of the closure of the braid. This quick computation leads to the fiber surfaces shown on the rightmost column of Table 5.1. □

Next, we will construct infinitely many pairwise independent pseudo-Anosov mapping class group elements using Corollary 5.2.2. The techniques utilized here were developed in [18]. In their work, the authors build a 2-parameter family of links which contains the figure-eight knot as a sublink in order to create their examples. Their method relies on Theorem 5.1.4, and thus, it is necessary for their sublink to have an exponentially growing Turaev-Viro invariant. By using the links in Corollary 5.2.2 where the Turaev-Viro invariant volume conjecture is known, we can consider similar steps to construct a 2-parameter family of links which also may be used to find examples satisfying the AMU conjecture. In this subsection, we will only focus on using the Borromean rings. This specific choice of link will be made clear in Remark 5.2.4.

We will begin to define our 2-parameter family of links $L_{n,m}$ for $n \geq 4$ and $m \geq 1$ where

n is the number of components. Necessary for the proof of our next proposition, we will build $L_{n,m}$ such that it is alternating and the closure of a homogeneous braid. We first let L be the Borromean rings which corresponds to the link L_{6a4} in Tables 4.1 and 5.1. As noted in Corollary 5.2.2, the Borromean rings have the property that they may be represented as the closure of a homogeneous braid $(\sigma_2^{-1}\sigma_1)^3 \in B_3$. We will now proceed to define C_i to be the component obtained as the closure of the i-th strand of the homogeneous braid such that $C_1 \cup C_2 \cup C_3 = L$.

We will begin by defining the link for the case $L_{5,m}$ which is the union of L with the additional components C_4 and C_5 shown in Figure 5.1. In Figure 5.1, the parameter m indicates the number of negative full-twists, or equivalently, $2m$ negative crossings. Additionally, we can notice that our braid contains the subword $\sigma_3^2\sigma_4^{-2}$. As mentioned in Subsection 5.2.1, this implies that we will be able to later utilize a non-trivial Stallings twist.

From $L_{5,m}$, we will inductively begin to add additional components C_i for $6 \leq i \leq n$ such that the union of the components defines our link $L_{n,m}$. In order to build $L_{n+1,m}$ from a given $L_{n,m}$, we add a new strand with closure C_{n+1} in the following way. From the viewpoint of following along C_n, we see that C_n has 2 crossings with C_{n+1}, followed by 2 crossings with C_{n-1}, and then ending with 2 more crossings with C_{n+1} where the signs of the crossings are chosen such that the link $L_{n+1,m}$ is always alternating. Each time we continue with this procedure of inserting a new component, we introduce 4 more crossings to the link.

Lastly, for the special case when $n = 4$, we simply replace the $2m$ negative crossings in $L_{5,m}$ with $(2m-1)$ negative crossings. The resultant link will be our 4-component link denoted by $L_{4,m}$.

We will now proceed with finding our elements in the mapping class group using the 2-parameter link family $L_{n,m}$.

Proposition 5.2.3. *Suppose that either $n = 4$ and $g \geq 3$, or $g + 2 \geq n \geq 5$, then there are infinitely many pairwise independent pseudo-Anosov elements of $Mod(\Sigma_{g,n})$ that satisfy the AMU conjecture.*

Proof. By construction, the 2-parameter link family $L_{n,m}$ contains the Borromean rings as a sublink for every $n \geq 4$ and $m \geq 1$. Now notice by Proposition 2.1.6, drilling out tori from our 3-manifold does not decrease the exponential growth rate of our Turaev-Viro invariant. In particular, if we start with any link where the Turaev-Viro invariant grows exponentially, then any new link obtained by adding additional components will also have the Turaev-Viro invariant growing exponentially. Since the Borromean rings have this property, this is also the case for the 2-parameter link family $L_{n,m}$ which contains the Borromean rings as a sublink. Now by Theorem 2.2.16, any mapping torus of the link complement of $L_{n,m}$ will have its corresponding element in the mapping class group satisfy the AMU conjecture.

Additionally, our link family $L_{n,m}$ will be hyperbolic by Menasco's criterion [41] which states that any prime, non-split, and alternating diagram of a link that is not the standard diagram of the $T(2, q)$ torus link is a hyperbolic link. By Theorem 2.2.8, this implies that the element in the mapping class group is also pseudo-Anosov.

Now by construction, our 2-parameter link family $L_{n,m}$ is the closure of a homogeneous braid such that we can consider its Stallings fibration with fiber surface $\Sigma_{g,n}$ for some g. As noted previously, our corresponding braid contains the subword $\sigma_3^2\sigma_4^{-2}$ such that we have a non-trivial Stallings twist. Now by Theorem 5.1.4, we can obtain infinitely many pairwise independent pseudo-Anosov elements satisfying the AMU conjecture for each fiber surface obtained from $L_{n,m}$ using the Stallings fibration.

We will end the proof by calculating the genus for each of the fiber surfaces $\Sigma_{g,n}$ of the Stallings fibration of $L_{n,m}$. From Equation (5.1), we can calculate the genus of the homogeneous braid as

$$g = \frac{2 + \#(\text{Crossings}) - n - s}{2}$$

where n is the number of components and s the index of the corresponding braid group.

We first consider the case when $n = 4$. By counting, we have $(2m + 11)$ crossings with

braid group B_5 such that $s = 5$. We can calculate that

$$g = \frac{2 + \#(\text{Crossings}) - n - s}{2} = \frac{2m + 4}{2} = m + 2,$$

therefore, $g = m + 2$ for $m \geq 1$.

Now we consider the case for $n \geq 5$. Here, the number of components is equal to the index of the braid group such that $n = s$. As mentioned earlier, each time we increase n by one, we add four additional crossings. This implies that there are $(2m + 4n - 8)$ crossings. From this, we calculate that

$$g = \frac{2 + \#(\text{Crossings}) - n - s}{2} = \frac{2m + 2n - 6}{2} = m + n - 3,$$

therefore, $g = m + n - 3$ for $m \geq 1$. These two cases imply our final result that our fiber surface $\Sigma_{g,n}$ has either $n = 4$ and $g \geq 3$, or $g + 2 \geq n \geq 5$. □

As mentioned previously, Proposition 5.2.3 and its proof should be compared to [18, Theorem 1.4]. Here, the authors similarly find infinitely many pairwise independent pseudo-Anosov elements for the surface $\Sigma_{g,n}$ where $n = 2$ and $g \geq 3$, or $g \geq n \geq 3$. Although the method is the same, by considering the Borromean rings as opposed to the figure-eight knot as our sublink, we gain additional infinite families for $Mod(\Sigma_{g,n})$ for certain g and n not previously discussed. Noticeably, their examples always have genus larger than or equal to the number of boundary components; however, with the Borromean rings, we can obtain infinitely many pairwise independent pseudo-Anosov elements where the genus is strictly less than the number of boundary components.

Remark 5.2.4. An important aspect of the proof of Proposition 5.2.3 is the use of Menasco's criterion. Because of this, we chose to use the Borromean rings from Table 5.1 as our example. In this case, our 2-parameter family $L_{n,m}$ will be alternating which will then imply that the link is hyperbolic by Menasco's criterion. Our previous construction would have worked with

any other homogeneous braid from Table 5.1; however, the resulting manifold may not be hyperbolic. In these cases, the Turaev-Viro invariant will still grow exponentially; however, the associated mapping class group element may not be pseudo-Anosov. Instead, the element may only be reducible and contain pseudo-Anosov parts. In either of these two settings, the conclusion of the AMU conjecture will still follow.

We will now end the subsection with a proof of Theorem 5.2.1.

Proof of Theorem 5.2.1. It is immediate that the combination of Corollary 5.2.2 and Proposition 5.2.3 provides a pseudo-Anosov element of $Mod(\Sigma_{g,4})$ for every $g \geq 1$. In particular, we see from Proposition 5.2.3 that for $g \geq 3$, there are infinitely many pairwise independent pseudo-Anosov elements satisfying the AMU conjecture. For the case when $g = 0$, Andersen, Masbaum, and Ueno in [3] verified the conjecture for every pseudo-Anosov element in $Mod(\Sigma_{0,4})$ as noted in Section 1.3. □

5.2.2 Applications of Corollary 4.5.4

In this subsection, we will demonstrate how Corollary 4.5.4 may be utilized to construct links fibering over S^1. As we will see in Subsection 5.2.3, Subsection 5.2.2 will be used in preparation of obtaining additional examples of pseudo-Anosov elements in the mapping class group which satisfy the AMU conjecture. We also note that the results of Theorem 5.2.5 are obtained using the fundamental shadow links. Therefore, any of the corresponding manifolds will also satisfy the Turaev-Viro invariant volume conjecture.

Our main result of the subsection states that given any complexity k, we can find a fundamental shadow link which fibers over S^1 with fiber surface a disk with punctures. In order to write the statement, we will first define the family of braids $\{b_k\}$ as follows:

- For $k = 1$, define $b_k := \sigma_1^{-2}\sigma_2^2 \in B_3$.

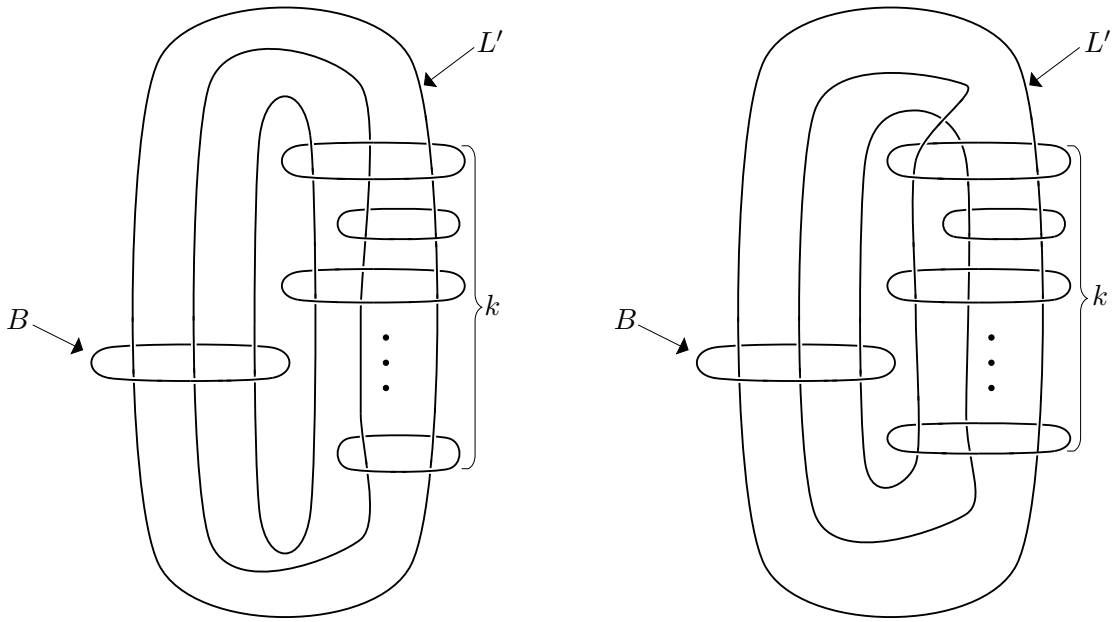

Figure 5.2: The complexity k fundamental shadow links realized in S^3 obtained from the braid family α_k. On the left, for k even, there are $(k+4)$ components, and on the right, for k odd, there are $(k+3)$ components. Here, our eventual braid axis component is labeled as B, and the component that bounds a $(k+1)$-punctured disk is labeled L'.

- For $k = 2m$, define $b_k \in B_{k+3}$ by

$$b_k := \prod_{i=1}^{m} (\sigma_{2i+1}\sigma_{2i} \cdots \sigma_3\sigma_2\sigma_1^2\sigma_2^{-1}\sigma_3\sigma_4 \cdots \sigma_{2i}\sigma_{2i+1})(\sigma_{2i+2}\sigma_{2i+1} \cdots \sigma_3\sigma_2^2\sigma_3 \cdots \sigma_{2i+1}\sigma_{2i+2}).$$

- For $k = 2m-1$, define $b_k \in B_{k+3}$ by

$$b_k := \sigma \prod_{i=2}^{m} (\sigma_{2i}\sigma_{2i-1} \cdots \sigma_3\sigma_2^2\sigma_3 \cdots \sigma_{2i-1}\sigma_{2i})(\sigma_{2i+1}\sigma_{2i} \cdots \sigma_3\sigma_2\sigma_1^2\sigma_2^{-1}\sigma_3\sigma_4 \cdots \sigma_{2i}\sigma_{2i+1}),$$

  where $\sigma = (\sigma_1)(\sigma_3\sigma_2\sigma_1^2\sigma_2^{-1}\sigma_3)$.

Theorem 5.2.5. *For $k \geq 1$, let $M_k := S^3 \backslash \mathrm{IntNbd}(\overline{b_k})$ denote the complement of the braided link $\overline{b_k}$. Then*

1.) M_k fibers over S^1 with fiber surface a disk with punctures,

2.) M_k is hyperbolic with volume $2kv_8$, and

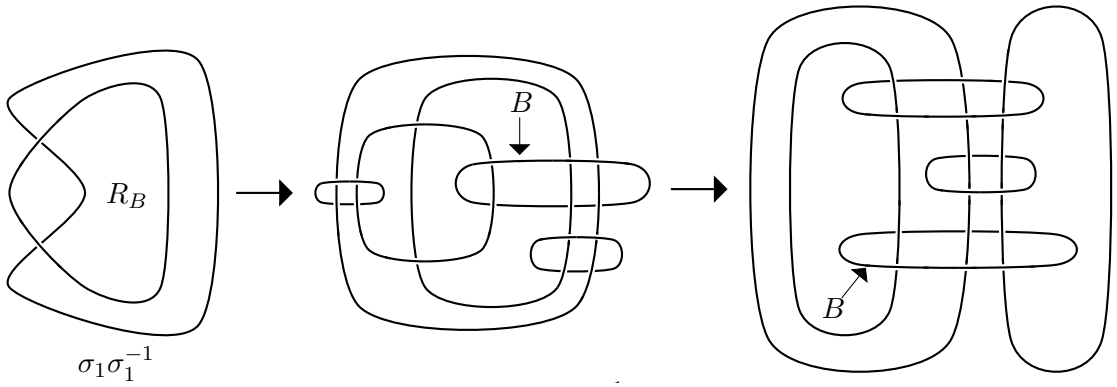

Figure 5.3: On the leftmost diagram, we have the closure of the braid $\alpha_2 = \sigma_1\sigma_1^{-1}$ with the region labeled R_B corresponding to the B labeled component in the second diagram. From the braid, we can apply Corollary 4.5.4 to obtain the link in the second diagram where B will eventual be the braid axis component. Through an isotopy, we obtain the link in the third diagram.

3.) M_k satisfies the Turaev-Viro invariant volume conjecture.

Proof. For $k \geq 2$, we will begin by considering the unreduced braids $\alpha_k = (\sigma_1\sigma_1^{-1})^{\frac{k}{2}}$, for k even, and $\alpha_k = \sigma_1(\sigma_1^{-1}\sigma_1)^{\frac{k-1}{2}}$, for k odd. Now from the braids α_k, we will apply Corollary 4.5.4 followed by an isotopy to obtain either the left link in Figure 5.2, for k even, or the right link, for k odd. For clarity, an example is shown in Figure 5.3 for when $k = 2$. In this case, the region corresponding to the component B is labeled as R_B. Now since our link is always constructed from the closure of a braid, we will always have an inside region R_B, and we can label the corresponding component in the link by B as shown in Figure 5.2. Eventually, the component B will be our braid axis in our fibered link. We note that when k is even, the sublink obtained from the braid closure of α_k contains two components. In the case when k is odd, the sublink obtained from the braid closure of α_k contains only one component. This accounts for the difference between the total components in the left and right diagrams of Figure 5.2.

Now we let L be a link of Figure 5.2 with link component L' as labeled. Notice that L' bounds a $(k+1)$-punctured disk where one of the punctures comes from the component B. We consider the self-homeomorphism obtained by performing a full-twist along the $(k+1)$-punctured disk that L' bounds. Under this self-homeomorphism, we will obtain a new link

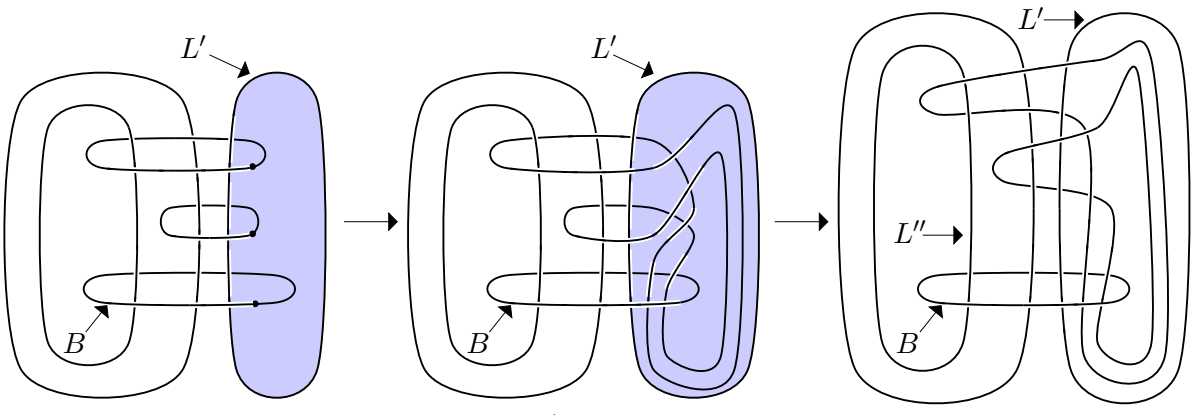

Figure 5.4: The case of obtaining a fibration for $k = 2$. Performing a full-twist on the 3-punctured disk shaded blue in the leftmost diagram results in the middle diagram. Through an isotopy of the link, we obtain a link fibering over S^1 with fiber surface D_5 as represented by the last diagram. Here, the monodromy may be written explicitly as $(\sigma_3\sigma_2\sigma_1^2\sigma_2^{-1}\sigma_3)(\sigma_4\sigma_3\sigma_2^2\sigma_3\sigma_4)$.

in S^3 where we define the complement of the manifold as M_k. In this new link, B, as a braid axis, now bounds a $(k+3)$-punctured disk D_{k+3}. The components of our new link in S^3 may now be isotoped to our defined braided link $\overline{b_k}$. Since we initially began with a fundamental shadow link of complexity k, our manifold M_k will be hyperbolic with volume $2kv_8$ and satisfy the Turaev-Viro invariant volume conjecture.

Now from the relationship between braided links and mapping tori, we will see that our link may be viewed as a mapping torus $M(\Gamma(b_k))$ where Γ is the surjective homomorphism between B_{k+3} and $MCG(D_{k+3})$ defined in Subsection 2.2.2. Additionally, the family b_k in B_{k+3} will be seen explicitly as the elements

$$\prod_{i=1}^{m}(\sigma_{2i+1}\sigma_{2i}\cdots\sigma_3\sigma_2\sigma_1^2\sigma_2^{-1}\sigma_3\sigma_4\cdots\sigma_{2i}\sigma_{2i+1})(\sigma_{2i+2}\sigma_{2i+1}\cdots\sigma_3\sigma_2^2\sigma_3\cdots\sigma_{2i+1}\sigma_{2i+2}),$$

when $k = 2m$, and

$$(\sigma_1\sigma_3\sigma_2\sigma_1^2\sigma_2^{-1}\sigma_3)\prod_{i=2}^{m}(\sigma_{2i}\sigma_{2i-1}\cdots\sigma_3\sigma_2^2\sigma_3\cdots\sigma_{2i-1}\sigma_{2i})(\sigma_{2i+1}\sigma_{2i}\cdots\sigma_3\sigma_2\sigma_1^2\sigma_2^{-1}\sigma_3\sigma_4\cdots\sigma_{2i}\sigma_{2i+1}),$$

when $k = 2m-1$ and $k \neq 1$.

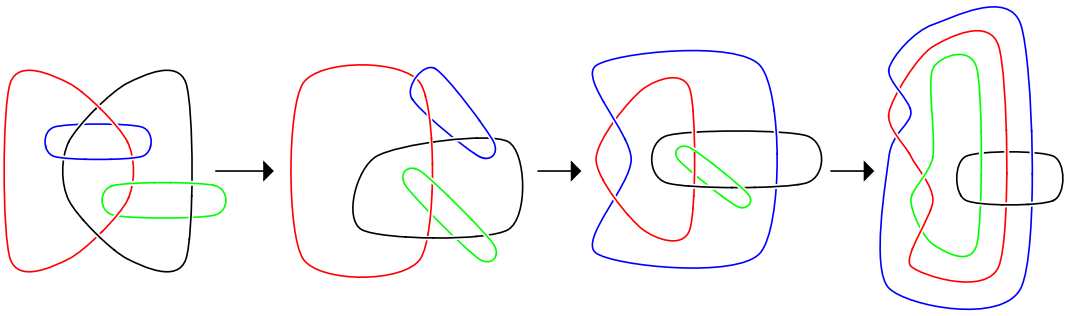

Figure 5.5: An isotopy of the Borromean twisted sister to a braided link where the braid axis is colored black. The resulting manifold has fiber surface D_3 with monodromy the braid group element $\sigma_1^{-2}\sigma_2^2 \in B_3$ under the surjective homomorphism Γ.

Obtaining this fibration of the link in S^3 with the given monodromy is straightforward, and we will demonstrate an example of this process for $k = 2$ in Figure 5.4. We begin by isotoping the component B so that locally we have a copy of $D_{k+3} \times [-\epsilon, \epsilon]$ for some ϵ. After this isotopy, we may cut along the surface bounded by B such that we obtain the braid element b_k which corresponds to our initial definition of the elements of the family. After this step, we have our desired fibration with monodromy $\Gamma(b_k)$.

Now lastly, we consider the case when $k = 1$. This will be done by showing an explicit isotopy of the Borromean twisted sister. For reference, the Borromean twisted sister appears as the rightmost diagram of Figure 4.3; however, it will be illustrated here again. As shown in Corollary 4.4.5, the complement of the Borromean twisted sister is a complexity one fundamental shadow link such that it satisfies the Turaev-Viro invariant volume conjecture with hyperbolic volume $2v_8$. Now from following the isotopies in Figure 5.5, we can see that one of the components is a braid axis that bounds a 3-punctured disk such that we have a fibered link. By cutting along the 3-punctured disk, we can see that our monodromy is the braid group element $\sigma_1^{-2}\sigma_2^2 \in B_3$ under the map Γ.

In conclusion, we can find a manifold with volume $2kv_8$, for any integer $k \geq 1$, which satisfies the Turaev-Viro invariant volume conjecture, fibers over S^1 with fiber surface a disk with punctures, and has explicit monodromy represented by b_k. □

Remark 5.2.6. Once we have a fibering link from Theorem 5.2.5, we may continue to

construct more examples of links satisfying the Turaev-Viro invariant volume conjecture by performing full-twists along the punctured disks the link components bound. Through this process, the new link with a homeomorphic complement may have a different fiber surface and monodromy. Additionally, there are self-homeomorphisms which may also remove the braid axis such that the resulting link is the closure of a braid. For example, a link with complement homeomorphic to the complement of a fundamental shadow link may be obtained as the braid closure of the element

$$(\sigma_4\sigma_3\sigma_2\sigma_1^2\sigma_2\sigma_3^{-1}\sigma_4)(\sigma_5\sigma_4\sigma_3^2\sigma_4\sigma_5)(\sigma_1\sigma_2\sigma_3\sigma_4\sigma_5^2\sigma_4\sigma_3\sigma_2\sigma_1) \in B_6.$$

This can be seen by performing a full-twist along the component labeled L'' in the rightmost diagram of Figure 5.4.

Remark 5.2.7. In the proof of Theorem 5.2.5, we obtained our results by applying Corollary 4.5.4 to a particular family of 2-braids. In general, this process may be repeated for other n-braids to obtain other links fibering over S^1 which satisfy the Turaev-Viro invariant volume conjecture; however, the monodromies may be more difficult to write down explicitly. In Subsection 5.2.3, we will follow the same steps for a particular family of 3-stranded braids such that we obtain fibered links satisfying similar properties. These links in combination with the links in Theorem 5.2.5 will be used to create explicit pseudo-Anosov elements in the mapping class group of a genus zero surface with n boundary components.

We will end this subsection with a result for obtaining additional fibered links which satisfy the extended Turaev-Viro invariant volume conjecture.

Corollary 5.2.8. *Let M_k be a manifold from Theorem 5.2.5 of volume $2kv_8$ that is realized as the complement of the braided link $\overline{b_k}$ where $b_k \in B_n$ for some n. Then for any $p \geq 2$, there exists a manifold M_k' obtained as the complement of a braided link $\overline{b_k'}$ where $b_k' \in B_{n+p-1}$*

such that

$$\lim_{r\to\infty} \frac{2\pi}{r} \log |TV_r(M'_k, q)| = v_4 \|M'_k\| = 2kv_8.$$

Here, r is odd, $q = \exp\left(\frac{2\pi\sqrt{-1}}{r}\right)$, $\|M'_k\|$ denotes the simplicial volume of M', and b'_k is obtained as an embedding of b_k into B_{n+p-1}.

Proof. For $p \geq 2$, we will first define T_p with distinguished boundary T to be the invertible cabling space as stated in Definition 2.1.7. To recall, T_p is the complement of a solid torus with p strands parallel to the core where the outer boundary torus of T_p is labeled T. For $k \geq 1$, the manifold M_k from Theorem 5.2.5 satisfies the Turaev-Viro invariant volume conjecture, and more generally, M_k satisfies the extended Turaev-Viro invariant volume conjecture. We will now define M'_k to be the manifold obtained by gluing $\partial(T_p)\backslash T$ for the manifold T_p to the boundary component of M_k which corresponds to the braid axis. Now by Proposition 2.1.8, the manifold M'_k satisfies the extended Turaev-Viro invariant volume conjecture with the following equalities

$$\lim_{r\to\infty} \frac{2\pi}{r} \log |TV_r(M'_k, q)| = \lim_{r\to\infty} \frac{2\pi}{r} \log |TV_r(M_k, q)| = v_4 \|M_k\| = 2kv_8$$

where r runs along the odd integers and $q = \exp\left(\frac{2\pi\sqrt{-1}}{r}\right)$.

Lastly, the manifold M'_k may be viewed explicitly as the complement of a braided link. This is because both the manifolds M_k and T_p are the complement of a link in a solid torus. By gluing the outer torus of M_k to one of the inner tori of T_p, our resultant manifold M'_k is still a complement of a link in a solid torus. In other words, the manifold M'_k is the complement of a braided link obtained by drilling out $(p-1)$ solid tori from M_k. □

Although Proposition 2.1.6 states that the exponential growth rate does not decrease by drilling out tori, it is not necessary for the growth rate to be related to the simplicial volume of the new manifold; however, Corollary 5.2.8 provides explicit examples where this holds.

5.2.3 Explicit Pure Braids Satisfying the AMU Conjecture

In this subsection, we will define explicit elements in the braid group which are pure braids. Because they are pure braids, they also represent elements in the mapping class group for genus zero surfaces as stated in Subsection 2.2.2. Additionally, since they will be constructed from fundamental shadow links, the explicit elements in the mapping class group will also satisfy the AMU conjecture. As a result, we provide the first known examples of pseudo-Anosov elements satisfying the conjecture in the mapping class group of $\Sigma_{0,n}$ for odd n.

Under the identification of elements of the pure braid group PB_n with $Mod(\Sigma_{0,n+1})$, we will now define the family of pure braids $\{\omega_m\}$, for $m \geq 4$, where we refer to $\{b_k\}$ as the family of braids obtained from Theorem 5.2.5:

- For $m = 4$, define $\omega_4 := b_1 \in Mod(\Sigma_{0,4})$.
- For $m \geq 6$ and even, define $\omega_m := b_{m-4} \in Mod(\Sigma_{0,m})$.
- For $m = 5$ and $m = 7$, define $\omega_m := \omega'_{m-1} \in Mod(\Sigma_{0,m})$ such that ω'_{m-1} is an embedding of $\omega_{m-1} \in Mod(\Sigma_{0,m-1})$ into $Mod(\Sigma_{0,m})$ sending each generator σ_j to σ_j.
- For $m = 9$, define $\omega_9 \in Mod(\Sigma_{0,9})$ by

$$\begin{aligned}\omega_9 :=&(\sigma_4\sigma_3^2\sigma_4)(\sigma_5\sigma_4\sigma_3\sigma_2^2\sigma_3\sigma_4\sigma_5)(\sigma_6\sigma_5\sigma_4\sigma_3\sigma_2\sigma_1^2\sigma_2^{-1}\sigma_3\sigma_4\sigma_5\sigma_6)\\ &(\sigma_7\sigma_6\sigma_5\sigma_4\sigma_3\sigma_2^2\sigma_3^{-1}\sigma_4\sigma_5\sigma_6\sigma_7).\end{aligned}$$

- For $m = 7 + 2s$ and $s \geq 2$, define $\omega_m \in Mod(\Sigma_{0,m})$ by

$$\begin{aligned}\omega_m :=&\omega'_9\prod_{i=2}^{s}(\sigma_{4+2i}\sigma_{3+2i}\cdots\sigma_4\sigma_3^2\sigma_4\cdots\sigma_{3+2i}\sigma_{4+2i})\\ &(\sigma_{5+2i}\sigma_{4+2i}\cdots\sigma_3\sigma_2^2\sigma_3^{-1}\sigma_4\sigma_5\cdots\sigma_{4+2i}\sigma_{5+2i})\end{aligned}$$

where ω_9' is an embedding of $\omega_9 \in Mod(\Sigma_{0,9})$ into $Mod(\Sigma_{0,m})$ sending each generator σ_j to σ_j.

Now in terms of the pure braid family $\{\omega_k\}$, we state the following result.

Corollary 5.2.9. *For $n \geq 4$, the element $\omega_n \in Mod(\Sigma_{0,n})$ satisfies the AMU conjecture. Additionally, if $n \notin \{5, 7\}$, then ω_n is a pseudo-Anosov element.*

Proof. We will first consider the case for genus zero surfaces with an even number of boundary components. We note that for every $m \geq 3$ and odd, there exists a link fibering over S^1 that has fiber surface D_m such that the complement satisfies the Turaev-Viro invariant volume conjecture. The examples of such manifolds are M_1 and M_k, for even k, obtained from Theorem 5.2.5. For reference, we will list the associated braids as follows:

- For $k = 1$, we defined $b_k := \sigma_1^{-2}\sigma_2^2 \in B_3$.
- For $k = 2j$, we defined $b_k \in B_{k+3}$ as

$$b_k := \prod_{i=1}^{j} (\sigma_{2i+1}\sigma_{2i} \cdots \sigma_3\sigma_2\sigma_1^2\sigma_2^{-1}\sigma_3\sigma_4 \cdots \sigma_{2i}\sigma_{2i+1})(\sigma_{2i+2}\sigma_{2i+1} \cdots \sigma_3\sigma_2^2\sigma_3 \cdots \sigma_{2i+1}\sigma_{2i+2}).$$

Notice that in these cases, the monodromies are obtained from pure braids. Under the identification of the pure braid group PB_m with $Mod(\Sigma_{0,m+1})$, this implies that we can view our manifolds as the mapping tori $M(b_k)$ with monodromy $b_k \in Mod(\Sigma_{0,m+1})$.

Now by Theorem 2.2.8, since our manifolds are hyperbolic, the element $b_k \in Mod(\Sigma_{0,m+1})$ is pseudo-Anosov. By Theorem 2.2.16, since our manifolds are mapping tori which satisfy the Turaev-Viro invariant volume conjecture where the elements are pseudo-Anosov, then b_k satisfies the AMU conjecture. This shows that for any $n \geq 4$ and even, we can find a pseudo-Anosov element $b_k \in Mod(\Sigma_{0,n})$ that satisfies the AMU conjecture.

We now consider the cases when our surface is $\Sigma_{0,n}$ for $n \in \{5, 7\}$. Our argument will follow the same logic in constructing elements in the mapping class group such that the

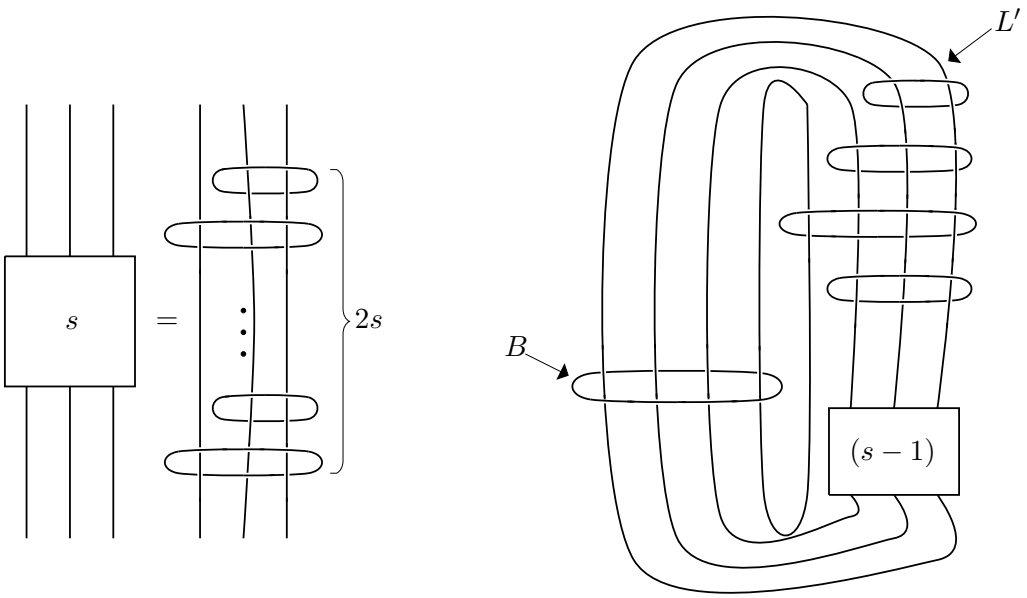

Figure 5.6: On the left, we define the boxed diagram as the identity 3-braid with $2s$ additional components. For a box labeled with 0, the diagram is the identity 3-braid without additional components. On the right, we show the link in S^3 obtained from applying Corollary 4.5.4 to the element $(\sigma_1\sigma_1^{-1})^s(\sigma_2\sigma_2^{-1}) \in B_3$. Here, the braid axis is labeled B, the link component that bounds a $(3+2s)$-punctured disk is labeled L', and the link contains $(7+2s)$ components.

corresponding mapping tori have exponential growth; however, we will choose to utilize Corollary 5.2.8. We first begin with any pure braid in PB_m for $m \leq (n-2)$ where the corresponding mapping torus satisfies the Turaev-Viro invariant volume conjecture. Now by Corollary 5.2.8, for $p \geq 2$, we may add an additional $(p-1)$ strands to obtain a pure braid in PB_{m+p-1} such that the corresponding mapping torus also has Turaev-Viro invariant with an exponential growth rate. This implies that the constructed element in the mapping class group $Mod(\Sigma_{0,m+p})$ will satisfy the AMU conjecture. For $n \in \{5, 7\}$, we can choose to use our previous pure braids from the case of a genus zero surface with an even number of boundary components.

It is important to note the following. By utilizing the previous procedure, any number of elements in different mapping class groups satisfying the AMU conjecture may be obtained. Although in these cases, the elements will only contain pseudo-Anosov parts, and they will not be pseudo-Anosov.

Lastly, we will consider the case when $n \geq 9$ and odd. Similar to the even boundary case, we will construct a pure braid through a combination of Corollary 4.5.4 and self-homeomorphisms of the manifold. For $s \geq 1$, consider $(\sigma_1\sigma_1^{-1})^s(\sigma_2\sigma_2^{-1}) \in B_3$ as the unreduced word of length $(2s+2)$. From Corollary 4.5.4, we can construct a hyperbolic manifold satisfying the Turaev-Viro invariant volume conjecture which is the complement of the link shown in the right diagram of Figure 5.6. Here, the box labeled with $(s-1)$ is defined on the left diagram. We also note that on the right diagram when $(s-1) = 0$, the boxed diagram is defined to be the identity 3-braid without any additional components. In the same manner of the proof of Theorem 5.2.5, we can perform a full-twist along the component L' to obtain a braided link $\overline{\omega_{7+2s}}$ with braid axis B such that ω_{7+2s} is a pure braid.

Now since L' and B bound a $(3+2s)$- and 4-punctured disk, respectively, then after the full-twist, our resultant link will have fiber surface D_{6+2s}. From the full-twist, we can describe the obtained elements in the pure braid group explicitly as follows:

- For $s = 1$, define $\omega_{7+2s} \in B_8$ by

$$\begin{aligned}\omega_{7+2s} :=&(\sigma_4\sigma_3^2\sigma_4)(\sigma_5\sigma_4\sigma_3\sigma_2^2\sigma_3\sigma_4\sigma_5)(\sigma_6\sigma_5\sigma_4\sigma_3\sigma_2\sigma_1^2\sigma_2^{-1}\sigma_3\sigma_4\sigma_5\sigma_6)\\ &(\sigma_7\sigma_6\sigma_5\sigma_4\sigma_3\sigma_2^2\sigma_3^{-1}\sigma_4\sigma_5\sigma_6\sigma_7).\end{aligned}$$

- For $s \geq 2$, define $\omega_{7+2s} \in B_{6+2s}$ by

$$\begin{aligned}\omega_{7+2s} :=&\omega_9' \prod_{i=2}^{s}(\sigma_{4+2i}\sigma_{3+2i}\cdots\sigma_4\sigma_3^2\sigma_4\cdots\sigma_{3+2i}\sigma_{4+2i})\\ &(\sigma_{5+2i}\sigma_{4+2i}\cdots\sigma_3\sigma_2^2\sigma_3^{-1}\sigma_4\sigma_5\cdots\sigma_{4+2i}\sigma_{5+2i})\end{aligned}$$

where ω_9' is an embedding of $\omega_9 \in B_8$ into B_{6+2s} sending each generator σ_j to σ_j.

Since $\omega_{7+2s} \in B_{6+2s}$ is a pure braid and the complement of the braided link $\overline{\omega_{7+2s}}$ satisfies the Turaev-Viro invariant volume conjecture, we can use the same argument as for the case of the

genus zero surface with an even number of boundary components. Under the identification of the pure braid group PB_{6+2s} with the mapping class group $Mod(\Sigma_{0,7+2s})$, we can find a corresponding element in $Mod(\Sigma_{0,7+2s})$ which is pseudo-Anosov and satisfies the AMU conjecture.

In conclusion, this shows that for every $n \geq 4$, our pure braid family $\{\omega_n\}$ satisfies the AMU conjecture such that ω_n is pseudo-Anosov for $n \notin \{5, 7\}$.

□

5.3 Cosets of the Pure Braid Group

In this section, we will construct additional examples of elements in the pure braid group which satisfy the AMU conjecture. This will be done by considering the forgetful maps for pure braid groups as well as utilizing the normal form of the pure braid group shown by Artin in [4]. Note that this consideration for using the normal form was found in Remark 5.7 of [18].

Definition 5.3.1. For $1 \leq i \leq n$, we define the i-th *forgetful map* on the pure braid group $F_i : PB_n \to PB_{n-1}$ to be the surjective homomorphism obtained by deleting the i-th strand of the pure braid. For $1 \leq l \leq n-1$, a forgetful map on the pure braid group $F : PB_n \to PB_{n-l}$ is a composition of i-th forgetful maps.

For a given forgetful map $F : PB_{m+l} \to PB_m$ and an element $b \in PB_m$, we can see that $F^{-1}(b) = \{\beta_k\}$ is a collection of pure braids $\beta_k \in PB_{m+l}$. Now notice that the corresponding complement of the braided link $\overline{\beta_k}$ is obtained from the complement of $\overline{b}$ by drilling out tori. If our initial braided link $\overline{b}$ has Turaev-Viro invariant with exponential growth rate, then $\overline{\beta_k}$ also has exponential growth rate by Proposition 2.1.6. Additionally, by Theorem 2.2.16, since the complement of $\overline{\beta_k}$ corresponds to the mapping torus of $\beta_k \in Mod(\Sigma_{0,m+l+1})$, then the element β_k also satisfies the AMU conjecture. Note that this is a more general construction for finding elements that satisfy the AMU conjecture than the one found in the proof of

Corollary 5.2.9 for the $n \in \{5, 7\}$ case. Here, the main difference is that our elements in the proof of Corollary 5.2.9 also satisfy the extended Turaev-Viro invariant volume conjecture which is not necessarily true for the general elements obtained from the inverses of the forgetful map. Using the forgetful maps, we see that we can obtain many elements that satisfy the AMU conjecture.

To add more structure to the elements, we will consider the normal form [4] of the pure braid group. This will allow us to view the elements which satisfy the AMU conjecture as cosets of the pure braid groups. It is well-known that for any $n > k$, the pure braid group PB_n may be written as a semidirect product of W_n and PB_k where W_n is itself a semidirect product of free subgroups of PB_n. Because of this, any braid $b \in PB_n$ has a unique representation as a product of $\beta \cdot \omega$ for $\beta \in P_k$ and $\omega \in W_n$. Now as before, notice that the braided link $\overline{b} = \overline{\beta \cdot \omega}$ contains the braided link $\overline{\beta}$ as a sublink such that if the complement of $\overline{\beta}$ has Turaev-Viro invariant with an exponential growth rate, then $\overline{b}$ also has Turaev-Viro invariant with an exponential growth rate. Once again, by Theorem 2.2.16, the element $b \in Mod(\Sigma_{0,n+1})$ will satisfy the AMU conjecture. This leads us into the following corollary where we define the collection of pure braids $\mathcal{P}$ to contain the elements from Table 5.2 and the elements from Corollary 5.2.9. Here, the elements in Table 5.2 are the links up to 11-crossings from Theorem 4.3.2 which can be obtained as the closure of a pure braid.

Corollary 5.3.2. *For a fixed n, let $\beta \in PB_s$ be an element of $\mathcal{P}$ with $n > s$. Now for any $b \in PB_n$ with normal form $b = \beta \cdot \omega$ where $\omega \in W_n$, the corresponding element b in $Mod(\Sigma_{0,n+1})$ satisfies the AMU conjecture.*

Proof. The proof follows from the previous discussion. The braided link of every element β in the collection $\mathcal{P}$ has Turaev-Viro invariant with an exponential growth rate. Now notice that the braided link of an element $b = \beta \cdot \omega \in PB_n$ also contains $\overline{\beta}$ as a sublink. Therefore, the complement of $\overline{b}$ which is the mapping torus of $b \in Mod(\Sigma_{0,n+1})$ also has Turaev-Viro invariant with an exponential growth rate. By Theorem 2.2.16, the element $b \in Mod(\Sigma_{0,n+1})$ satisfies the AMU conjecture. □

LinkInfo Name	Pure Braid Group PB_s	Pure Braid Element
L_{6a4}	$s=3$	$(\sigma_1\sigma_2^{-1})^3$
L_{6a4}	$s=3$	$(\sigma_1^{-1}\sigma_2)^3$
L_{8n5}	$s=3$	$(\sigma_1^{-1}\sigma_2)^2\sigma_1^{-1}\sigma_2^{-3}$
L_{8n7}	$s=4$	$\sigma_1\sigma_2\sigma_3^{-1}\sigma_2\sigma_1^{-2}\sigma_2\sigma_3\sigma_2\sigma_1$
L_{8n7}	$s=4$	$\sigma_1^{-1}\sigma_2^{-1}\sigma_3^{-1}\sigma_2\sigma_1^{-2}\sigma_2\sigma_3\sigma_2^{-1}\sigma_1^{-1}$
L_{8n7}	$s=4$	$\sigma_1\sigma_2^{-2}\sigma_3\sigma_2^{-2}\sigma_1^{-1}\sigma_2^2\sigma_3^{-1}\sigma_2^{-2}$
L_{8n7}	$s=4$	$\sigma_1^{-1}\sigma_2^{-1}\sigma_3^{-1}\sigma_2\sigma_1^{-2}\sigma_2\sigma_3\sigma_2^{-1}\sigma_1^{-1}$
L_{8n7}	$s=4$	$\sigma_1\sigma_2^2\sigma_1\sigma_3\sigma_2^{-2}\sigma_3$
L_{8n7}	$s=4$	$\sigma_1\sigma_2^{-2}\sigma_1\sigma_3^{-1}\sigma_2^{-2}\sigma_3^{-1}$
L_{8n7}	$s=4$	$\sigma_1\sigma_2\sigma_3^{-2}\sigma_2\sigma_1^{-1}\sigma_2\sigma_3^2\sigma_2$
L_{10n87}	$s=3$	$\sigma_1^3\sigma_2^2\sigma_1^2\sigma_2^2\sigma_1$
L_{10n97}	$s=4$	$\sigma_1\sigma_2\sigma_3^{-1}\sigma_2^{-3}\sigma_1^{-2}\sigma_2^{-1}\sigma_3\sigma_2\sigma_1$
L_{10n97}	$s=4$	$\sigma_1^{-3}\sigma_2^{-2}\sigma_1^{-1}\sigma_3^{-1}\sigma_2^{-2}\sigma_3^{-1}$
L_{10n97}	$s=4$	$\sigma_1\sigma_2^{-3}\sigma_3^{-2}\sigma_2^{-1}\sigma_1^{-1}\sigma_2\sigma_3^2\sigma_2$
L_{10n105}	$s=4$	$\sigma_1^{-1}\sigma_2\sigma_1\sigma_2^{-1}\sigma_1\sigma_3^{-1}\sigma_2^{-1}\sigma_3\sigma_2^{-1}\sigma_3^{-1}$
L_{10n105}	$s=4$	$\sigma_1\sigma_2\sigma_1^{-1}\sigma_2\sigma_1\sigma_3^{-1}\sigma_2\sigma_3^{-1}\sigma_2^{-1}\sigma_3$
L_{10n105}	$s=4$	$\sigma_1(\sigma_2\sigma_3)^2\sigma_2\sigma_1^{-1}\sigma_2^{-1}\sigma_3\sigma_2\sigma_3^{-1}\sigma_2$
L_{10n105}	$s=4$	$\sigma_1\sigma_2^{-1}\sigma_3\sigma_2^{-1}\sigma_3^{-1}\sigma_2\sigma_1^{-1}\sigma_2\sigma_3\sigma_2^{-1}\sigma_3\sigma_2$
L_{10n105}	$s=4$	$(\sigma_1^{-1}\sigma_2^{-1})^2\sigma_1^{-1}\sigma_3\sigma_2^{-1}\sigma_3^{-1}\sigma_2\sigma_3^{-1}$
L_{10n105}	$s=4$	$\sigma_1\sigma_2^{-1}\sigma_1\sigma_2\sigma_1^{-1}(\sigma_3\sigma_2)^2\sigma_3$
L_{10n105}	$s=4$	$\sigma_1\sigma_2\sigma_3^{-1}\sigma_2^{-1}\sigma_3\sigma_2^{-1}\sigma_1^{-1}(\sigma_2^{-1}\sigma_3^{-1})^2\sigma_2^{-1}$
L_{10n105}	$s=4$	$\sigma_1\sigma_2^{-1}\sigma_3^{-1}\sigma_2\sigma_3^{-1}\sigma_2^{-1}\sigma_1^{-1}\sigma_2\sigma_3^{-1}\sigma_2\sigma_3\sigma_2^{-1}$
L_{10n108}	$s=4$	$(\sigma_1^{-1}\sigma_2^{-1})^3\sigma_3\sigma_2^{-2}\sigma_3$
L_{10n108}	$s=4$	$\sigma_1\sigma_2\sigma_3^{-2}\sigma_2\sigma_1^{-1}(\sigma_2^{-1}\sigma_3^{-1})^3$
L_{10n108}	$s=4$	$\sigma_1\sigma_2^{-2}\sigma_3\sigma_2^{-2}\sigma_1^{-1}\sigma_2^{-1}\sigma_3\sigma_2\sigma_3^{-1}\sigma_2$
L_{10n108}	$s=4$	$\sigma_1\sigma_2^{-1}\sigma_1\sigma_2\sigma_1^{-1}\sigma_3^{-2}\sigma_2\sigma_3^{-2}$
L_{10n108}	$s=4$	$\sigma_1\sigma_2\sigma_1^{-1}\sigma_2\sigma_1\sigma_3\sigma_2^{-2}\sigma_3\sigma_2^{-1}$
L_{10n108}	$s=4$	$\sigma_1\sigma_2\sigma_3^{-2}\sigma_2\sigma_1^{-1}\sigma_3^{-1}\sigma_2\sigma_3\sigma_2^{-1}\sigma_3\sigma_2$

Table 5.2: The fundamental shadow links from Theorem 4.3.2 which can be written as the closure of a pure braid.

Corollary 5.3.2 allows us to construct cosets of elements in the pure braid group which satisfy the AMU conjecture; however, there is a key distinction compared to the elements in Corollary 5.2.9. For Corollary 5.2.9, we were careful in ensuring that all but finitely many of the elements are pseudo-Anosov. In the case of Corollary 5.3.2, there is no guarantee on whether the elements are pseudo-Anosov or whether they only contain pseudo-Anosov pieces.

Remark 5.3.3. Although the braided links $\overline{\beta}$ formed from the braids β in Table 5.2 are not necessarily fundamental shadow links, β as an element in the mapping class group of a genus zero surface still satisfies the AMU conjecture. This is because the mapping torus of the element β as an element in the mapping class group of a genus zero surface corresponds to the link complement of a braided link which inherently contains the braid axis. Now the braided link $\overline{\beta}$ contains the braid closure of β as a sublink such that the complement of $\overline{\beta}$ is a fundamental shadow link realized in S^3 with a drilled out torus from the braid axis. Since drilling out a torus does not decrease the exponential growth rate of the Turaev-Viro invariant, the complement of the braided link $\overline{\beta}$ also has Turaev-Viro invariants with an exponential growth rate, and we can apply Theorem 2.2.16 to see that β as an element in the mapping class group of a genus zero surface satisfies the AMU conjecture.

BIBLIOGRAPHY

BIBLIOGRAPHY

[1] I. Agol. "Small 3-Manifolds of Large Genus". In: *Geometriae Dedicata* 102 (2003), pages 53-64.

[2] J. W. Alexander. "A Lemma on Systems of Knotted Curves". In: *Proc. Nat. Acad. Sci. USA* 9.3 (1923), pages 93-95.

[3] J.E. Andersen, G. Masbaum, and K. Ueno. "Topological Quantum Field Theory and the Nielsen-Thurston classification of $M(0,4)$". In: *Mathematical Proceedings of the Cambridge Philosophical Society* 141.3 (2006), pages 477-488.

[4] E. Artin. "Theory of braids". In: *Ann. of Math. (2)* 48 (1947), pages 101-126.

[5] M. Baker. "All links are sublinks of arithmetic links". In: *Pacific Journal of Mathematics* 203.2 (2002), pages 257-263.

[6] G. Belletti. "A maximum volume conjecture for hyperbolic polyhedra". In: *arXiv preprint arXiv:2002.01904* (2020).

[7] G. Belletti, R. Detcherry, E. Kalfagianni, and T. Yang. "Growth of quantum $6j$-symbols and applications to the Volume Conjecture". In: *Journal of Differential Geometry* (to appear).

[8] R. Benedetti and C. Petronio. "On Roberts' proof of the Turaev-Walker theorem". In: *Journal of Knot Theory and Its Ramifications* 5.4 (1996), pages 427-439.

[9] C. Blanchet, N. Habegger, G. Masbaum, and P. Vogel. "Three-manifold invariants derived from the Kauffman bracket". In: *Topology* 31.4 (1992), pages 685-699.

[10] C. Blanchet, N. Habegger, G. Masbaum, and P. Vogel. "Topological Quantum Field Theories derived from the Kauffman bracket". In: *Topology* 34.4 (1995), pages 883-927.

[11] J. Brock. "Weil-Petersson Translation Distance and Volumes of Mapping Tori". In: *Communication in Analysis in Geometry* 11 (2003), pages 987-999.

[12] J. Brock, H. Mazur, and Y. Minsky. "Asymptotics of Weil-Pertersson Geodesics II: Bounded Geometry and Unbounded Entropy". In: *Geometric and Functional Analysis* 21 (2011), pages 820-850.

[13] Q. Chen and T. Yang. "Volume conjectures for the Reshetikhin-Turaev and the Turaev-Viro invariants". In: *Quantum Topology* 9.3 (2018), pages 419-460.

[14] F. Constantino. "$6j$-symbols, hyperbolic structures and the volume conjecture". In: *Geom. Topol.* 11.3 (2007), pages 1831-1854.

[15] F. Constantino and D. Thurston. "3-manifolds efficiently bound 4-manifolds". In: *Journal of Topology* 1.3 (2008), pages 703-745.

[16] M. Culler, N. M. Dunfield, M. Goerner, and J. R. Weeks. *SnapPy, a computer program for studying the geometry and topology of* 3*-manifolds*. Available at http://snappy.computop.org (01/12/2018)

[17] R. Detcherry. "Growth of Turaev-Viro invariants and cabling". In: *Journal of Knot Theory and Its Ramifications* 28.14 (2019), 8 pages.

[18] R. Detcherry and E. Kalfagianni. "Quantum representations and monodromies of fibered links". In: *Advances in Mathematics* 351 (2019), pages 676-701.

[19] R. Detcherry and E. Kalfagianni. "Gromov norm and Turaev-Viro invariants of 3-manifolds". In: *Ann. Sci. de l'Ecole Normale Sup.* 53.6 (2020), pages 1363-1391.

[20] R. Detcherry and E. Kalfagianni. "Cosets of monodromies and quantum representations". In: *Indiana Univ. Mathematics Journal* (To Appear).

[21] R. Detcherry, E. Kalfagianni, and T. Yang. "Turaev-Viro invariants, colored Jones polynomial and volume". In: *Quantum Topology* 9.4 (2018), pages 775-813.

[22] J.K. Egsgaard and S.F. Jorgensen. "The homological content of the Jones representations at $q = -1$". In: *Journal of Knot Theory and Its Ramifications* 25.11 (2016), 25 pages.

[23] B. Farb and D. Margalit. *A primer on mapping class groups*. Vol. 49, Princeton Mathematical Series. Princeton University Press, 2012.

[24] W. Floyd and A. Hatcher. "Incompressible surfaces in punctured-torus bundles". In: *Topology and its Applications.* 13 (1982), pages 263-282.

[25] D. Futer and F. Guéritaud. "On canonical triangulations of once-punctured torus bundles and two-bridge link complements". In: *Geometry & Topology.* 10 (2006), pages 1239-1284.

[26] P. M. Gilmer and G. Masbaum. "Integral TQFT for a one-holed torus". In: *Pac. J. Math.* 252.1 (2011), pages 93-112.

[27] M. Gromov. "Volume and bounded cohomology". In: *Inst. Hautes Études Sci. Publ. Math.* 56 (1982), pages 5-99.

[28] A. Hatcher. *Algebraic Topology*. Cambridge University Press, 2001.

[29] M. Ishikawa and Y. Koda. "Stable maps and branched shadows of 3-manifolds". In: *Mathematische Annalen* 367.3 (2017), pages 1819-1863.

[30] V. F. R. Jones. "A polynomial invariant for knots via von Neumann algebras". In: *Bull. Amer. Math. Soc. (N.S.)* 12.1 (1985), pages 103-111.

[31] V. F. R. Jones. "Hecke algebra representations of braid groups and link polynomials". In: *Ann. of Math. (2)* 126.2 (1987), pages 335-388.

[32] R. M. Kashaev. "A link invariant from quantum dilogarithm". In: *Modern Phys. Lett. A* 10.19 (1995), pages 1409-1418.

[33] R. M. Kashaev. "The hyperbolic volume of knots from the quantum dilogarithm". In: *Lett. Math. Phys.* 39.3 (1997), pages 269-275.

[34] E. Kin, S. Kojima, and M. Takasawa. "Entropy versus volume for pseudo-Anosovs". In: *Experimental Mathematics* 18.4 (2009), pages 397-407.

[35] R. Kirby. "A calculus for framed links in S^3". In: *Invent. Math.* 45 (1978), pages 35-36.

[36] S. Kumar. "Fundamental shadow links realized as links in S^3". In: *Algebraic & Geometric Topology.* (To Appear).

[37] H. Levine. *Classifying immersions into* $\mathbb{R}^4$ *over stable maps of* 3*-manifolds into* $\mathbb{R}^2$. Vol. 1157, Lecture Notes in Mathematics. Springer, Berlin, 1985.

[38] W. B. R. Lickorish. *An Introduction to Knot Theory.* Springer-Verlag New York, Inc., 1997.

[39] C. Livingston and A. H. Moore. *KnotInfo: Table of Link Invariants.* http://www.indiana.edu/ knotinfo (May 18, 2020)

[40] J. Marché and R. Santharoubane. "Asymptotics of quantum representations of surface groups". In: *Annales Scientifiques de l'Ecole Normal Supérieure* (To Appear).

[41] W. Menasco. "Closed incompressible surfaces in alternating knot and link complements". In: *Topology* 23.1 (1984), pages 37-44.

[42] Y. Minsky. "Teichmüller Geodesics and Ends of Hyperbolic 3-Manifolds". In: *Topology* 32 (1993), pages 625-647.

[43] G. D. Mostow. "Quasi-conformal mappings in n-space and the rigidity of hyperbolic space forms". In: *Inst. Hautes Études Sci. Publ. Math.* 34 (1968), pages 53-104.

[44] H. Murakami and J. Murakami. "The colored Jones polynomials and the simplicial volume of a knot". In: *Acta Math.* 186.1 (2001), pages 85-104.

[45] T. Ohtsuki. "On the asymptotic expansion of the quantum $SU(2)$ invariant at $q = \exp(4\pi\sqrt{-1}/N)$ for closed hyperbolic 3-manifolds obtained by integral surgery along the figure-eight knot". In: *Algebraic & Geometric Topology* 18.7 (2018), pages 4187-4274.

[46] G. Prasad. "Strong rigidity of Q-rank 1 lattices". In: *Invent. Math.* 21 (1973), pages 255-286.

[47] V.V. Prasolov and A.B. Sossinsky. *Knots, Links, Braids and* 3*-Manifolds: An Introduction to the New Invariants in Low-Dimensional Topology.* Vol. 154, American Mathematical Society, 1997.

[48] N. Reshetikhin and V. Turaev. "Invariants of 3-manifolds via link polynomials and quantum groups". In: *Invent. Math.* 103.3 (1991), pages 547-597.

[49] J. Roberts. "Skein theory and Turaev-Viro invariants". In: *Topology.* 34.4 (1995), pages 771-787.

[50] O. Saeki. "Simple stable maps of 3-manifolds into surfaces". In: *Topology* 35.3 (1996), pages 671-698.

[51] R. Santharoubane. "Limits of quantum $SO(3)$ representations for the one-holed torus". In: *Journal of Knot Theory and Its Ramifications* 21.11 (2012).

[52] R. Santharoubane. "Action on $M(0, 2n)$ on some kernel spaces coming from $SU(2)$-TQFT". In: *J. Lon. Math. Soc* 95.3 (2017), pages 785-803.

[53] J. R. Stallings. "Constructions of fibered knots and links". In: *Proceedings of Symposia in Pure Mathematics* 32 (1978), pages 55-60.

[54] W. Thurston. "The geometry and topology of three-manifolds". In: *Princeton Univ. Math. Dept. Notes.* (1979).

[55] W. Thurston. "On the geometry and dynamics of diffeomorphisms of surfaces". In: *Bull. Amer. Math. Soc.* 19.2 (1988), pages 417-431.

[56] V. Turaev. *Quantum invariants of knots and 3-manifolds.* de Gruyter Studies in Mathematics. de Gruyter, 1994.

[57] V. Turaev and O. Viro. "State sum invariants of 3-manifolds and quantum $6j$-symbols". In: *Topology* 31.4 (1992), pages 865-902.

[58] R. Van Der Veen. "Proof of the volume conjecture for Whitehead chains". In: *Acta. Math. Vietnamica* 33.3 (2008), pages 421-431.

[59] R. Van Der Veen. "The volume conjecture for augmented knotted trivalent graphs". In: *Algebraic & Geometric Topology* 9.2 (2009), pages 691-722.

[60] E. Witten. "Quantum Field Theory and the Jones Polynomial". In: *Commun. Math. Phys.* 121 (1989), pages 351-399.

[61] K. H. Wong. "Asymptotics of some quantum invariants of the Whitehead chains". In: *arXiv preprint arXiv:1912.10638* (2019).

[62] K. H. Wong, and T. Yang. "On the Volume Conjecture for hyperbolic Dehn-filled 3-manifolds along the figure-eight knot". In: *arXiv preprint arXiv:2003.10053* (2020).